

N O T I C E

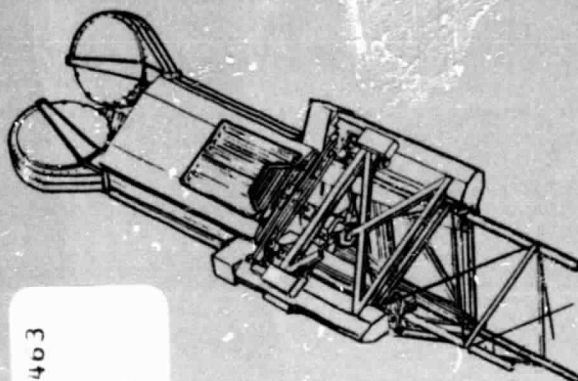
THIS DOCUMENT HAS BEEN REPRODUCED FROM
MICROFICHE. ALTHOUGH IT IS RECOGNIZED THAT
CERTAIN PORTIONS ARE ILLEGIBLE, IT IS BEING RELEASED
IN THE INTEREST OF MAKING AVAILABLE AS MUCH
INFORMATION AS POSSIBLE

TM: L. Jenkins EW4

7. GDC-ASP-80-007

NASA CR-

160932



N81-20463

UUCIAS
19422

CSCL 20K G3/39

(NASA-CR-100932) GRAPHITE COMPOSITE TRUSS
WELDING AND CAP SECTION FORMING SUBSYSTEMS.
VOLUME 2: PROGRAM RESULTS Final Report
(General Dynamics/Convair) 104 P
HC A06/MF A01

2. GRAPHITE COMPOSITE TRUSS WELDING AND CAP SECTION FORMING SUBSYSTEMS

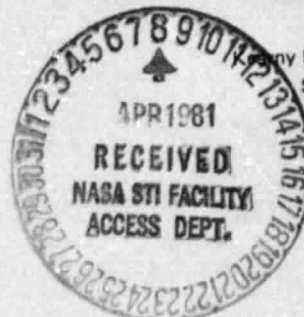
FINAL REPORT
VOLUME II + PROGRAM RESULTS

5. CONTRACT NO. NAS9-15973
DPL NO. T-1562
DRD NO. MA-179T
LINE ITEM NO. 3

6. Oct 31, 1980

4. **GENERAL DYNAMICS**
Convair Division

Convair Mesa Plant, P.O. Box 80847
San Diego, California 92138
Advanced Space Programs



GDC-ASP-80-007

**GRAPHITE COMPOSITE TRUSS WELDING
AND CAP SECTION FORMING SUBSYSTEMS**

**FINAL REPORT
VOLUME II • PROGRAM RESULTS**

CONTRACT NO. NAS9-15973
DRL NO. T-1562
DRD NO. MA-179T
LINE ITEM NO. 3

31 October 1980

Submitted to
National Aeronautics and Space Administration
LYNDON B. JOHNSON SPACE CENTER
Houston, Texas 77058

Prepared by
GENERAL DYNAMICS CONVAIR DIVISION
P. O. Box 80847
San Diego, California 92138

FOREWORD

This final report was prepared by General Dynamics Convair Division for NASA-JSC in accordance with Contract NAS9-15973, DRL No. T-1562, DRD No. MA-179, File Item No. 3. It consists of two volumes: (I) a brief Executive Summary and (II) a comprehensive set of program results.

The principal program results were developed from October 1979 through June 1980 followed by final documentation. Reviews were presented at JSC on 18 March 1980 and 16 July 1980.

During this program, many individuals were involved in providing technical and manufacturing support and assistance. We specifically wish to acknowledge the efforts of the following General Dynamics Convair personnel who significantly contributed to the program.

Structural Design & Analysis	-	Lee Browning, Ed Spier, Des Vaughan
Mechanical Design	-	John Bodle, Hans Stocker, Bob Clemens
Manufacturing R&D	-	Steve Hardy, Gerry Peddie
Materials R&D	-	Gay Liskay, Ray Adsit, Mal Campbell, Chuck Horst, Jim Prather, Jose Villa, Carlos Portugal, Mel Wood, Dave Harris, Hector Camacho
Environmental Test	-	Don Page, Bill Brunnhoelzl
Experimental Shop	-	Don Tibb, Norm Taylor, Dick Renick, Lou Schlife
Electronics & Instrumentation	-	Hugh Arrendale, Ralph Wickwire, Steve Cunningham, Wally Butts, Bob Hayes

The program was managed through Convair's Advanced Space Programs department, directed by R. H. (Russ) Thomas. The program manager was Lee Browning until 21 April 1980. Mr Browning accepted a new position at Convair and was succeeded by his Mechanical and Structural tasks leader, John Bodle. The NASA-JSC COR is Lyle Jenkins of the Spacecraft Design Division, under George Franklin, Chief.

For further information contact:

Lyle M. Jenkins, Code EW4
NASA-JSC
Houston, Texas 77058
(713) 483-2478

John G. Bodle, MZ 21-9504
General Dynamics Convair Division
P.O. Box 80847
San Diego, California 92138
(714) 277-8900, Ext. 2815

TABLE OF CONTENTS

<u>Section</u>		<u>Page</u>
1	INTRODUCTION	1-1
	1.1 Scope	1-1
	1.2 Program Overview	1-1
	1.2.1 Objectives	1-1
	1.2.2 Task Summary	1-1
2.	CAP FORMING TECHNOLOGY	2-1
	2.1 Roller/Heater Geometry	2-1
	2.1.1 Cap Forming Machine Modification	2-2
	2.1.2 Cap Forming Machine Operation	2-5
	2.1.3 Cap Forming Test & Evaluations	2-9
	2.2 Drive Rate Effects	2-14
	2.2.1 Drive Section Modifications	2-14
	2.2.2 Drive Rate Test & Evaluation	2-17
3	ULTRASONIC WELDING TECHNOLOGY	3-1
	3.1 Welding Task Objectives and Approach	3-1
	3.2 Weld Test Instrumentation	3-1
	3.2.1 Welder Controls	3-3
	3.2.2 Weld Specimen Drive System	3-4
	3.2.3 Data Recording	3-6
	3.3 Weld Schedule Determination	3-6
	3.4 Ultrasonic Welding Tests	3-7
	3.4.1 Preliminary Checkout	3-7
	3.4.2 Weld Specimen Configuration and Identification	3-8
	3.4.3 Vacuum & Gravity Effects Test	3-8
	3.5 Welding Test Results	3-10
	3.5.1 Lap Shear Strength Analysis	3-10
	3.5.2 Weld Visual Examinations	3-11
	3.5.3 Weld Head Temperature Characteristics	3-18
	3.5.4 Weld Specimen Temperature Effects	3-19
	3.5.5 Power Curve Analysis	3-20
4	PROTOTYPE TRUSS SEGMENT	4-1
	4.1 PTS Fabrication	4-1
	4.1.1 PTS Structural Members	4-2
	4.1.2 PTS Tools & Fixtures	4-2
	4.1.3 PTS Assembly	4-4
	4.2 PTS Test Preparation	4-7
	4.2.1 PTS Load Introduction Fittings	4-7
	4.2.2 PTS Instrumentation	4-8

TABLE OF CONTENTS (Continued)

<u>Section</u>	<u>Page</u>
4 (Contd)	
4.3 Local Effects	4-9
4.3.1 Cap Material Properties	4-10
4.3.2 Local Stability Analysis and Test	4-10
4.3.3 Crippling Tests	4-12
4.3.4 Torsional Instability Analysis	4-16
4.3.5 Column Tests & Displacement Measurement	4-19
4.4 Test Plan	4-23
4.5 PTS Test Results	4-23
4.5.1 Test Sequence 1: Cap Transverse Stiffness	4-23
4.5.2 Test Sequence 2: Torsional Stiffness Test	4-24
4.5.3 Test Sequence 3: Torsional Damping Test	4-27
4.5.4 Test Sequences 4 & 5: Flexural Stiffness and Damping Tests	4-27
4.5.5 Test Sequence 6: Axial Compression Test	4-27
4.5.6 Discussion of PTS Test Results	4-30
5 GRAPHITE COMPOSITE MATERIAL	5-1
5.1 Forming, Welding, & Truss Material	5-1
5.2 Space Environmental Test Material	5-2
6. CONCLUSIONS AND RECOMMENDATIONS	6-1
6.1 Conclusions	6-1
6.1.1 Cap Forming Technology	6-1
6.1.2 Ultrasonic Welding Technology	6-2
6.1.3 Prototype Test Truss	6-2
6.2 Recommendations	6-3
6.2.1 Beam Builder Technology	6-3
6.2.2 Graphite Thermoplastic Material Technology	6-4
6.2.3 Large Space Structures Technology	6-4
7 REFERENCES	7-1
<u>Appendix</u>	
A INSTRUMENTATION AND TEST REQUIREMENTS FOR PROTOTYPE TRUSS SEGMENT (PTS)	A-1

LIST OF FIGURES

<u>Figure</u>		<u>Page</u>
1-1	Summary of tasks and ground rules	1-2
1-2	Task relationships and flow	1-2
2-1	Effects of previous heater/roller geometry problems	2-3
2-2	Prototype cap forming machine	2-4
2-3	Cap forming process controller	2-4
2-4	Forming section changes	2-6
2-5	Roller/heater geometry changes	2-7
2-6	Cap strip preparation for forming	2-8
2-7	Cap forming operations	2-8
2-8	Cap forming results	2-11
2-9	Irregularities due to heating	2-12
2-10	Forming section trouble spot	2-12
2-11	Irregularities due to material processing limitations	2-13
2-12	Effects of step-wise consolidation	2-14
2-13	Original cap displacement measurement	2-15
2-14	Drive control and speed recording changes	2-16
2-15	Drive section modifications	2-16
2-16	Drive rate effects test procedure	2-18
2-17	Drive rate effects summary	2-19
3-1	Welding task approach	3-2
3-2	Welder instrumentation and controls diagram	3-2
3-3	Welding test instrumentation and controls	3-3
3-4	Ultrasonic weld head stack	3-4
3-5	GR/TRF weld test strip configuration	3-5
3-6	Vacuum chamber 0° setup	3-5
3-7	Vacuum chamber 45° setup	3-9
3-8	Vacuum chamber 90° setup	3-9
3-9	Specimen coupon tests	3-10
3-10	Weld head temperature characteristics in air and in vacuum	3-18
3-11	Thermocouple locations for air and vacuum temperature flow tests	3-20
3-12	Weld specimen heat flow characteristics in air and in vacuum	3-20
3-13	Smooth surface power curve	3-21
3-14	Rough surface power curve	3-21
3-15	Low weld strength power curve	3-21
4-1	Prototype truss segment configuration	4-1
4-2	Truss welding and assembly fixture details	4-3
4-3	Crossmember forming tools and process	4-3
4-4	Truss fabrication plan	4-4
4-5	Truss assembly operations	4-4
4-6	Truss ultrasonic welder	4-6
4-7	Finished weld joint	4-6

LIST OF FIGURES (Continued)

<u>Figure</u>		<u>Page</u>
4-8	Truss load introduction fittings installation	4-7
4-9	Truss strain gage installation	4-8
4-10	Finished prototype test truss segment	4-9
4-11	Local effects data development	4-10
4-12	Flexural and buckling properties tests	4-11
4-13	Finite-difference model for STAGS	4-11
4-14	Predicted local buckling and end shortening for crippling test specimens	4-12
4-15	Cap column crippling test setup	4-13
4-16	Crippling test results	4-14
4-17	Nondimensional buckling curves	4-15
4-18	Cap cross-section	4-16
4-19	Predicted compression load versus tangential displacement of free edges due to torsional instability	4-18
4-20	Cap column test setup	4-19
4-21	Cap rotation measurement	4-20
4-22	Cap column test no. 1 results	4-22
4-23	Cap column test no. 2 results	4-22
4-24	Cap transverse stiffness test setup	4-23
4-25	Cap transverse stiffness characteristic	4-24
4-26	PTS torsional stiffness and damping test setup	4-25
4-27	Torsional stiffness test results	4-26
4-28	PTS axial compression test	4-28
4-29	Cap displacement and rotation versus end load	4-30
5-1	Material characteristics	5-1

LIST OF TABLES

<u>Table</u>		<u>Page</u>
2-1	Summary of cap forming operations	2-9
2-2	Drive rates test sequence	2-17
3-1	Weld test specimen requirements	3-8
3-2	Weld test sequence	3-9
3-3	Summary of lap shear and peel tests	3-11
3-4	0° in-air weld specimens	3-12
3-5	0° in-vacuum weld specimens	3-13
3-6	45° in-air weld specimens	3-14
3-7	45° in-vacuum weld specimens	3-15
3-8	90° in-air weld specimens	3-16
3-9	90° in-vacuum weld specimens	3-17
3-10	Weld head heating effects	3-19

1

INTRODUCTION

1.1 SCOPE

This is the second of two volumes comprising the Final Report for the Graphite Composite Truss Welding and Cap Section Forming Subsystems Program. Volume I is an Executive Summary.

This section provides a program overview and a top level summary of the program effort.

1.2 PROGRAM OVERVIEW

1.2.1 OBJECTIVES. The overall objective of this development program is to advance the technology required to develop a beam builder which will automatically fabricate long, continuous, lightweight, triangular truss members in space from graphite/thermoplastic composite materials. The primary program objectives are:

- a. Continue the development of forming and welding methods for graphite/thermoplastic (GR/TP) composite material.
- b. Continue GR/TP materials technology development.
- c. Fabricate and structurally test a lightweight truss segment.

1.2.2 TASK SUMMARY. The Space Construction Automated Fabrication Experiment Definition Study (SCAFEDS), performed under Contract NAS9-15310 by General Dynamics Convair Division for the NASA Lyndon B. Johnson Space Center, in parallel with a Convair Independent Research and Development (IRAD) program, produced a concept for an efficient beam builder system for use in the on-orbit construction of large space structures (See Reference 1). This program's major task groups are structured, as summarized in Figure 1-1, to build on the SCAFEDS design and technology base in the three key areas of: forming; ultrasonic welding; and GR/TP composite materials development, test and evaluation.

The task flow shown in Figure 1-2 indicates the interrelationship between Task I and III. After modification and test of Convair's existing bench model cap roll forming machine, the machine was used to roll-form caps for the prototype test truss as well as for column test specimens used to test local buckling and torsional instability characteristics.

TOPIC	INPUT	DETAIL TASKS	GROUND RULES
TASK I CAP FORMING TECHNOLOGY	SCAFEDS PARTS I/II, III	101 ROLLER/HEATER GEOMETRY	• ON EXISTING BENCH MODEL MACHINE
		102 DRIVE RATE EFFECTS	
TASK III PROTOTYPE TEST TRUSS SEGMENT		301 TRUSS FABRICATION	• GEOMETRY, ELEMENT/JOINT DETAILS, MATERIAL PER SCAFEOS
		302 LOCAL EFFECTS	• LENGTH: 4.90m (3 BAYS + STD END CUTOFF)
		303 TRUSS TEST PREP/SUPPORT	• DIE-FORMED CROSS-MEMBERS
		304 MATERIAL	• STRAIN GAGES & LOAD INTRO FITTINGS PROVIDED
			• TESTS CONDUCTED AT JSC
TASK II ULTRASONIC WELDING TECHNOLOGY		201 VACUUM EFFECTS	• CONSOLIDATED STRIP FOR TESTING AT LARC: WOVEN SINGLE-PLY GRAPHITE/GLASS; POLYSULFONE RESIN
		202 GRAVITATIONAL EFFECTS	• ON EXISTING COMMERCIAL WELDER
			• GENERAL DYNAMICS CONVAIR-DEVELOPED HORN/TIPS/SCHEDULES

Figure 1-1. Summary of tasks and ground rules.

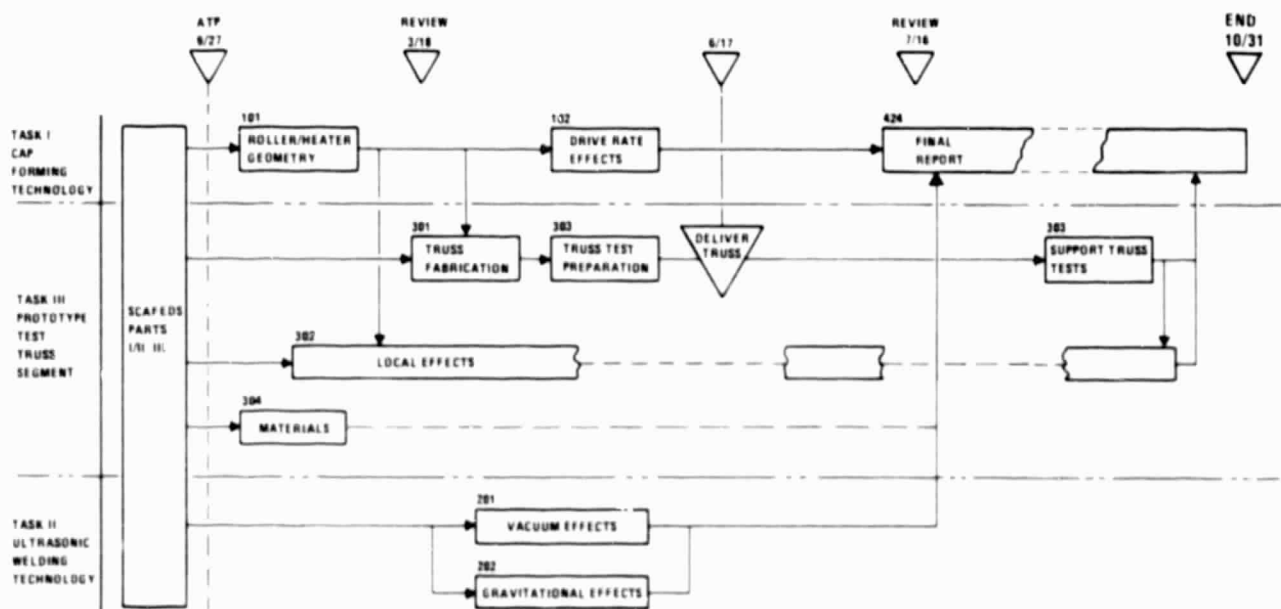


Figure 1-2. Task relationships and flow.

2

CAP FORMING TECHNOLOGY

In 1976, Convair engineers invented a process for forming flat strips of graphite/thermoplastic (GR/TP) material into structural shapes by heating the strips to the plastic temperature and passing them through sets of forming and cooling rollers. The patented roll-forming process was termed "Rolltrusion" as opposed to "Pulltrusion" whereby fabric strips are saturated with liquified resin material then pulled through a forming die which impregnates and consolidates the strip in-process. Rolltrusion allowed the material to be preprocessed (impregnated, coated, and consolidated) before forming.

It also took little energy to heat and drive the strip material because only the bend zones were exposed to heating and the forming rollers created little friction drag on the material. By 1978, a machine for automatically roll-forming GR/TP open-section cap members configured for the SCAFEDS space structure triangular truss and beam builder was demonstrated. This early bench model of a beam builder cap forming module showed the need for improvements of the roller and heater arrangements. It had also never been tested at forming rates faster than 1.27 cm/sec (0.5 in./sec). This section presents the results of modification, test, and evaluation tasks performed to improve performance of and identify drive rate effects for the cap forming machine.

2.1 ROLLER/HEATER GEOMETRY

The objective of this task was to evaluate and further optimize the operation of Convair's prototype cap forming machine. The goal was to be able to produce "operational quality" cap members, except for conditions caused by lack of sophistication of the machine elements or limited capability to produce uniform, top quality GR/TP strip material. The factors known to affect cap quality and appearance which could not be resolved within the scope of this task included the following:

- a. Use of surface contacting thermocouples for temperature control of the heated strips create scuff marks along the band zone surfaces.
- b. The GR/TP material, described in Section 5.1 is procured as a pre-pregged, uncoated, partially compacted fabric strip. Preprocessing includes spray coating with titanium dioxide TiO_2 mixed with polysulfone, and consolidation, compaction, and coating of the material by compression between plates which are heated to plasticize the polysulfone resin, then cooled to solidify the resin. This process squeezes the white coating into the graphite fibers causing the graphite to show through the coating. Processes for continuously coating and consolidating GR/TP strip material are not currently available.

Following modification and test, the cap forming machine would then be used to produce caps for the prototype test truss segment discussed in Section 4, and to produce cap test specimens for evaluation of column buckling and torsional instability effects.

2.1.1 CAP FORMING MACHINE MODIFICATION. Previous tests of the roll forming machine revealed some undesirable effects on the quality of the caps produced. Two of the most noticeable effects are shown in Figure 2-1. Wavy edges were common due to: a) inability to control the heating of the material within the bend zones; and b) too much strain on the material during forming because the forming stages were too close together. The use of numerous quartz lamps throughout the forming section without proper reflectors caused too much heating and softening of the side flats, which made the material more prone to wrinkling.

The modified cap forming machine shown in Figure 2-2 incorporated a new forming section and an improved process controller. The process controller shown in Figure 2-3 contains a control panel for manual and automatic control of the machine functions, and a heater power control panel for adjusting the power supplied to the heaters in the heating section and forming section through the strip temperature controllers shown on the process control panel.

The controller improvements were not a specified part of this contract, but were tasks planned and implemented as part of Convair's IRAD for in-space fabrication processes development. They included incorporation of the heater power control panel, which was previously a breadboard setup, and changes in the process control logic to eliminate some redundant functions which were causing periodic interruptions of the drive cycle.

The contracted task required redesign, fabrication, assembly, and development testing of the forming section. Each section of the cap forming machine was designed as a separate module to allow each function (i.e. heating, forming, cooling, drive) to be exchanged with different designs as required to evaluate alternative approaches. The forming section was thus replaced without changes to the heating, cooling, and drive sections.

The new forming section used much of the hardware from the original forming section, such as the forming rollers, lead-in rollers, bearings, shafts, and thermocouples. The new forming section used a 25.4 cm (10 in.) wide aluminum channel as a support base for all hardware. This provided better access to and greater visibility of the heaters and rollers.

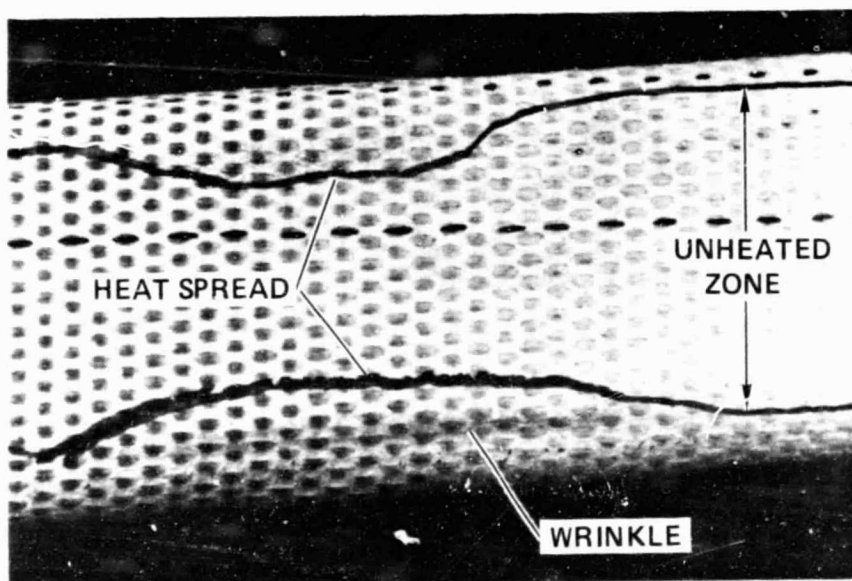
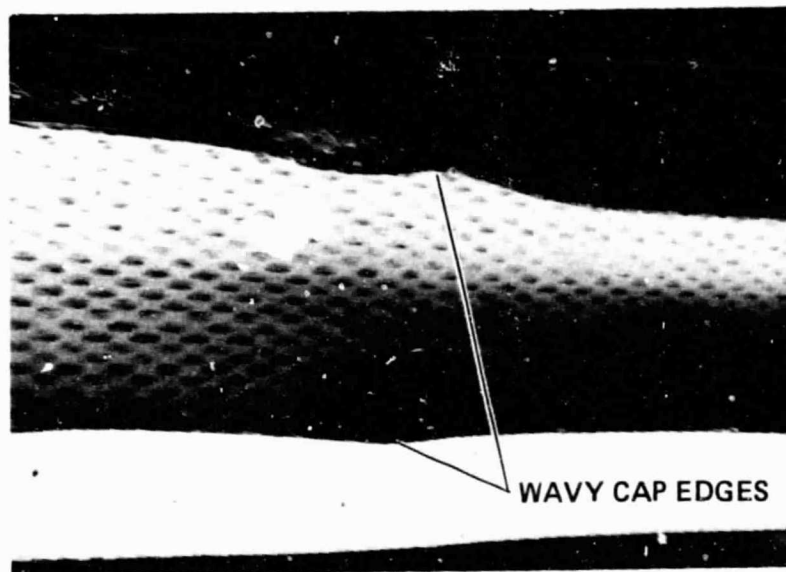


Figure 2-1. Effects of previous heater/roller geometry problems.

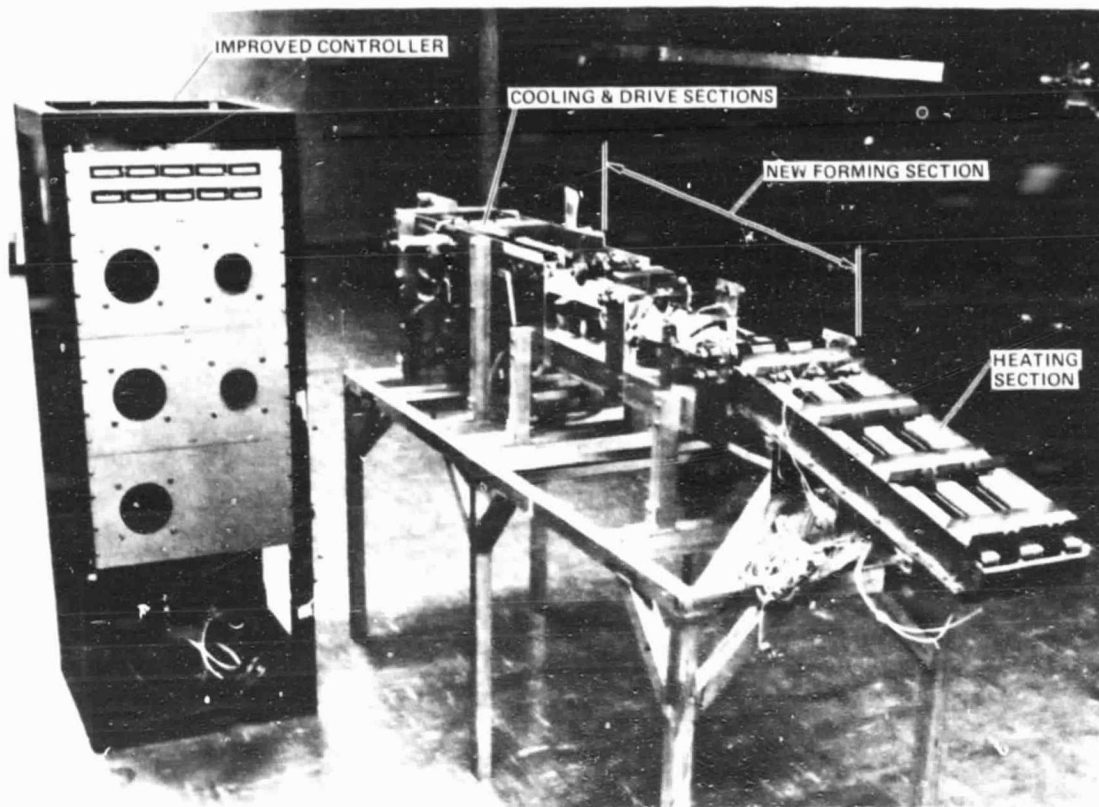


Figure 2-2. Prototype cap forming machine.

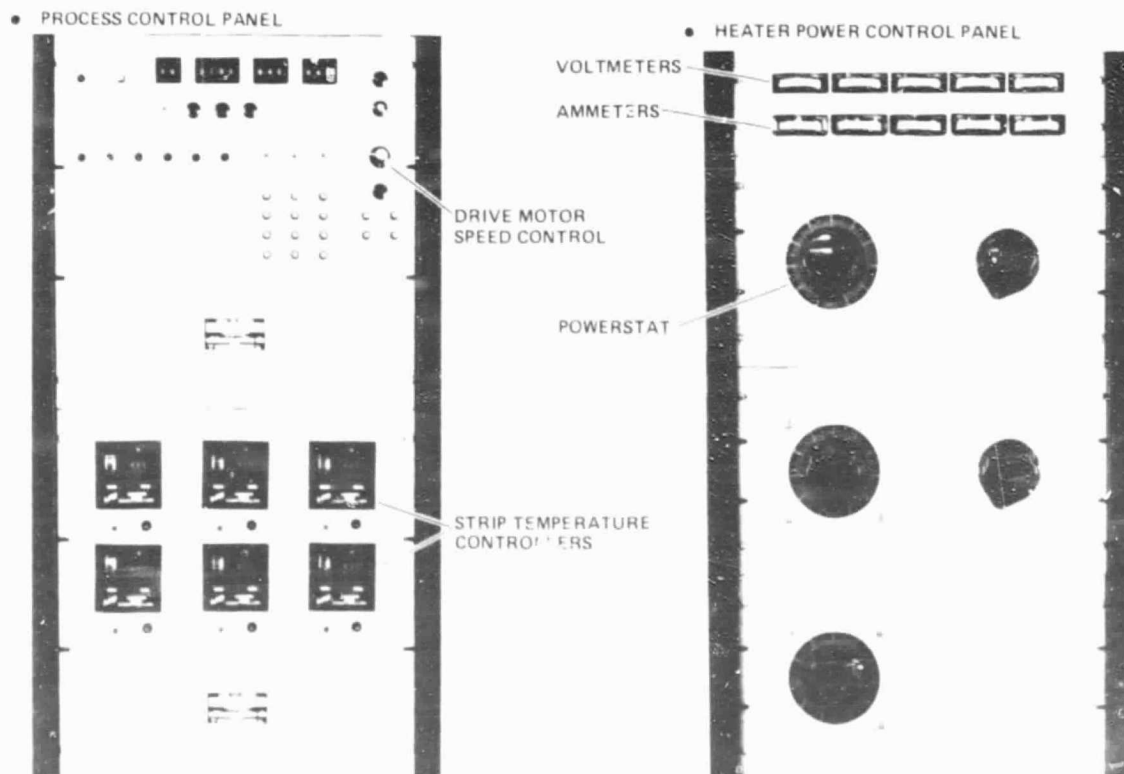


Figure 2-3. Cap forming process controller.

As shown in Figure 2-4, the original forming section employed numerous quartz lamps beneath and above the strip material. This was to allow flexibility in the adjustments of heaters during early development. The new design employs only four quartz lamp heaters located beneath the strip with specially shaped reflectors to direct the infrared heating at the bend zones. External reflector strips are provided along the length of the heated zones to help maintain the temperature of the strips.

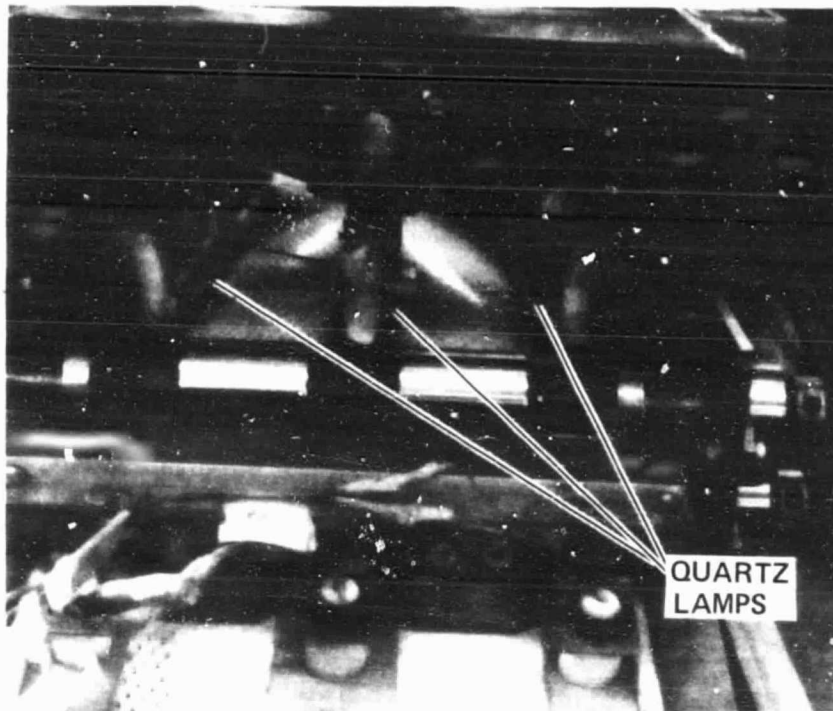
The distance between the lead-in set of straight rollers and the first forming stage was increased 6.35 cm (2.5 in.) to reduce the strains on the unheated side flats as the strip transitioned from flat to form the 60-degree apex angle. This alleviated the tendency of the center heated strip to fold to a peak just in front of the apex forming rollers, which made it difficult to control the width of the heat zone in this area during the pause period.

The distance between the first and final forming stage was increased 8.89 cm (3.5 in.), as shown in Figure 2-5. This reduced the strain on the unheated edges of the strip as the 90-degree side bends were formed. The strain had caused the edges to become crimped and wavy during the pause period and had also caused small cracks to occur in the edges. These problems were further alleviated by the addition of some teflon guides to support the edges before and after passing through the final forming rollers.

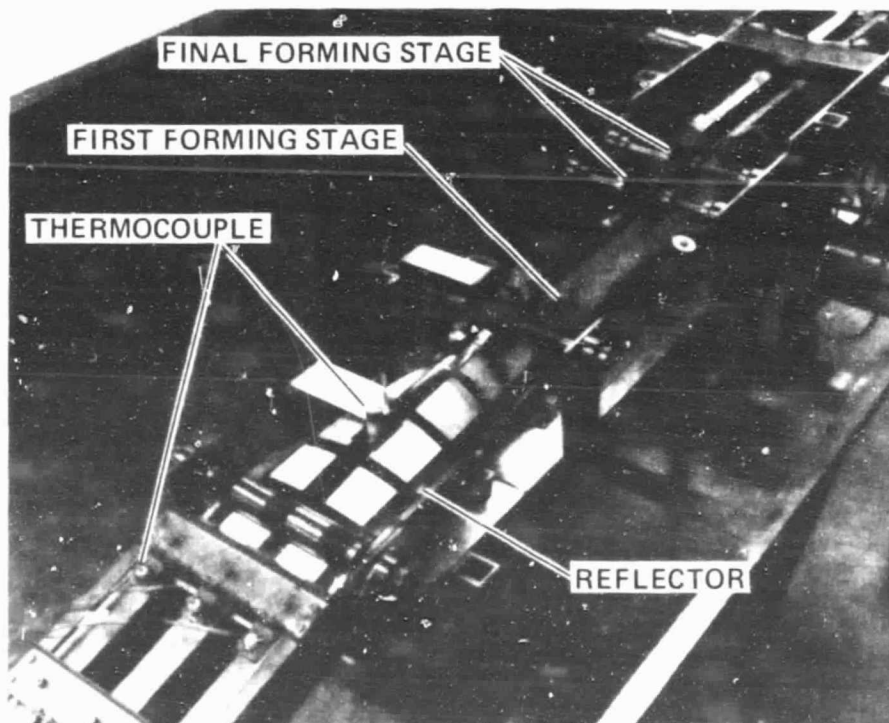
Surface contacting thermocouples were installed for control and measurement of strip temperatures. Three thermocouples in the forming section connect to three temperature controllers in the control panel which are preset to maintain strip temperatures within a range of 466K (380F) to 522K (480F). Two thermocouples in the forming section were connected to a temperature recorder to monitor temperatures at two critical locations during operation.

2.1.2 CAP FORMING MACHINE OPERATION. Cap forming specimens were prepared as shown in Figure 2-6. The 2.43 cm (8 ft) flexible glass leaders are installed on each strip to provide a means of starting the strip into the machine. The leader is fed by hand through the machine from the heating section to the drive section. After 15-minute warm-up period, the forming run is initiated and the glass leader pulls the strip through the heating, forming, and cooling sections and into the drive rollers. At that point, the leader is quickly cut off and the strip continues to completion. A short glass trailer is attached to the end of each strip. This is to stabilize the last few feet of strip material as it passes through the forming section. When the cap forming machine is in operation, as shown in Figure 2-7, the strip is automatically pulled through the process in cycles of 40 seconds run and 30 seconds pause. The controller measures a 58.4 cm (23 in.) stroke for each run cycle, then stops the motor and closes the water-cooled cooling platens. After 30 seconds, the controller opens the cooling platens and starts the motor. The motor is driven open-loop (i.e., no velocity feedback) so it is preadjusted to a strip speed of approximately 1.46 cm/sec (0.58 in./sec) so that the run time is 40 seconds.

- ORIGINAL FORMING SECTION



- NEW FORMING SECTION

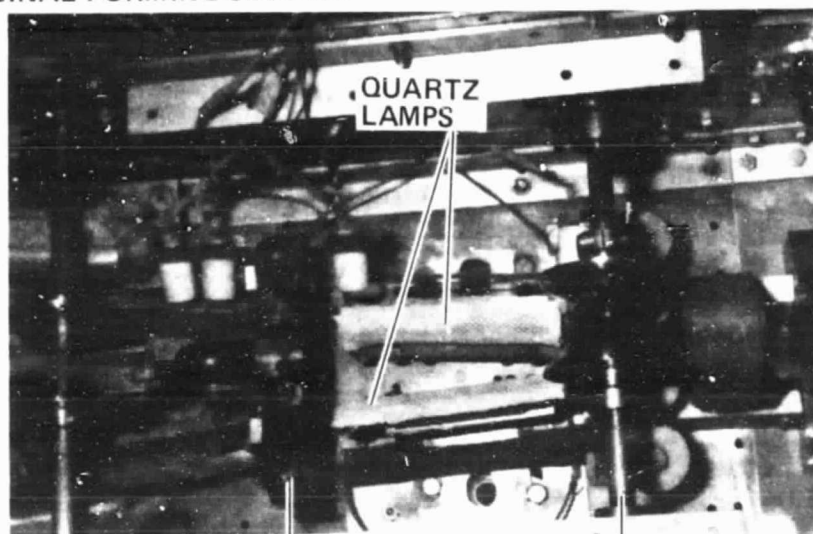


- NUMBER OF HEATERS IN FORMING SECTION REDUCED BY 79%
- OVERALL LENGTH INCREASED ~ 15.2 CM

Figure 2-4. Forming section changes.

ORIGINAL PAGE IS
OF POOR QUALITY

- ORIGINAL FORMING SECTION



- NEW FORMING SECTION

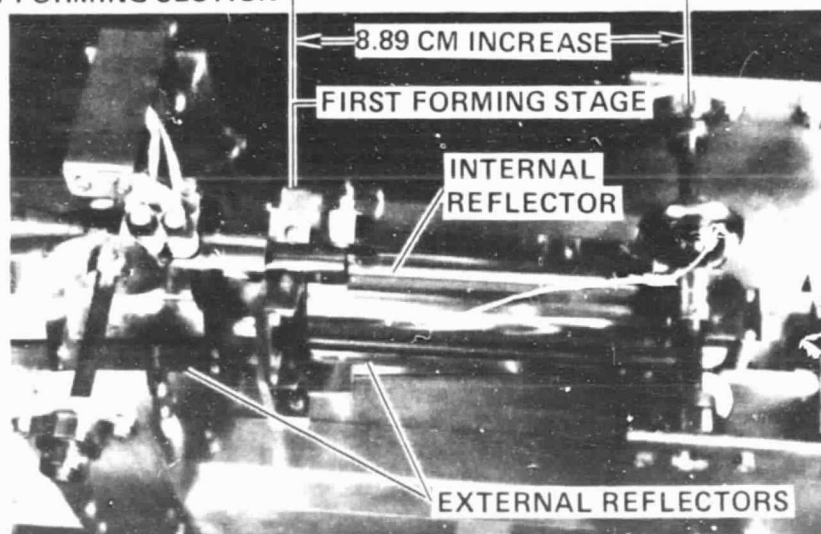
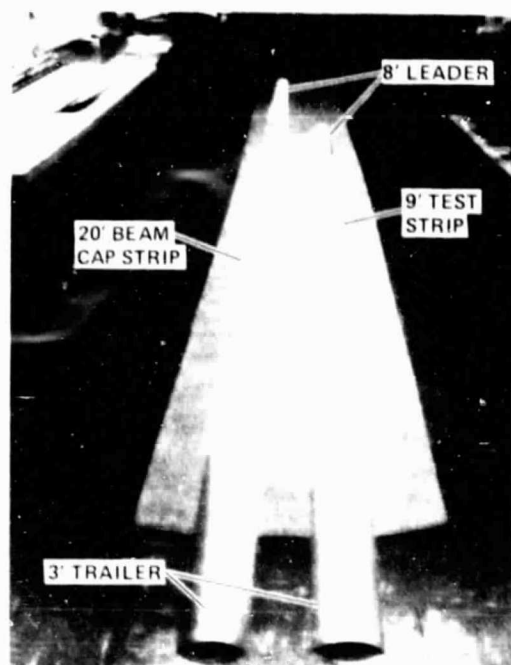


Figure 2-5. Roller/heater geometry changes.

• CAP STRIP ASSEMBLIES



• LEADER & TRAILER DETAILS

E-GLASS
181 P-1700
25% RESIN BY WT

BONDED
3.61 cm
LAP JOINT

COATED &
COMPACTED
GRAPHITE/GLASS/
POLYSULFONE
COMPOSITE STRIPS

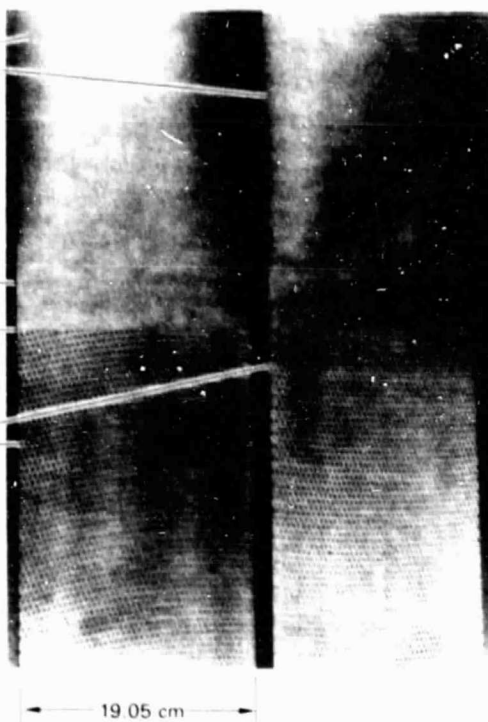


Figure 2-6. Cap strip preparation for forming.

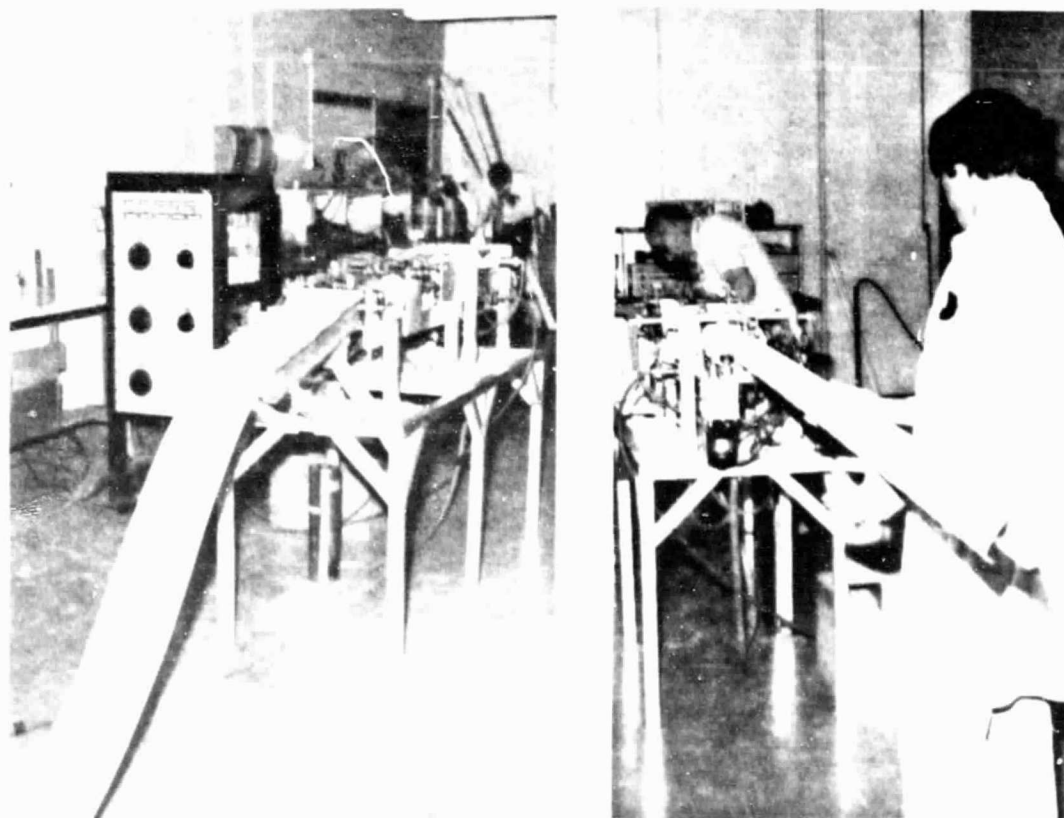


Figure 2-7. Cap forming operations.

Cyclic feed is a beam-builder consideration to allow a pause period during which beam assembly functions are accomplished.

The strip material is heated only along the bend zones to the forming temperature in the heating section, during the 70 second run and pause period. The forming section heaters are required to maintain the forming temperature due to the convective cooling effect of air. Analysis has shown that for operation in space, the forming section heaters could be turned off after the initial warm-up, and the heating section heaters would require less energy to heat the material in vacuum. In-air operation is, however, a consideration for ground test and checkout, which must be provided for an operational beam builder.

The prototype (bench model) cap forming machine operates in 58.4 cm (23 in.) strokes because it was intentionally designed with short heating and cooling sections to save cost. For a SSAFE beam builder, the stroke would be 1.439 cm (56.46 in.). For a run time of 40 seconds, the maximum strip speed would be approximately 3.8 cm/sec (1.5 in./sec). The effects of forming at this speed are discussed in Section 2.2.2.

2.1.3 CAP FORMING TEST & EVALUATIONS. A summary of all cap forming tests and operations performed on this program is given in Table 2-1. The first test performed after initial buildup of the forming section resulted in a very poor specimen. This test revealed the following deficiencies in the forming section:

Table 2-1. Summary of cap forming operations.

RUN NO.	DATE	CAP LENGTH	END USE	RESULTS & ACTION
1	14 MAR	2.74m (9 FT)	TEST RUN ONLY	POOR - HEATING ELEMENTS ADJUSTED - SUPPORT GUIDES ADDED
2	9 MAY	2.74m (9 FT)	TEST RUN ONLY	FAIR - MINOR ADJUSTMENTS MADE
3	13 MAY	6.1m (20 FT)	TEST RUN - CRIPPLING SPECIMENS	GOOD - MINOR IRREGULARITIES - INSULATED SUPPORT BRACKETS
4	14 MAY	<div><div></div><div></div></div>	COLUMN TEST SPECIMEN	GOOD
5	14 MAY		PROTOTYPE TRUSS CAP	GOOD
6	15 MAY		PROTOTYPE TRUSS CAP	GOOD
7	15 MAY		PROTOTYPE TRUSS CAP	GOOD

TOTAL 36m (118 FT)

- a. The heater reflectors needed adjustment and modification in some areas.
- b. The heating elements required some repositioning to improve heat distribution. Some areas were over-heating and others were not getting enough heat.
- c. The edge guides required further modification.
- d. The side flats required additional support.

A substantial number of modifications were made to improve performance. Heating profiles were tested by installing flexible fiberglass strips in the forming section and measuring temperatures along the heat zones with a surface probe thermocouple and digital thermometer. This pinpointed problem areas requiring adjustments and modifications. More edge guides and side support guides were added to prevent waviness of the free edges and wrinkling along the bend zones.

The second test showed a marked improvement in the uniformity of the finished cap; however, further adjustment of guides was required to correct minor creases along the bend zones.

The third test specimen was the first 6.1 m (20 ft) specimen to be run. It was generally uniform in crosssection with some minor irregularities, which will be discussed later. One set of support brackets in the forming section was wrapped with fiberglass to eliminate a potential hot spot in the edges.

It was decided at this point to proceed with the forming of the specimens for column test and caps for the prototype test truss. It was recognized that further efforts to eliminate minor irregularities would require more time, money, and material than was available. It should be noted, however, that the causes of every irregularity observed was eventually identified, and none were found that could not be remedied by either improving the material processing techniques or by some minor changes in forming section reflectors.

The last four caps were run in sequence without further change or adjustment of the cap forming machine. The results achieved on the prototype truss caps is shown in Figure 2-8.

• LENGTHWISE VIEW

• SIDE VIEW

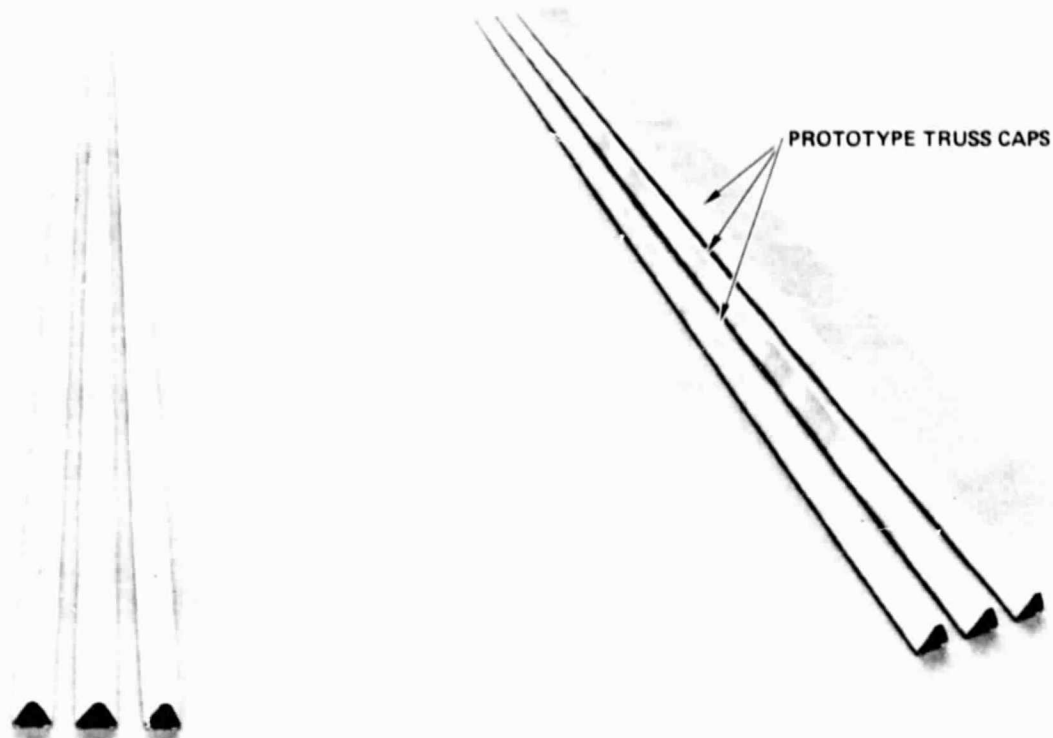


Figure 2-8. Cap forming results.

There were two noticeable irregularities in the finished caps. The first was a local edge deformation shown in Figure 2-9, which occurred at regular stroke length intervals. This suggested a local hot spot somewhere in the forming section that was radiating enough heat on the edges to cause them to soften and subsequently be deformed. Post test analysis of this problem identified a 2.54 cm (1.0 in.) wide reflector support just forward of the first forming stage as the cause. This support, shown in Figure 2-10, was attached directly to the internal and external reflector, which would allow it to become heated enough to melt the cap edges locally.

The second noticeable irregularity was that all of the formed caps exhibited a relatively constant curvature in the plane of symmetry as seen in Figure 2-11. A careful check of the alignment of the axially linear element in the cap forming machine failed to identify anything that would account for this curvature. The machine, in fact, would tend to correct this type of curvature due to the offset of the drive pull force from the cap section center of gravity.

• LOCAL EDGE DEFORMATION



Figure 2-9. Irregularities due to heating.

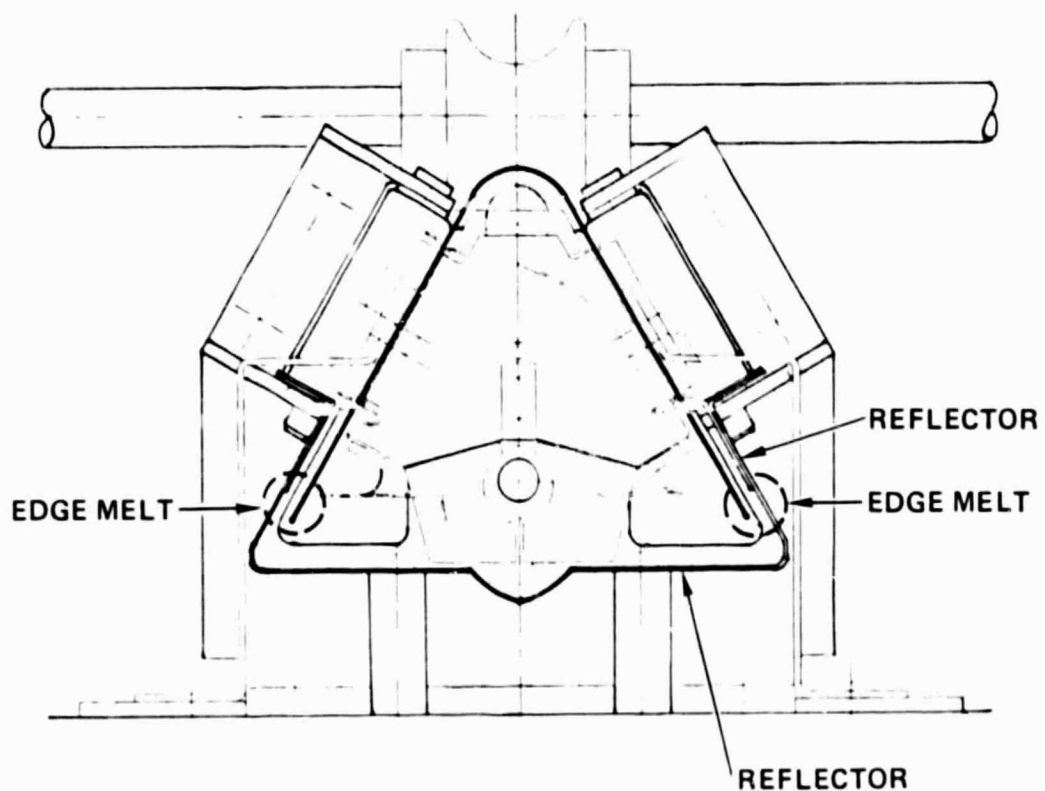


Figure 2-10. Forming section trouble spot.

• CAP CURVATURE



Figure 2-11. Irregularities due to material processing limitations.

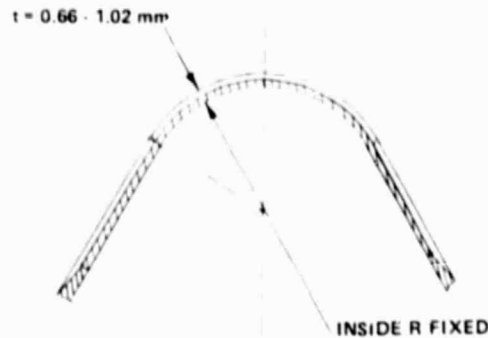
After general inspection of the strip material thickness, it was theorized that the curvature may be induced by the nonuniformity of the material thickness. Step-wise compaction of the strip results in alternately varying material thickness over its entire length. This thickness varies from 0.66 to 1.02 mm (0.026 to 0.040 in.). The thickest areas are characterized by a whiter color and rougher surface texture, and do not lay perfectly flat. These thick zones are approximately 12.7 cm (5 in.) long and occur at 22.9 cm (9 in.) intervals along the strip length.

The thinner zones are characterized by a generally darker color due to more graphite fibers showing through the coating. Separation between the graphite strands is measurably greater than in the thicker zones. The greater squeeze of the fabric in the thin zone obviously creates a zone of nonuniform intra-material stress concentration.

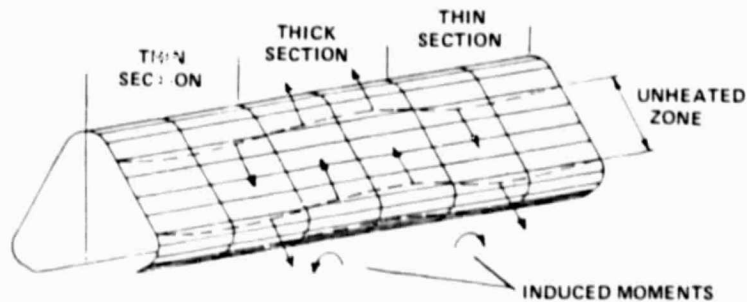
The effect of the alternating thickness variation on cap shape is illustrated in Figure 2-12. Since the inside geometry of the cap section is fixed by the forming rollers and cooling platens, the arc perimeters of the outside radii changed with thickness. This alternating shortening and lengthening of the arc perimeters causes stresses along the boundaries of the unheated side flats and edges as shown. These stresses induce moments along the length of the cap. Since the open section allows the cap to distort

under the influence of these stresses, the cap will tend to bow in the direction of least resistance.

1. NON-UNIFORM THICKNESS



2. THICKNESS VARIATION ALTERNATES



3. OTHER EFFECTS

- GRAPHITE SHOWS THRU COATING
- NON-UNIFORM COATING

Figure 2-12. Effects of step-wise consolidation.

The curvature of the caps did not affect truss assembly because it took very little force to straighten the caps out on the truss welding fixture described in Subsection 4.1.2. The curvature did, however, introduce an unexpected variable to the cap crippling and column test specimens.

2.2 DRIVE RATE EFFECTS

An experiment was performed to determine the effects of driving the strip material through the forming section at increased rates of speed. This section describes the changes made to the drive section to perform this experiment, and the test method and results of testing.

2.2.1 DRIVE SECTION MODIFICATIONS. The original drive section and cap displacement measurement is shown in Figure 2-13. The molded elastomeric drive rollers were driven in unison by a 1/50 horsepower DC shunt-wound motor through a gear train. A resolver wheel created pulses from an optoelectronic interrupter which were

input to the cap displacement controller in the cap forming machine controller. There was a resolution of approximately 96 pulses per inch of cap travel.

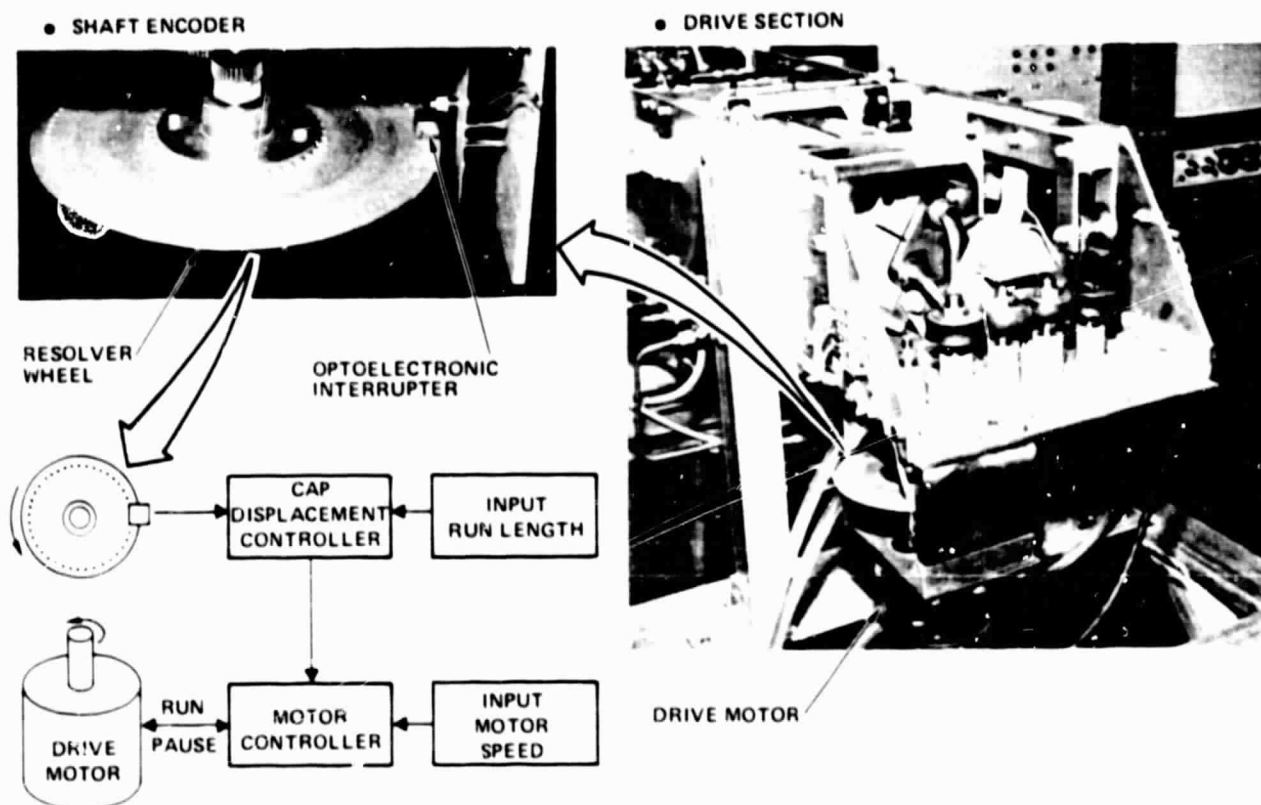


Figure 2-13. Original cap displacement measurement.

By setting the desired run length on the control panel, the cap displacement controller stopped the drive motor when the required pulse count accumulated. This measurement technique was not very accurate because the elastomeric rollers introduced an error in the actual-versus-indicated cap displacement.

To improve accuracy of the displacement measurement and provide for recording of cap speed, the changes illustrated in Figure 2-14 were incorporated. To permit driving the cap at increased speeds the drive motor and gear ratio were changed. These drive section modifications are shown in Figure 2-15.

The optical shaft encoder pulses output signals at the rate of 100 pulses per inch of cap travel in response to the rotation of the displacement driven wheel. The wheel is equipped with an elastomeric O-ring to provide traction on the cap. This technique improved the accuracy of cap displacement measurement by an order of magnitude.

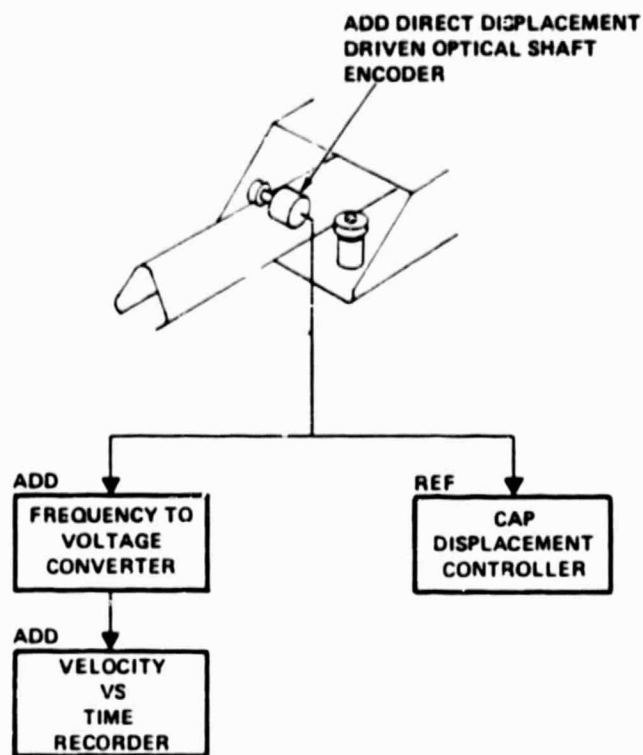


Figure 2-14. Drive control and speed recording changes.

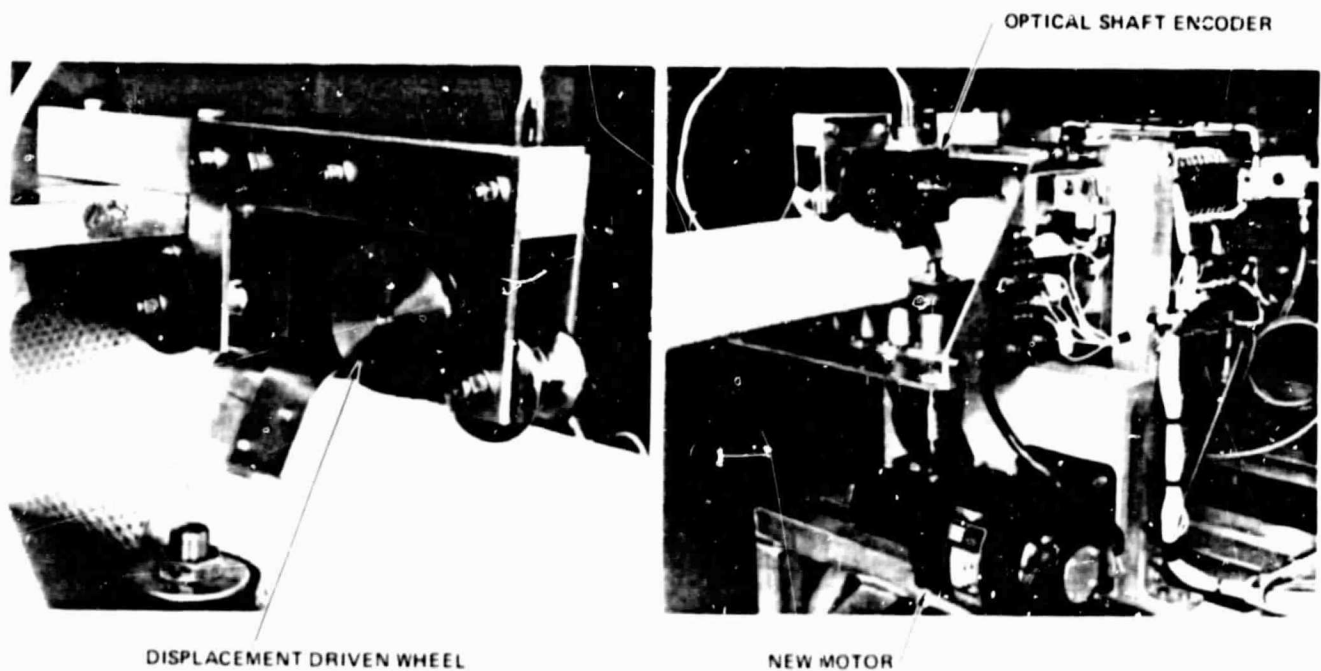


Figure 2-15. Drive section modifications.

ORIGINAL PAGE 2
OF FOUR QUALITY

The new drive motor is a 1/15 horsepower DC shunt-wound. As mentioned previously, the motor is driven open-loop, with no velocity feedback or control. The motor thus tends to slow down under increased load, which results in variable velocity during test runs if the strip material encounters a change in drag force for some reason. For a beam-builder system, a more sophisticated drive control would be required to ensure uniform displacement of caps during the run phase, and highly accurate displacement control of each beam cap to ensure straightness of long beams. This differential drive concept is discussed in detail in Reference 1.

2.2.2 DRIVE RATE TEST & EVALUATION. Because of a limited amount of strip material available for this program, the drive rate effects test had to be run using 6.1 m (20 ft) length of strip material. This allowed eight different speeds to be run. The speeds were selected between the minimum speed of 3.8 cm/sec (1.50 in./sec), which is the baseline speed for the SCAFEDS beam building, and 31.8 cm/sec (12.5 in./sec) which is the speed derived for the Solar Power Satellite growth version of the beam builder, per Reference 1. These speed increments are listed in Table 2-2.

Table 2-2. Drive rates test sequence.

Run	Speed cm/sec (in/sec)	Pause Time (sec)	Remarks
1	3.8 (1.50)	68	SCAFEDS Baseline
2	8.9 (3.50)		
3	14.0 (5.50)		
4	19.0 (7.50)		
5	24.1 (9.50)		
6	26.7 (10.50)		
7	29.2 (11.50)		
8	31.8 (12.50)	68	SPS Growth BB

Because the pause time required at the maximum speed would be 68 seconds, it was decided that all test runs would use the same pause time. This would eliminate pause time as a variable from run-to-run and also preclude another adjustment of the control settings that would have to be made between test runs.

The drive rate effects test procedure was as diagrammed in Figure 2-16. Prior to test, the speed control dial was calibrated by driving lengths of cap through the cooling and drive sections, recording velocity, and marking the speed on the dial.

A pretest practice run was made with a flexible glass leader to proof the procedure and calibrate the operators. The machine was then loaded with the test strip and leader. After the initial warm-up, the test was started.

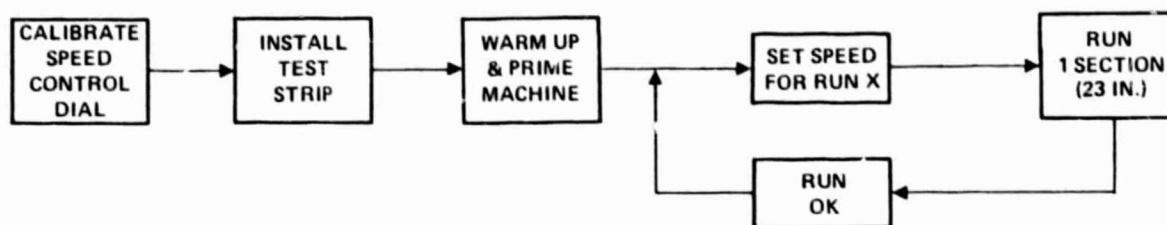


Figure 2-16. Drive rate effects test procedure.

The first three run cycles are required to feed the strip from the input end to the drive section. These runs were made at 3.8 cm/sec (1.5 in./sec). On the third test run, the material encountered a high drag load at some point in the machine which sheared the roll pin in the motor drive coupler. From this point on the strip was manually pulled through the machine at ever increasing speeds; however, the maximum speed that could be reached by this method was 30.5 cm/sec (12.0 in./sec).

The drive rate effects identified during this experiment are summarized in Figure 2-17. There were no speed related effects noted until the velocity reached 10.2-12.7 cm/sec (4.0-5.0 in./sec). The irregularities in the cap section at the lower speeds were all related to the larger than normal pause time and were all heating or cooling effects.

The cold spot on the apex occurred at regular stroke intervals and corresponded to the one area of the machine that has poor heat distribution, that is the zone between the heating section and the lead-in rollers of the forming section. This cold spot was not present on previous runs because the material had less time to cool in this zone and more time to become heated as it passed from the lead-in rollers to the first stage forming rollers. Better heater design at the inlet to the forming section would resolve this condition.

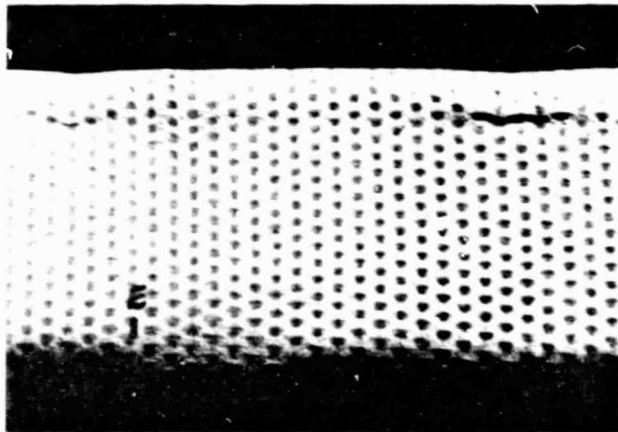
The long pause resulted in more heat on the sides of the cap and more softening of the free edges, which caused wrinkles and distortions to occur. The basic cause of this is too much exposure time to back-side radiation from the heater reflectors. Additional shielding or insulation of the reflectors would eliminate these problems.

The first noticeable drive rate effects were wrinkles in the apex side bend as shown in Figure 2-17. These effects repeated for all speeds above 10.2 cm/sec (4.0 in./sec). The apex wrinkles occurred under the apex forming rollers in the final forming stages and were apparently caused by the sudden strip acceleration compressing the still-soft

• MAJOR EFFECTS

IRREGULARITY	CAUSE		NORMAL SPEED REF							
	SPEED	PAUSE	(SPEED (in/sec))							
			0.5	1.5	3.5	5.5	7.5	9.5	11.5	12.0 MAX
• 2.8 IN. COLD SPOT ON APEX		X		X						
• HEAT SPREAD ON SIDES		X		X						
• EDGE RIPPLE & MELTING		X		X						
• EDGES LOCALLY DISTORTED (SAME REFLECTOR SUPPORT)		X		X						
• WRINKLES IN APEX	X					X				
• WRINKLES ON SIDE BEND	X					X				
• SEVERE EDGE RIPPLE	X	X					X			

• WRINKLES IN APEX



• WRINKLES ON SIDE BEND

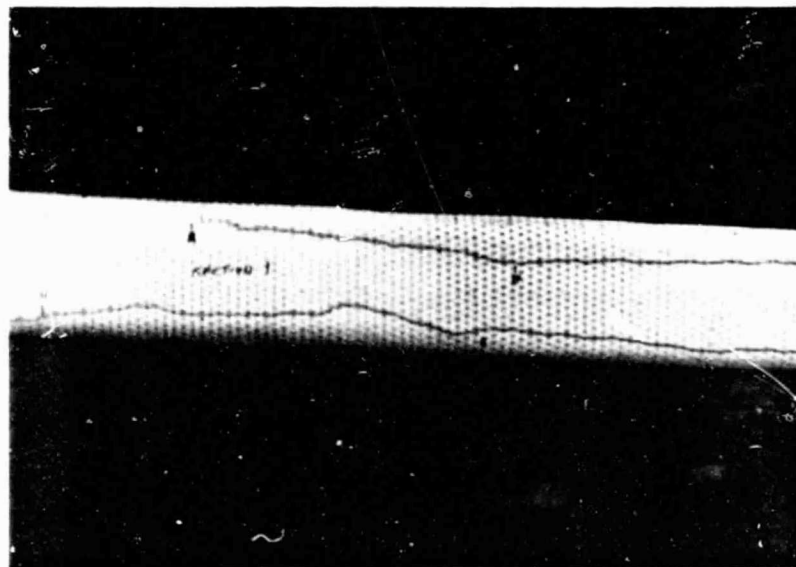
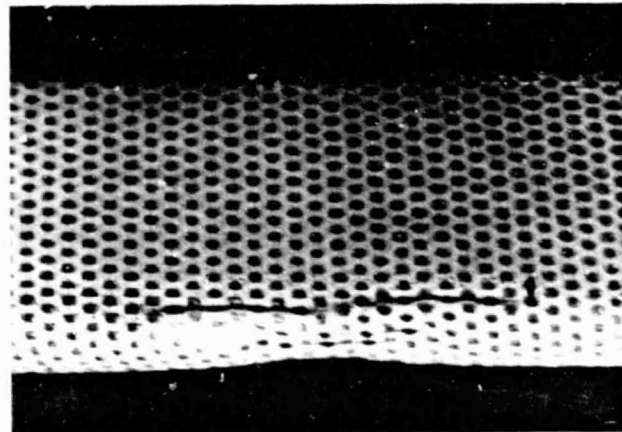


Figure 2-17. Drive rate effects summary.

apex against the outer forming rollers. This effect could be avoided by controlling the accelerations of the strip.

At speeds from 17.8 cm/sec to 30.5 cm/sec (7.0 in./sec to 12.0 in./sec) the edges of the cap developed very severe ripples. This is believed to be the result of softening of the edges combined with drag created by the edge guides.

This one brief test indicated that careful attention will be required in the design of forming section heaters for the beam builder cap forming modules to achieve uniform heating. This basic forming process is compatible with drive speeds required for near term beam builders and can be adapted to higher drive speeds through further development.

3

ULTRASONIC WELDING TECHNOLOGY

Ultrasonic welding of composite materials has been developed extensively in the environment of air and gravity. Prior to final selection of this method for joining structural members together in the environment of space, experiments to investigate the effects of gravity and vacuum on the composite material and welding apparatus were required. This section describes the procedures, hardware, and results of these experiments.

3.1 WELDING TASK OBJECTIVES AND APPROACH

The objectives of the ultrasonic welding task were to investigate and evaluate the following:

- a. Solidification of ultrasonic welds by investigating weld heat buildup and dissipation during the welding operation in a thermal-vacuum simulation.
- b. Ultrasonic weld flow in a zero-g environment by determining the effect of gravity on the molten weld.

Investigation of the effects of gravity and vacuum on the ultrasonic welding process was conducted by instrumenting an off-the-shelf Branson Sonic Power Co. Model 4120 ultrasonic welder to operate in a vacuum chamber and in three different angles to gravity. The experimental procedure, illustrated in block diagram form in Figure 3-1, was developed to identify any vacuum, gravitational, or combined effects on the welder, material, or final weld strength.

3.2 WELD TEST INSTRUMENTATION

The instrumentation setup, illustrated in Figure 3-2, allowed for control and monitoring of the welder from outside the vacuum chamber. Figure 3-3 shows the actual setup and identifies the major monitoring devices.

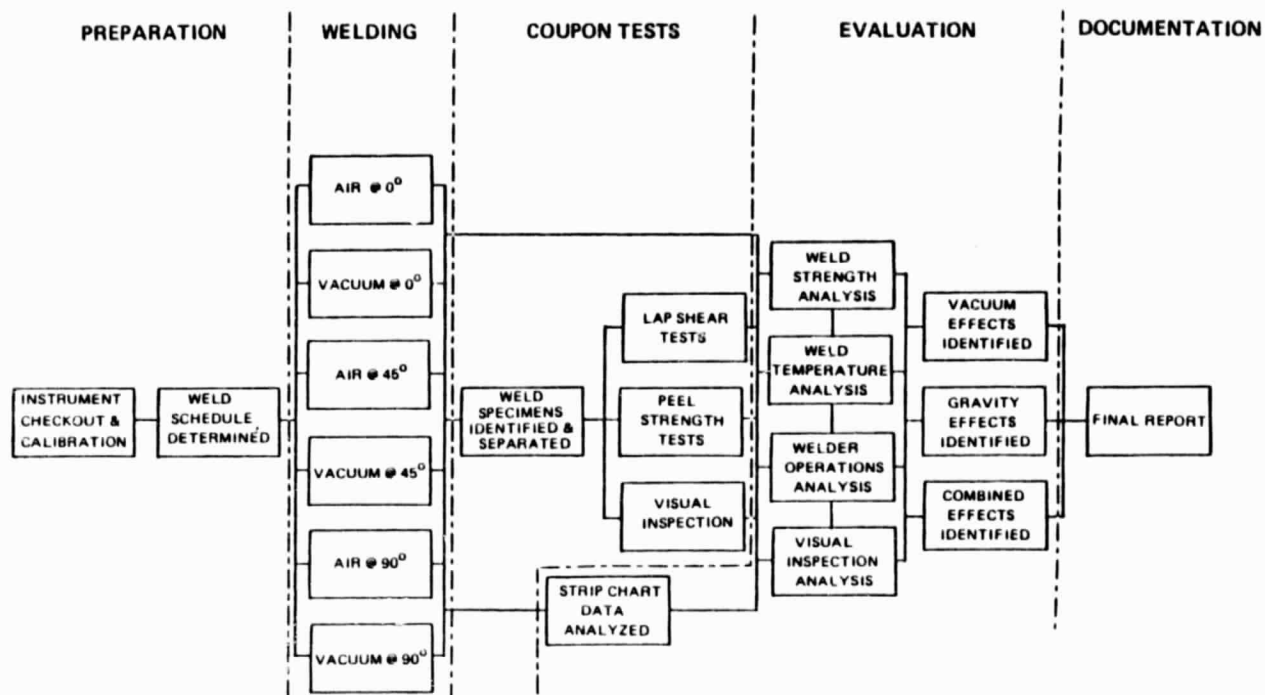


Figure 3-1. Welding task approach.

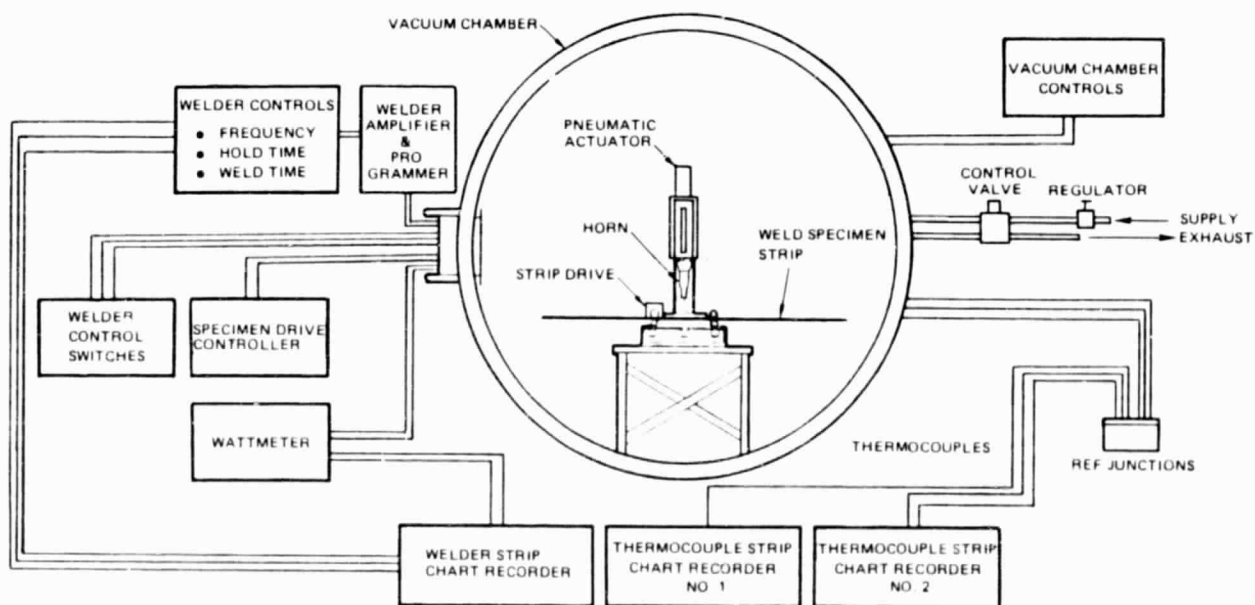


Figure 3-2. Welder instrumentation and controls diagram.



Figure 3-3. Welding test instrumentation and controls.

3.2.1 WELDER CONTROLS. For consistent weld schedules, the weld time, hold time, weld pressure, and frequency must be accurately controlled. Timing control of the welder was accomplished by using a special controller, designed and built by Convair to control weld time and hold time to an accuracy of ± 0.02 seconds.

Weld pressure was controlled by setting a pneumatic regulator located outside the chamber to supply a predetermined air pressure to the welder pneumatic actuator. Air pressure to the actuator and exhaust from the actuator was conducted by tubing through a solenoid control valve outside the chamber. The pneumatic actuator and tubing were carefully leak-tested with helium prior to conducting vacuum testing. Weld frequency was monitored by a digital counter with a readout capability of 10 times per second. Weld frequency readout was displayed and recorded 0.5 second into the weld time. This point in the weld cycle was selected because it is the time at which power is at a maximum for a normal weld.

The weld stack, shown in Figure 3-4, is designed to oscillate at 20,000 Hz. However, this natural frequency will decrease as the stack heats and expands during operation. Therefore, retuning of the amplifier to produce the optimum frequency for best efficiency is occasionally required. The optimum frequency is determined by finding the frequency with the lowest resistance or lowest power required to oscillate the welder stack.

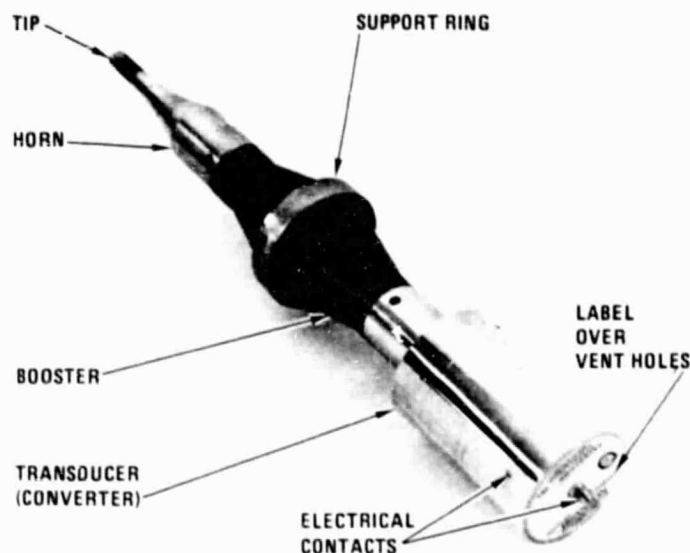


Figure 3-4. Ultrasonic weld head stack.

The wattmeter shows an obvious drop in power at this natural frequency. Tuning is conducted without a load on the stack (horn not touching anything). During welding operations the weld stack will shorten due to pressure and the sound waves will travel slightly faster over a shorter distance. Therefore the natural frequency during welding will increase about 1% or to about 20,200 Hz. This retuning requirement would not be required after the first 30 welds or when the temperature stabilizes. Automatic tuning devices have been designed by welder manufacturers which retune the welder in-process, insuring optimum frequency for all welds regardless of welder stack temperature fluctuations.

3.2.2 WELD SPECIMEN DRIVE SYSTEM. To allow a series of welds to be performed inside the vacuum chamber, two 122 cm x 6.35 cm strips of GR/T₂ composite material were joined together as shown in Figure 3-5 with a 2.54 cm overlap. The strips were incrementally moved under the weld head by a remotely controlled, variable speed, reversible motor drive system. A wire cord was attached to both ends of the weld specimen strip and drawn around pulleys at both ends of a support beam. The "L" shaped support beam with drive motor and pulleys attached, was bolted to the base of the welder as shown in Figure 3-6. Teflon guide blocks were attached to the welder base to provide specimen alignment and reduce drag for best incrementing accuracy.

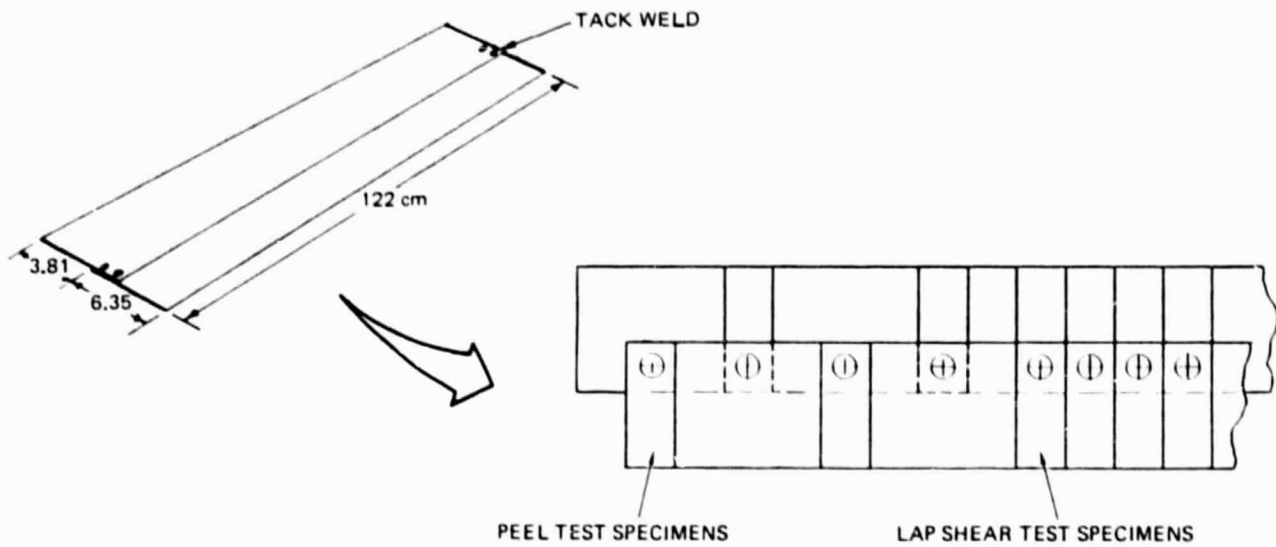


Figure 3-5. GR/TP weld test strip configuration.

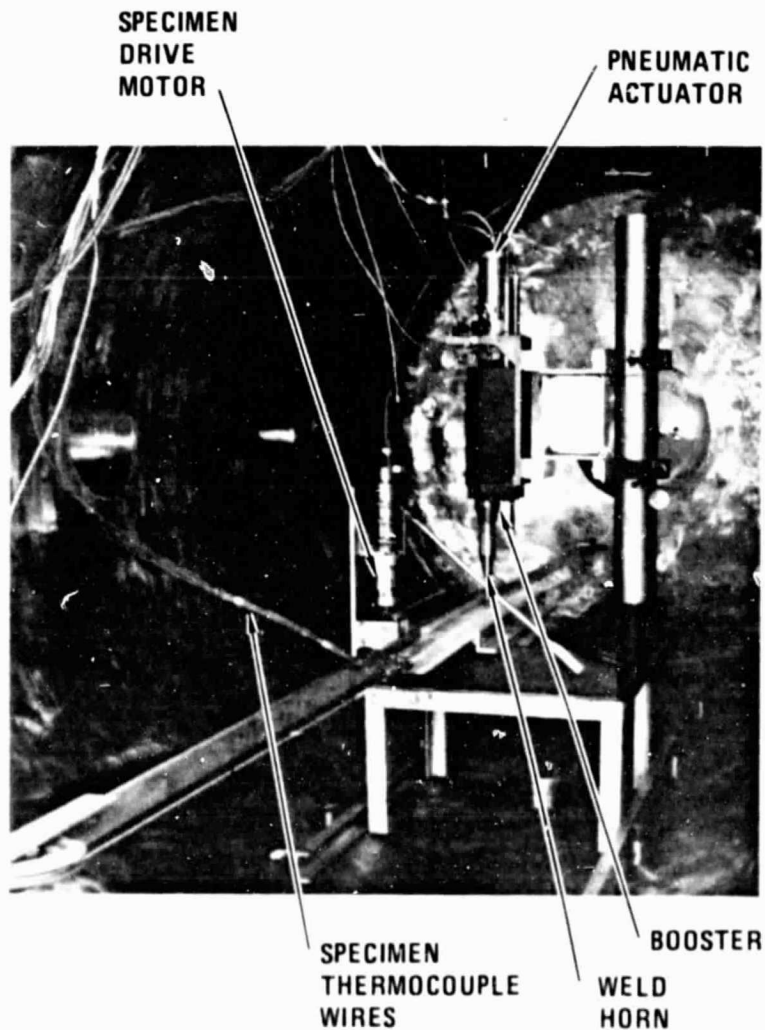


Figure 3-6. Vacuum chamber 0° setup.

3.2.3 DATA RECORDING. Two 8-channel rapid-read strip chart recorders were used to monitor the operation of the welder, temperature of the weld stack, and temperature of specimens for heat flow tests. These recorders were run at speeds of 10 cm/sec during weld tests and 0.5 cm/sec during the 80-second delay between welds. The high speed allowed detailed characteristics of the power curve, weld time, hold time, and temperature increases to be recorded during the 0.7 sec weld cycle. The low speed allowed continuous reading of temperature changes between welds on a minimum amount of strip chart paper.

Each recorder was equipped with eight recording channels. The welder performance and temperature recorder monitored weld power, horn down time, weld time, and temperatures of the converter (piezoelectric transducer), booster, horn mid-point (area of maximum strain), and weld tip.

The other recorder was used for temperature sensing eight places on the welded specimens to determine heat flow characteristics.

3.3 WELD SCHEDULE DETERMINATION

Previous weld tests conducted using the GR/TP composite material welded with a 1.27 cm diameter knurled tip have shown that the weld strength is directly related to energy (Joules) input to the weld (assuming uniform material).

These tests have shown that the weld strength obtainable from any given weldable material will reach a peak as a function of energy input. As more energy is input to the bond area, degradation of the material eventually begins to weaken the weld. For the GR/TP composite material used in this program, the peak weld strength will occur within a range of energy between 310 J/cm^2 and 496 J/cm^2 of weld area. For the series of welds performed, it was assumed that the identification of a relatively minor weld strength degradation caused by gravity direction or vacuum around the weld area might not be apparent if a peak strength weld schedule were used. Consequently the weld schedule selected was approximately 155 J/cm^2 so that small deviations in welder efficiency, resin flow, material uniformity, temperature flow, etc. would cause an easily identified change in weld strength. Effects of vacuum and gravity on the welding process would also be more likely to be identified.

Weld testing was performed with a 1.27 cm (1/2 in.) diameter coarse knurled tip (total surface area approximately 2.53 cm^2 (0.393 in.^2)) attached to an ultrasonic weld horn with a gain of 6.6. Total tip motion with a 1:1 gain booster is $6.6 (0.00191) = 0.01257 \text{ cm}$ (0.00495 in.).

The weld schedule used for all weld tests specimens was as follows

- a. Weld Time: 0.7 seconds
- b. Hold Time: 1.0 seconds
- c. Pneumatic Pressure: 27.6 N/cm^2 (40 psig)

3.4 ULTRASONIC WELDING TESTS

3.4.1 PRELIMINARY CHECKOUT. Following the checkout and calibration of all instruments, a preliminary test of the total system was conducted. A 20-weld test specimen was welded with all instruments operational, the welder oriented in the 0-degree configuration (Figure 3-6) and at normal atmospheric pressures. The total welder, with its amplifiers and programming module, was inside the chamber. All welds were successfully accomplished.

The chamber was then pumped down to a pressure of $2.8 \times 10^{-3} \text{ N/M}^2$ (2.1×10^{-5} Torr). Attempts to weld at this pressure were unsuccessful. This failure to weld in vacuum initiated a "trouble shooting" procedure and attempts to isolate the welder components affected by operation in vacuum.

The initial attempt to weld in vacuum showed: there was erratic and generally very low power to the transducer; the weld and hold time were altered and inconsistent; and the frequency being generated was erratic, there was no weld or melt in the composite material because of these factors. Actions and results of the investigation are summarized below:

- a. Trouble shooting of the electronics and actuator were inconclusive.
- b. Factory checkout and repair of the amplifiers and programmer, and replacement of the transducer had no effect.
- c. Removal of amplifiers from the vacuum chamber was not successful due to wiring problems between the amplifiers and the programmer inside the chamber.
- d. Removal of all electronics from the chamber resulted in normal weld and hold times and frequency (tuning), but welding was intermittent.
- e. Removal of an aluminum label over the top of the transducer to insure proper venting of internal air pressure during pump down resulted in normal welder operation in vacuum.

From the preceding actions, it was concluded that when the chamber was pumped down, some of the electronic components in the amplifiers, programming module, and

transducer malfunctioned, probably due to internal corona effects causing electrical short circuiting. Air pressure inside the converter was probably lowered into the corona region of approximately 10^{-1} to 10^{-3} Torr. The problem was overcome by insuring proper venting of the transducer (see Figure 3-4) to allow air to escape during pump down of the chamber.

3.4.2 WELD SPECIMEN CONFIGURATION AND IDENTIFICATION. The weld test specimens required for the test series are summarized in Table 3-1. The weld strips were designed to accommodate 35 to 38 weld specimens of the number and type indicated in Table 3-1. The technique used to obtain lap shear and peel test specimens is shown in Figure 3-5. Thermocouples were installed near the weld strip temperature specimens. Identification of each weld specimen was accomplished by applying a mylar tape along the upper edge of the strip, marked off in one inch increments. These were marked to indicate weld number, weld condition (Air or Vacuum), and weld orientation to gravity (0° , 45° , or 90°). This identification method also insured that each weld could be correlated to the strip chart data.

Table 3-1. Weld test specimen requirements.

Usage	Air			Vacuum		
	0°	45°	90°	0°	45°	90°
Preliminary	20	5	5	5	5	5
Lap Shear	40	25	25	25	25	25
Peel	5	5	5	5	5	5
Visual Insp.	5	5	5	5	5	5
Temperature	3			3		
Total	58	35	35	35	35	35

3.4.2.1 Weld Strip Preparation. Each weld strip was baked at 533K (500F) for 3 hours then vacuum bagged and baked for 18 hours at 389K (350F) to remove moisture and volatiles which can effect weld strength and vacuum chamber pressures. These were then compacted and aluminum/mylar bagged to prevent moisture absorption.

3.4.3 VACUUM & GRAVITY EFFECTS TESTS. The vacuum and gravity effects welding tests were conducted in the sequence shown in Table 3-2.

Vacuum pressures ranged from 4.8×10^{-3} N/m² (3.6×10^{-5} Torr) maximum to 1.07×10^{-3} N/m² (0.8×10^{-5} Torr). A separate test strip was installed for each run.

Table 3-2. Weld test sequence.

Run No.	Environment	Welder Orientation	Ref. Figure No.
1	Air	0°	3-6
2	Vacuum	0°	3-6
3	Air	90°	3-8
4	Vacuum	90°	3-8
5	Air	45°	3-7
6	Vacuum	45°	3-7

No changes were made in weld schedule and no adjustments made to the welding apparatus except for periodic tuning of the weld stack.

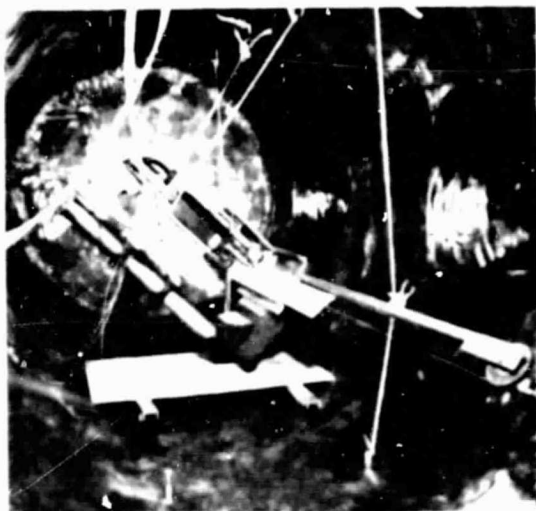


Figure 3-7. Vacuum chamber 45° setup

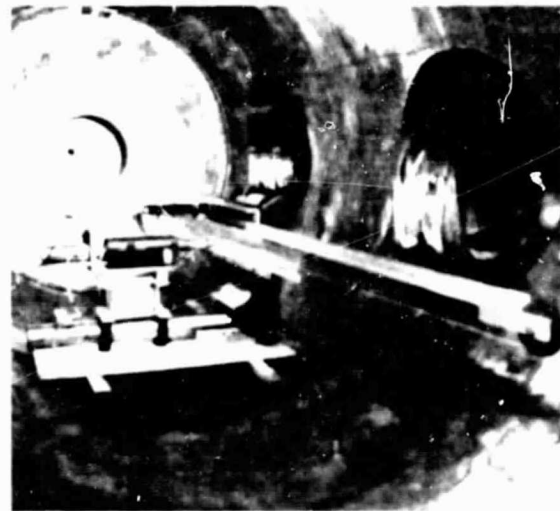


Figure 3-8. Vacuum chamber 90° setup

3.5 WELDING TEST RESULTS

Upon completion of each weld test the weld strip was removed from the drive mechanism and the individual welds were separated into test groups as shown in Table 3-1 and Figure 3-5, and bagged according to the evaluations required for each set of welds: lap shear tests (25 welds), peel strength (5 welds), visual inspections (5 welds), or temperature flow specimens (3 welds each for Air and Vacuum at 0°). The tests performed on these coupons are summarized in Figure 3-9. The results of these tests are described below.

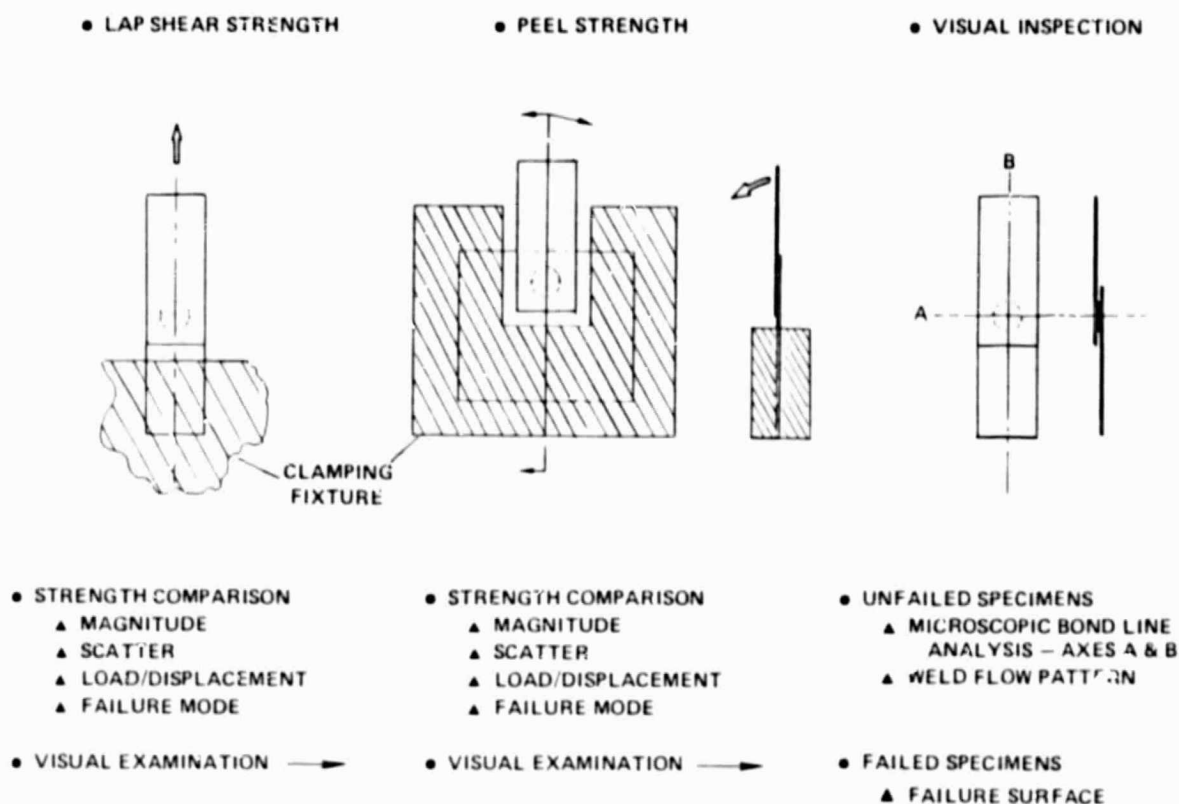


Figure 3-9. Specimen coupon tests.

3.5.1 LAP SHEAR STRENGTH ANALYSIS. Table 3-3 summarizes the lap shear and peel test data presented in detail in Tables 3-4 through 3-9. Air and vacuum welds made at 90-degrees were notably lowest in strength and had the lowest ratio of success; i.e., 8 out of 25 in air and 16 out of 25 in vacuum. A possible explanation for the lower weld strength at the 90-degree angle is that the motion of the weld tip is 90-degrees to the force of gravity. Since the horn is slender and tapered from 6.35 cm at the top to 1.27 cm at the weld tip, some of the weld energy may be converted into transverse motion due to cantilevered vibration of the horn. This condition is a gravity effect on weld strength which would not exist in a zero-g earth orbit environment.

Table 3-3. Summary of lap shear and peel tests.

Welder Angle	In-Air						In-Vacuum					
	Lap Shear			Peel			Lap Shear			Peel		
	n	(N)		n	(N)		n	(N)		n	(N)	
		P _L	±σ		P _p	±σ		P _L	±σ		P _p	±σ
0°	25	814.0	333.6	3	24.9	17.3	18	582.7	213.5	0	0	—
45°	24	619.4	155.7	5	20.0	10.2	25	796.2	253.5	5	16.0	8.5
90°	8	431.5	155.7	0	0	—	16	471.5	124.6	4	8.9	7.1

In earth gravity environment, this whipping condition can be compensated for simply by increasing weld pressure and/or time. This tendency of the weld horn to whip would be less pronounced using a horn of greater cross section such as that designed for the truss welder.

3.5.2 WELD VISUAL EXAMINATIONS. All weld specimens were examined for resin flow, resin melt, and general appearance differences which might result from welding in vacuum or from gravitational effects. There was no difference in tip penetration or flow on the surface of the welds which could be related to the gravitational or ambient conditions under which the weld was made. Flow of thermoplastic in the faying surfaces was very similar with the only variations resulting from material resin content and thickness as noted in Tables 3-4 through 3-9.

Table 3-4. 0° in-air weld specimens.

Specimen No.	Energy (J)	Type Specimen	Strength (lb)	Frequency Hz	Remarks
A-0-1	230	Lap	77	20130	Low power - slight melt
2	280		208	20157	Irregular power - poor joint
3	300		290	20274	Resin rich - good joint
4	345		260	-	Resin rich - good joint
5	350		272	20253	Resin rich - good joint
6	215		34	20307	Low power - no weld
7	345		199	20233	Poor joint
8	355		182	20233	Poor joint - no fibers
9	340		238	20235	Poor joint
10	305		127	20227	Poor joint - no fibers
11	340		158	20237	" " " "
12	335		107	20273	" " " "
13	315		175	20250	" " " "
14	225		114	20098	Poor joint: Rough surface-irregular power
15	240		235	20173	Power dipped - poor joint, no fibers, rough & thick
16	225		303	20300	Good joint
17	335		225	20283	Good joint
18	200		68	20385	Low power - no weld
19	340		172	20299	Poor joint
20	335		165	20193	Poor joint
21	310		166	20170	Poor joint - no fibers
22	240		86	20139	Low power - no weld, rough & thick
23	260		167	20105	Power dipped - poor joint
24	350		303	20276	Good joint
25	335	Lap	235	20235	Good joint
A-0-26	—	Visual	N/A	20339	Power dipped
27	—			20277	
28	—			20271	
29	—			20217	
30	—	Visual	N/A	20303	Irregular power
A	340			20329	
B	345	Peel	5.7	20282	
C	340		9.5	20307	
D	335		1.6	20294	
E	245	Peel	0	20287	

Table 3-5. 0° in-vacuum weld specimens.

Specimen No.	Energy (J)	Type Specimen	Strength (lb)	Frequency Hz	Remarks
V-0-1	245	Lap 	0	20378	No weld - some melt - dark/burned material
2	240		0	20337	No weld - no melt - dark/burned material
3	265		0	20378	No weld - no melt - dark/burned material
4	260		69	20319	Poor weld
5	225		52	20114	Irregular power - poor weld - rough material
6	270		174	20238	Irregular power - rough material - good joint
7	250		163	20244	Good joint
8	245		140	20298	Partial weld - resin poor
9	130		0	20469	No weld - retune required
10	310		159	20323	Good joint
11	340	Lap 	72	20362	Resin poor - burned/dark material
12	310		88	20297	Poor weld - irregular power
13	305		98	20216	Poor weld - rough material
14	300		0	20194	No weld - irregular power - rough material
15	115		0	21839	No weld - irregular power & frequency - rough material
16	310		171	20283	Good joint - rough material - irregular power
17	85		0	29492	No weld - negative power reading
18	275		159	20333	Rough material - good joint
19	360		178	20318	Good joint
20	280		123	20329	Irregular power - rough material
21	275	Lap 	120	20371	Burned dark material - resin poor
22	315		154	20339	Good joint
23	310		219	20406	Good joint - resin rich
24	300		155	20333	Resin poor
25	145		62	0	Very low power - partial weld
V-0-26	—	Visual	N/A	20368	Irregular power Irregular power
27	—			20219	
28	—			20235	
29	—			20351	
30	—	Visual	N/A	20257	Irregular power Low power - programmer malfunctioned - short weld Irregular power Low power at end of cycle " " " " " "
A	290	Peel	0	20247	
B	200			20309	
C	265			20292	
D	270			20224	
E	260	Peel	0	20270	

Table 3-6. 45° in-air weld specimens.

Specimen No.	Energy (J)	Type Specimen	Strength (lb)	Frequency Hz	Remarks
A-45-1	225	Lap	114	20247	Resin poor
2	195		126	20259	" "
3	215		178	20306	Irregular power - resin poor - good joint
4	225		146	20267	Good joint
5	230		155	20226	" "
6	90		0	20208	No weld - rough material - low power
7	140		95	20439	Poor joint - rough material - low power
8	300		221	20266	Good joint
9	295		185	20315	Good joint
10	290		157	20254	Resin poor
11	295		149	20270	Resin poor
12	275		137	20274	Irregular material
13	280		129	20294	Resin poor
14	270		174	20277	Good joint
15	280		144	20409	" "
16	270		164	20265	Good joint
17	275		155	20223	" "
18	260		127	20210	Irregular power - rough material
19	295		227	20216	Good joint - rough material - irregular power
20	280		147	20261	Good joint
21	280		93	20325	Resin poor
22	280		92	20261	Resin poor
23	270		116	20257	Resin poor
24	280		113	20306	Resin poor
25	280	Lap	155	20299	Good joint
A-45-26	—	Visual	N/A	20265	
27	—			20257	
28	—			20238	
29	—			20253	
30	—	Visual	N/A	20266	
A	300	Peel	5.2	20219	
B	285		6.7	20261	
C	270		2.5	20271	
D	275		3.7	20111	
E	275	Peel	2.3	20293	

Table 3-7. 45° in-vacuum weld specimens.

Specimen No.	Energy (J)	Type Specimen	Strength (lb)	Frequency Hz	Remarks
V-45-1	205	LAP	100	20235	Resin poor
2	205		130	20258	" "
3	220		183	20233	" "
4	225		173	20229	Good joint
5	220		118	20234	Resin poor
6	245		149	20357	
7	245		200	20208	Good joint
8	220		157	20212	Rough material - irregular power
9	260		186	20199	Good joint
10	270		212	20284	" "
11	265		184	20253	Rough material
12	285		164	20271	Rough material
13	275		141	20281	
14	115		30	14889	Low power - low frequency - converter malfunction
15	280		261	20346	Good weld joint
16	285		239	20413	" " "
17	230		325	20225	Irregular power curve - rough material
18	245		183	20280	" " " " " "
19	280		236	20287	Rough material
20	280		157	20241	Rough material
21	270		157	20238	Good weld bond separation
22	290		197	20338	
23	290		206	20264	Good weld bond separation
24	285		190	20255	Good weld
25	295	Lap	205	20249	" "
V-45-26	—	Visual	N A	20336	
27	—			20246	
28	—			20291	
29	—			20190	Irregular power
30	—	Visual	N A	20240	
A	300	Peel	5.3	20239	
B	310		3.0	20270	
C	315		5.8	20291	
D	290		2.7	20237	
E	290	Peel	1.3	20258	Erratic power

Table 3-8. 90° in-air weld specimens.

Specimen No.	Energy (J)	Type Specimen	Strength (lb)	Frequency Hz	Remarks
A-90-1	310	Lap	0	20300	Material burned/brown both surfaces <u>all welds</u>
2	285			20282	
3	150			20316	Material rough & burned - low power
4	225			20285	Irregular power - rough material
5	200			20072	" " " "
6	170			20143	Irregular power - rough material - low power
7	170			20140	Irregular power - " " " "
8	245		0	20237	" " " " " "
9	290		78	20276	Rough material - irregular power
10	275		111	20268	" " " "
11	295		30	20327	Smooth but very dark surface
12	305		0	20363	
13	305			20286	
14	305			20300	
15	245			20253	Irregular power - rough material
16	240			20178	Irregular power - rough material
17	250			20186	" " " "
18	215			20223	" " " "
19	225		0	20323	" " " "
20	275		116	20314	Rough material
21	135		0	20434	Low power - irregular power - rough material
22	310		112	20340	Resin poor
23	315		121	20368	
24	290		137	20334	
25	295	Lap	73	20297	
A-90-26	—	Visual	N A	20362	
27	—			20320	
28	—			20320	
29	—			20232	Irregular power
30	—	Visual	N A	20248	" " "
A	285	Peel	0	20316	
B	290			20354	
C	300			20564	
D	280			20346	
E	275	Peel	0	20288	

Table 3-9. 90° in-vacuum weld specimens.

Specimen No.	Energy (J)	Type Specimen	Strength (lb)	Frequency Hz	Remarks
V-90-1	280	Lap	0	20358	Lower surface burned brown-rough material
2	265			20288	
3	245			20293	No melt
4	250			20380	
5	235			20247	Converter - negative power - re-welded
6	225			—	Irregular power curve - rough surface
7	225		0	20169	Irregular power - rough surface
8	235		121	20150	Irregular power - rough material
9	225		117	20259	" " " "
10	275		173	20329	
11	285		106	—	Converter failure - re-weld retune
12	280		99	20051	Normal weld spot
13	275		78	20266	
14	270		118	20324	Resin poor
15	270		0	20267	
16	295		97	20268	Rough surface - normal power
17	290		95	20170	Irregular power - rough surface
18	285		110	20226	Rough surface
19	215		90	20233	Irregular power - rough surface
20	215		82	20240	
21	235		106	20224	
22	230		129	20180	Resin poor
23	245		44	20209	Resin poor
24	250		134	20203	
25	125	Lap	0	20265	Low power - programmer malfunction (0.6 sec weld)
V-90-26	N/A	Visual	N/A	20255	
27				20276	
28				20180	
29				20161	
30	N/A	Visual	N/A	20126	Irregular Power
A	280	Peel	0	20178	
B	260		0.8	20163	
C	275		2.0	20229	
D	265		3.8	20178	
E	275	Peel	6.5	20261	

3.5.3 WELD HEAD TEMPERATURE CHARACTERISTICS. Thermocouples attached to the weld head during the welding experiments were continually monitored to determine the effects of additional strain in the welder due to direction of gravity or lack or presence of air to conduct heat away from the weld head. Figure 3-10 illustrates the weld head thermocouple locations. Table 3-10 shows the maximum change in temperatures from start of weld sequence to completion of the last test weld using the prescribed weld schedule with 80-second intervals between welds. Weld tip operating temperature data was lost during test due to separation of the thermocouple and fractional heating interaction between the thermocouple and the weld tip. It is assumed that the weld tip temperatures after 80 seconds of cooling approached the temperature of the horn. The maximum temperature changes occurred in the horn in vacuum. This change was not significant; however, the total welding time was not long enough to allow the weld horn to reach an equilibrium temperature.

• THERMOCOUPLE LOCATIONS

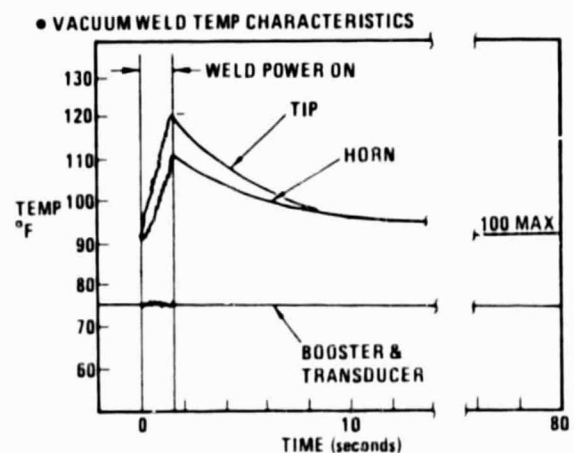
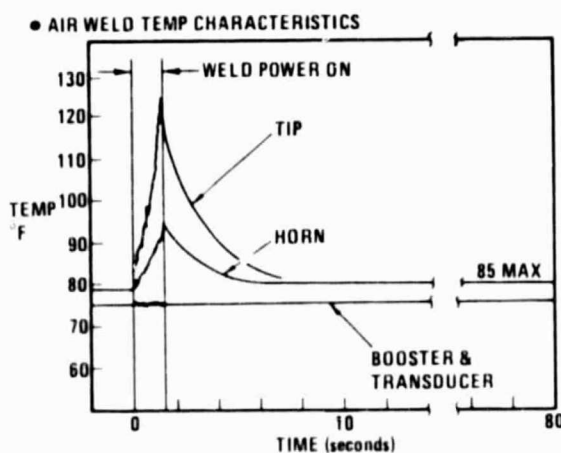
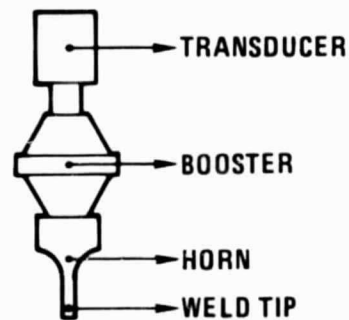


Figure 3-10. Weld head temperature characteristics in air and in vacuum.

Table 3-10. Weld head heating effects.

Angle	Environment	$\Delta T^*(^{\circ}F)$			
		Tip**	Horn	Bstr	Trans
0°	Air	-	3	3	3
45°		-	2	2	2
90°		-	9	1	1
0°	Vacuum	-	21	6	4
45°		-	14	4	5
90°		-	23	9	8

*Rise in preweld temp in ~50 min (35 weld cycles)

**Tip thermocouple separated

Figure 3-10 illustrates the maximum temperature change characteristics of each weld head component during weld cycles in air and in vacuum. There were no more than a few degrees increase in booster or transducer temperatures, regardless of weld direction or atmosphere. In air, the horn temperature increased approximately 35°F during weld, but returned to near ambient within 10 seconds. In-vacuum temperature changes were similar to air welds but with slower decay rates apparently due to the lack of convective cooling. In both air and vacuum welds, the maximum change in temperature occurred at the 90-degree weld direction, which suggests increased heating due to bending strain in the horn.

3.5.4 WELD SPECIMEN TEMPERATURE EFFECTS. Figure 3-11 illustrates the thermocouple locations and material fiber orientation on the weld strips for the 0-degree air and vacuum tests. Figure 3-12 shows the temperature changes that occurred at the thermocouples 7 and 10 in air and in vacuum. Temperature recording began two welds prior to the T1 weld.

Results of these tests showed only minor heating external to the weld area in the direction of the glass fibers. The peak temperatures at thermocouples 6, 9, and 12 (nearest the weld) showed an increase of 10 to 20°F. Average temperatures at 5, 6, 8, 9, 11, and 12 during the welding of T1, T2 and T3 were 83°F in air and 105°F in vacuum.

Figure 3-12 shows how the maximum peak temperatures occurred along the graphite direction nearest the weld. The differences in peak temperatures between TC7 and TC10 are attributable to inaccuracy in positioning the strip under the weld tip. Examination of the weld specimens indicated the welds made closest to a thermocouple corresponded with the maximum peak temperatures for that thermocouple.

• WELD STRIP & THERMOCOUPLES

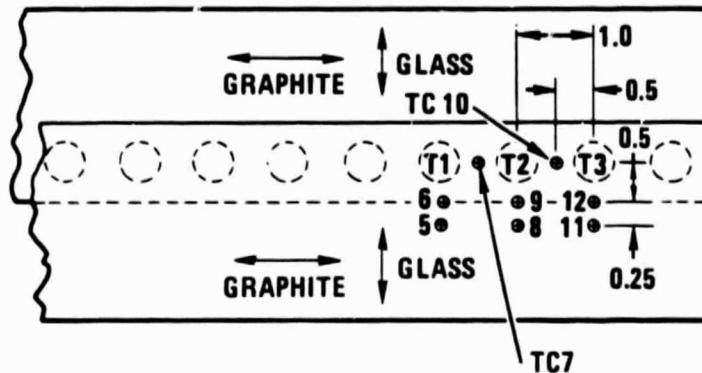


Figure 3-11. Thermocouple locations for air and vacuum temperature flow tests.

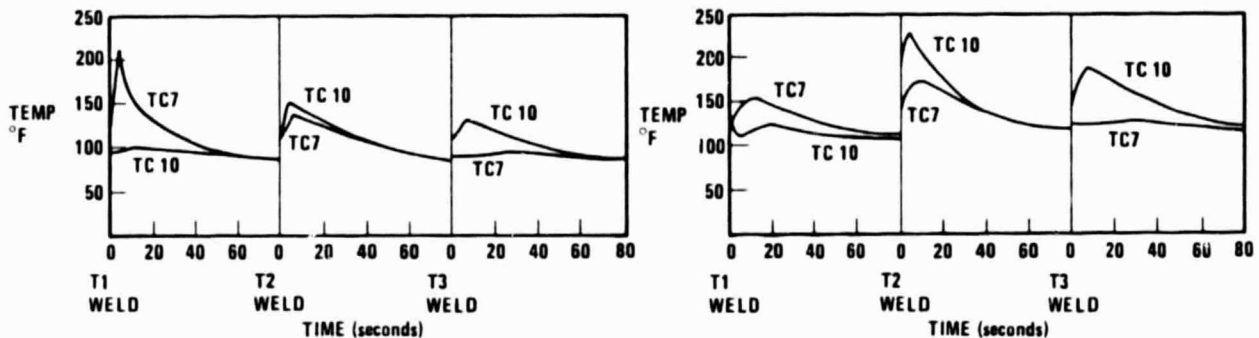


Figure 3-12. Weld specimen heat flow characteristics in air and in vacuum.

3.5.5 POWER CURVE ANALYSIS. During preliminary air weld tests it was found that two distinct power curves were being generated. On further analysis of the material it was determined that the power curve profiles were a result of the GR/TP surface roughness on the faying surfaces. Figures 3-13 and 3-14 illustrate these two power curves. Figure 3-13 shows a typical power curve for GR/TP with smooth faying surfaces. Figure 3-14 illustrates the power curve caused by rough faying surfaces.

The total area under these curves is similar, indicating nearly equal energy - Joules input to each weld. Weld strength is also similar as would be expected with equal energy input with equal time and pressure.

A third power curve, shown in Figure 3-15, was also created when welder efficiency was affected by gravity or variations in material thickness and resin content. In each case, where this type of power curve was created, the resulting weld strength was significantly reduced. Monitoring the power curve during the weld can thus be a major in-process method of weld quality verification. Weld

energy can be electronically monitored and controlled to insure optimum weld quality.

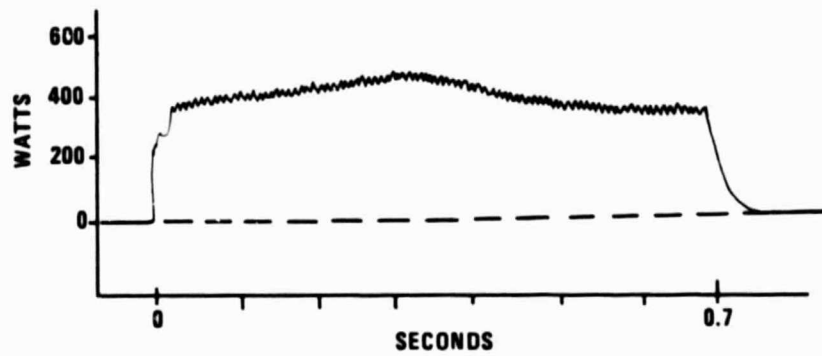


Figure 3-13. Smooth surface power curve.

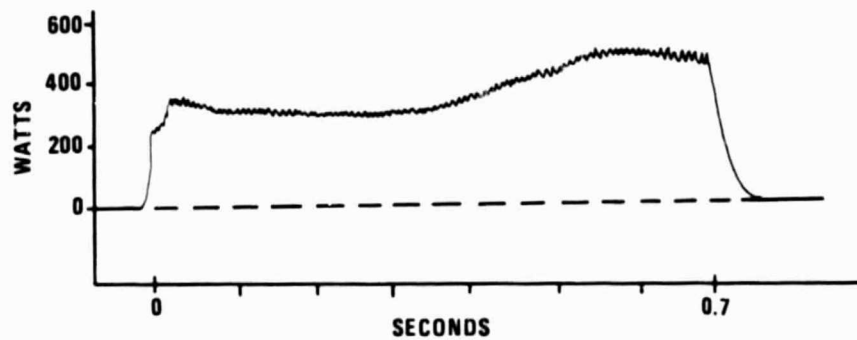


Figure 3-14. Rough surface power curve.

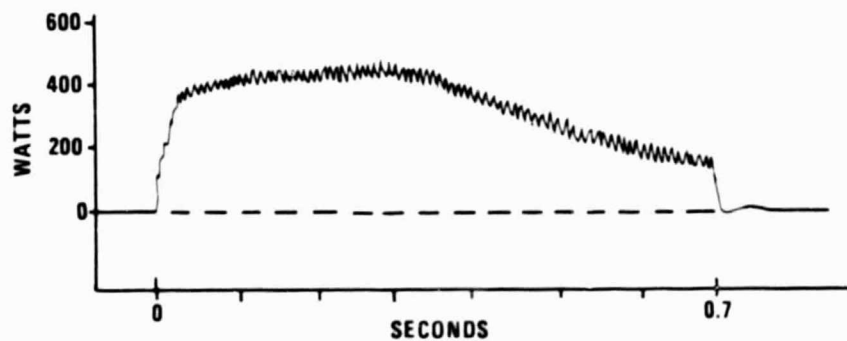


Figure 3-15. Low weld strength power curve.

4

PROTOTYPE TRUSS SEGMENT

The requirement to fabricate, test, and evaluate a three-bay prototype triangular truss segment which conformed to the design developed for the SCAFEDS (Reference 1), comprised three major tasks: (1) truss fabrication for the manufacture of the Prototype Test Truss (PTS); (2) truss test preparation and support to prepare test plans, install strain gages and load introduction fittings, and provide technical support to NASA/JSC during test; and (3) local effects analyses and tests to characterize cap crippling, buckling, and torsional instability effects for comparison with PTS test results as a means of determining end fixity of the PTS as tested. This section presents the results of these three activities and includes a report of the test results achieved by JSC.

4.1 PTS FABRICATION

The PTS configuration is shown in Figure 4-1. The materials, tooling, and manufacturing techniques used to fabricate the PTS are described in the following paragraphs.

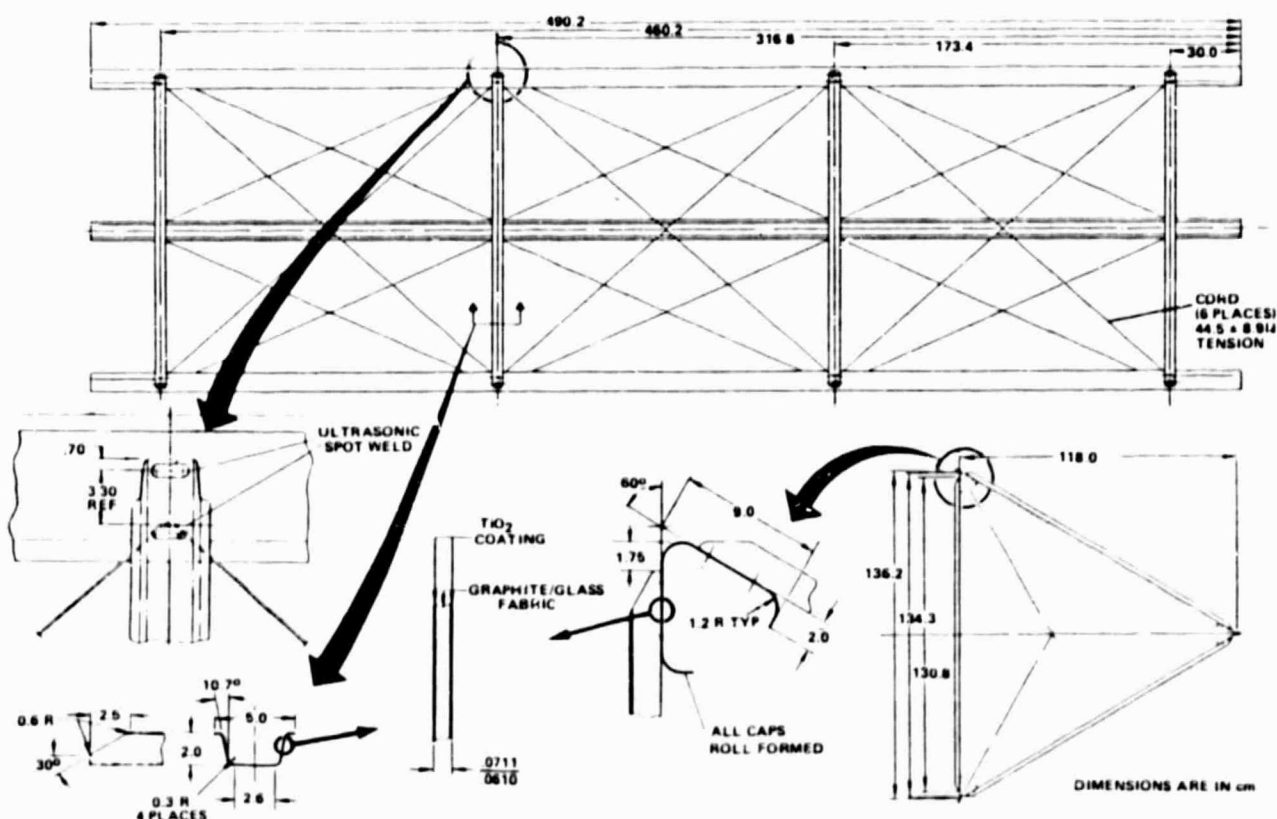


Figure 4-1. Prototype truss segment configuration.

4.1.1 PTS STRUCTURAL MEMBERS. The cap members for the PTS were manufactured from graphite/glass/polysulfone, single-ply woven composite material described in Subsection 5.1. All three caps were automatically roll-formed from flat preprocessed composite strips using the roll forming machine which had been modified as described in Subsection 2.1.1.

The crossmembers were manufactured from the same composite material as the caps. Each crossmember was individually formed using a die form tool as described in Subsection 4.1.2. This is in keeping with the SCAFEDS beam builder design, which uses preformed crossmembers.

The diagonal cord material is a 20-end S-glass roving impregnated with P-1700 polysulfone resin and manufactured by U. S. Polymeric. The cord, as received, was in a flat ribbon-like form partially consolidated with the polysulfone. The cord was consolidated to a more circular cross section to improve its strength properties by immersing it in a polysulfone and solvent bath and pulling it through a circular die. The finished cord is characterized as follows:

- a. Area of cross section: $4.56 \times 10^{-3} \text{ cm}^2$ ($7.07 \times 10^{-4} \text{ in}^2$)
- b. Tensile strength: $1.56 \times 10^5 \text{ N/cm}^2$ ($2.26 \times 10^5 \text{ psi}$)
- c. Modulus of elasticity: $4.55 \times 10^6 \text{ N/cm}^2$ ($6.6 \times 10^6 \text{ psi}$)

4.1.2 PTS TOOLS & FIXTURES. To assure dimensional accuracy and minimize assembly time for the PTS, a rigid welding and assembly fixture was designed and built. The fixture, shown in Figure 4-2, consisted of a steel pipe with twelve arms attached. Each arm supported an aluminum anvil shaped to fit the internal geometry of the caps. The fixture was supported on each end by tooling stands. The pipe rested on steel rollers attached to the end stands. This allowed the entire fixture to be rotated to facilitate truss assembly.

The crossmember forming tool shown in Figure 4-3 consisted of two matching dies. Each crossmember was formed by placing a strip of coated and consolidated composite material between the dies, as shown, using guide pins to center the strip and upper die. When placed in an oven and heated to 232°C (450°F), the weight of the upper die formed the softened strip. The dies were then placed on a hot press to compact the formed member to the proper thickness. The tool was then cooled under pressure, removed from the press, and the formed crossmember cut to width using the upper die as a guide. The crossmember was removed from the dies and the ends were trimmed to length and shape, using a trim tool made from pieces of the forming dies. The welder pierce-pin location holes were then pre-drilled in each crossmember using a locating template. Fiberglass cloth inserts were bonded to the work surface of each crossmember at each spotweld location with polysulfone.

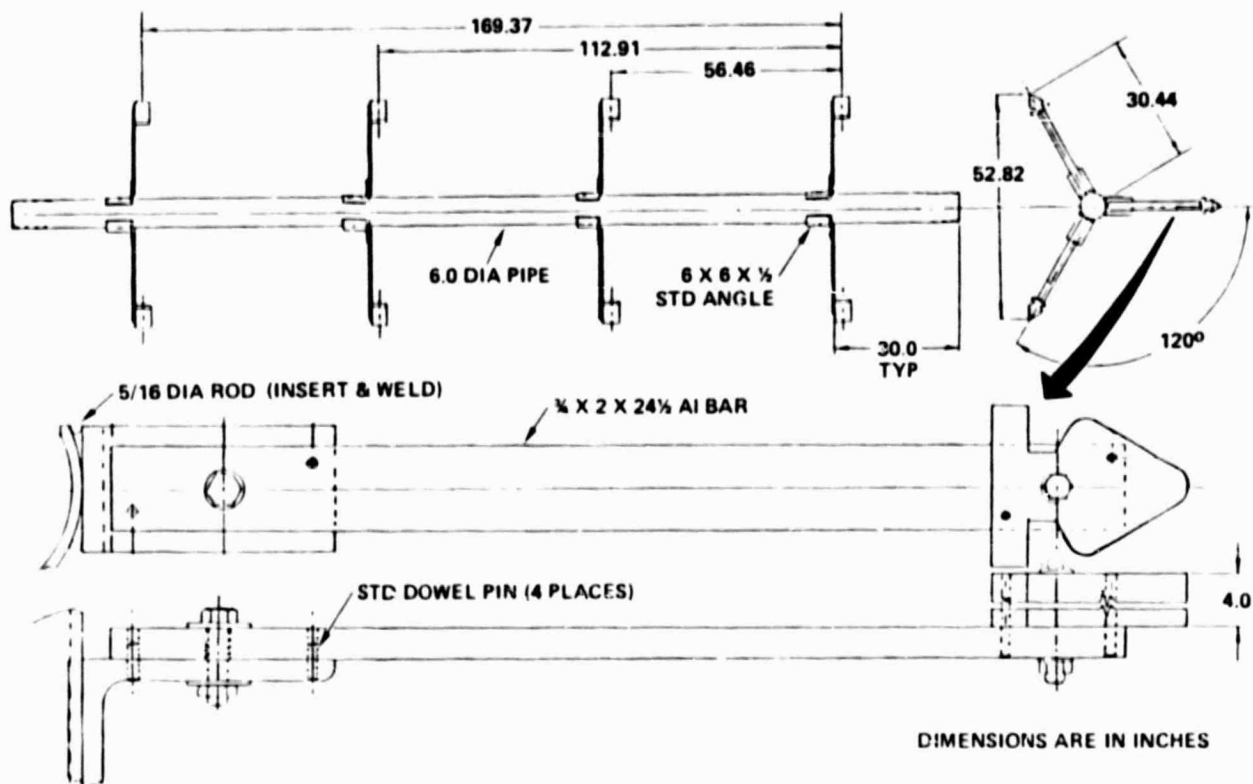


Figure 4-2. Truss welding and assembly fixture details.

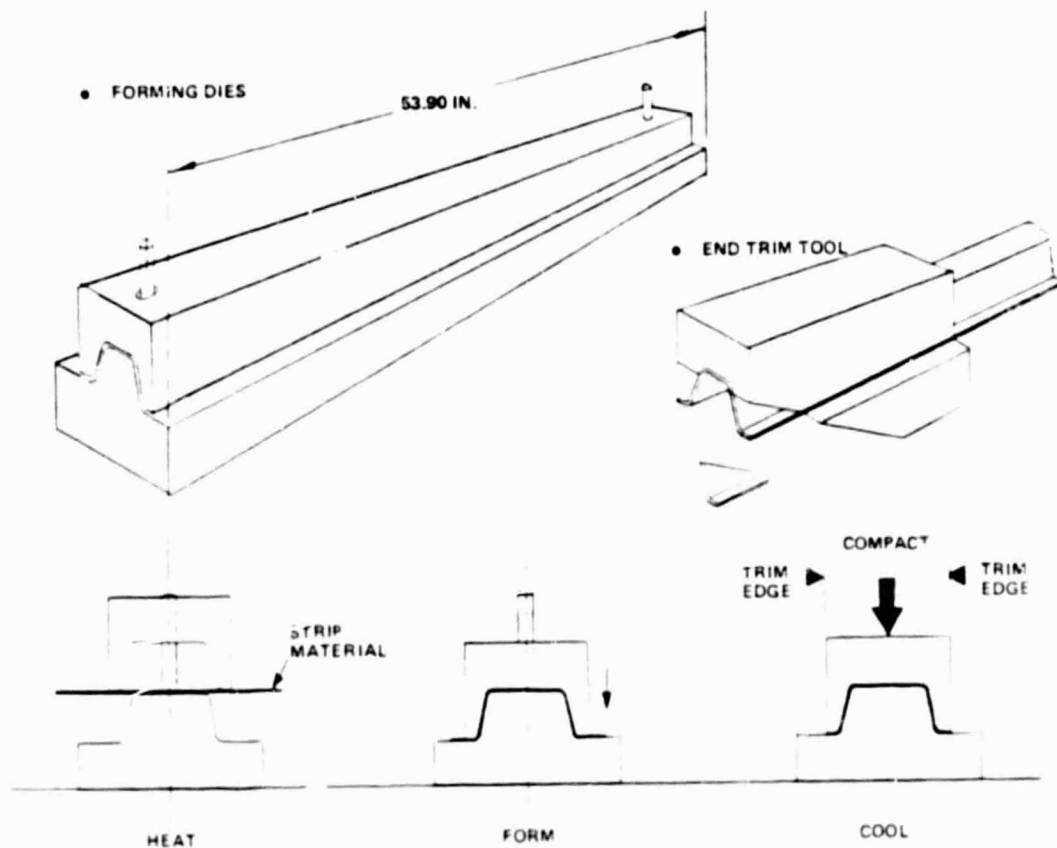


Figure 4-3. Crossmember forming tools and process.

4.1.3 PTS ASSEMBLY. The steps followed in assembling the PTS are illustrated in Figures 4-4 and 4-5. After trimming the caps to length, they were placed on the tool and the crossmember stations measured and marked off on each cap. Pierce-pin locator holes were then located on each cap at each weld location. With the caps aligned with their ends in-plane and the crossmember centerline stations centered on the weld

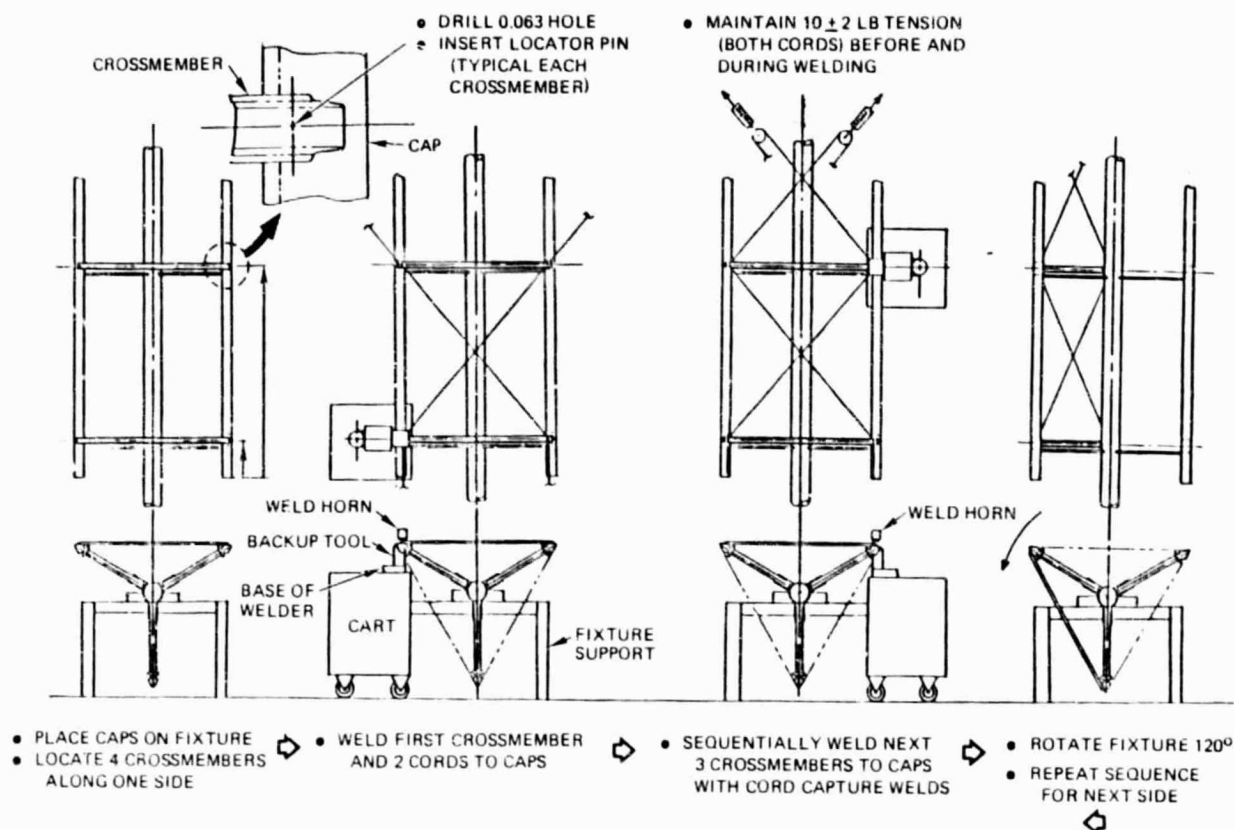


Figure 4-4. Truss fabrication plan.

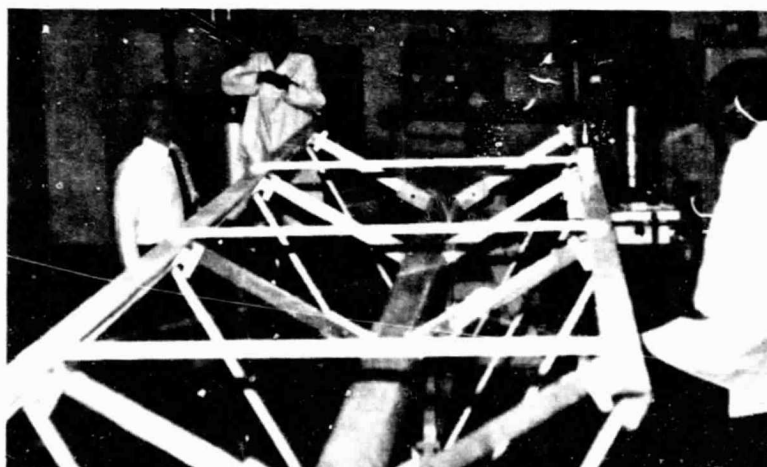


Figure 4-5. Truss assembly operations.

anvils, each locator hole was predrilled through the cap to a depth of 1.3 cm into the anvil.

The caps were removed from the fixture and the locator holes in the anvils deburred. Short pieces of cap were then installed on each anvil along one side of the fixture and drilled to match the locator holes in the anvils. This was done to prepare for a practice run made using short pieces of crossmember and lengths of cord so that all steps required to assemble one set of side members could be performed. This procedure proved to be valuable in working out some procedural and technical problems.

The ultrasonic welder was set up to perform truss welding, as shown in Figure 4-6. A standard commercial welder (Branson Model 3600) was placed on a table equipped to raise and lower the welder with a hydraulic lift mechanism, and move it from station to station on wheels. An anvil support, bolted to the base of the welder, straddled the adjacent crossmember and provided the load path for the force applied to the weld horn during welding.

The Convair-developed multi-spot weld horn is equipped with a short 1.6mm (0.063 in.) diameter piercing pin. This pin is provided as part of the beam builder operating concept to act as a fulcrum over which the diagonal cord is wrapped. The wrapping is done before start of the weld cycle, which attaches the crossmember to the cap and captures the cord within the weld zone. For assembly of the PTS, all crossmembers were positioned on the predrilled pierce-pin holes and maintained in position by locating pins inserted in each hole as shown in Figure 4-7.

After positioning the welder on the anvil, the locating pin was removed and the weld horn manually lowered to insert the pierce-pin in the drilled hole. After leveling and aligning the horn and anvil support, the cord was positioned against the pin and between the cap and crossmember. For the first crossmember, the cords were aligned but not tensioned, since it was only necessary to capture the cords on this first weld. On subsequent welds, the cords were first aligned against the pierce-pin, pulled in tension using a fish scale, then wrapped over the pierce-pin while maintaining tension until the cord just touched the locating pin at the next crossmember station. At this point, the weld pressure was applied to clamp the cord between the crossmember and cap and the tension load at the fish scale was reduced to approximately 8.8N (2 lb). The weld sequence was then initiated.

During the practice run, it was found that maintaining applied tension on the cord during welding caused the cord to break. This was attributable to an oversight in the design of the weld tip pierce-pin which allowed the cord to bear on the pin during welding. This could have been remedied by modifying the weld tip. It was found that reducing the applied cord tension just before welding did not cause loss of tension in the installed segment of cord. This was verified by checking the tension in each cord segment after it was welded. This alternative assembly method was used to prevent further delay in assembling the PTS.

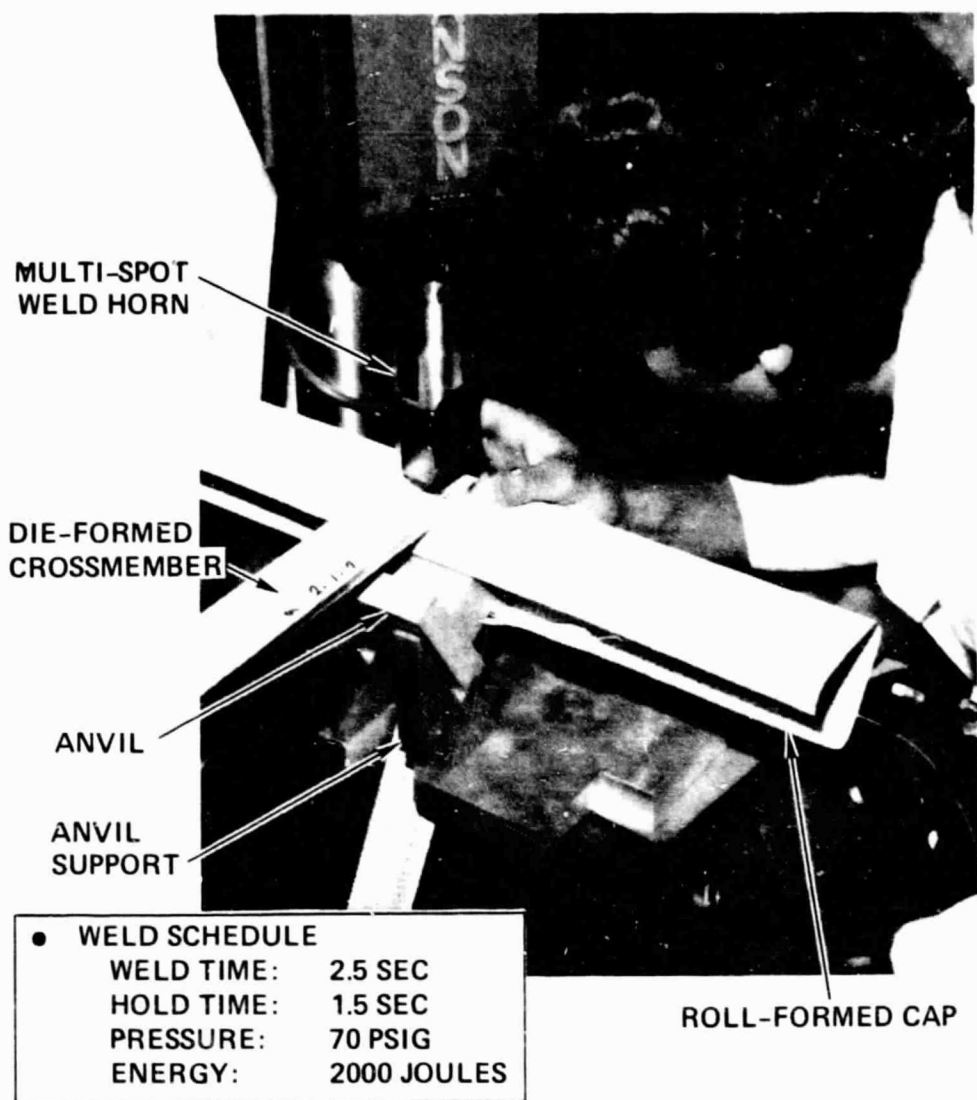


Figure 4-6. Truss ultrasonic welder.

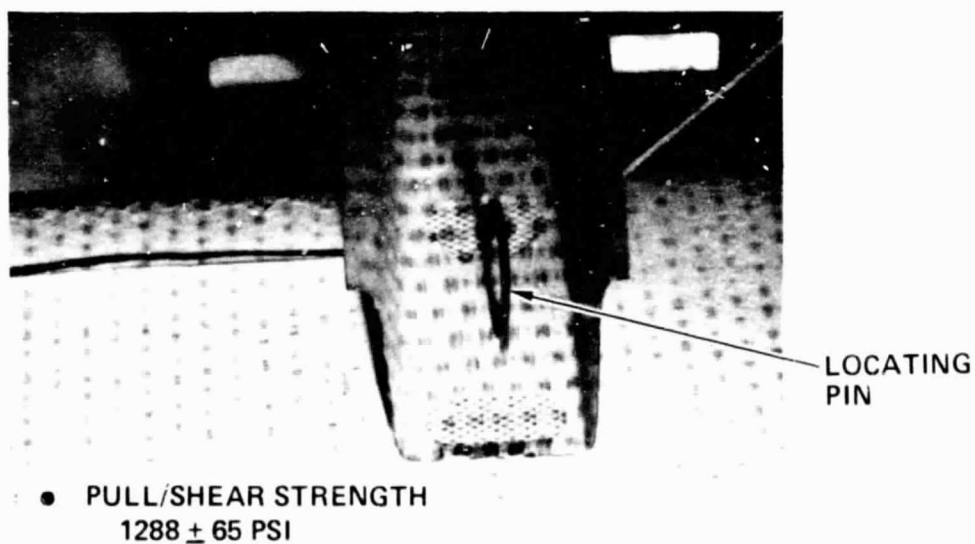


Figure 4-7. Finished weld joint.

4.2 PTS TEST PREPARATION.

4.2.1 PTS LOAD INTRODUCTION FITTINGS. After the PTS was assembled, the end load introduction fittings were positioned and installed with the truss still on the assembly fixture. The load introduction fittings consisted of aluminum form blocks inserted into the end of each cap and braced with aluminum angles as shown in Figure 4-8.

Before bonding the form blocks inside the caps, all parts were fabricated, installed and inspected for perpendicularity of the end planes to the centerline of the truss and for parallelism of the end planes to each other. Only one set of form blocks at one end were bonded in place while the truss was still on the fixture. This was to allow the truss to be removed from the fixture by sliding it off at one end.

Final alignment checks and permanent bonding of the second set of form blocks took place after the PTS was removed from the fixture. Alignment inspections were made before and after bonding the form blocks in place.

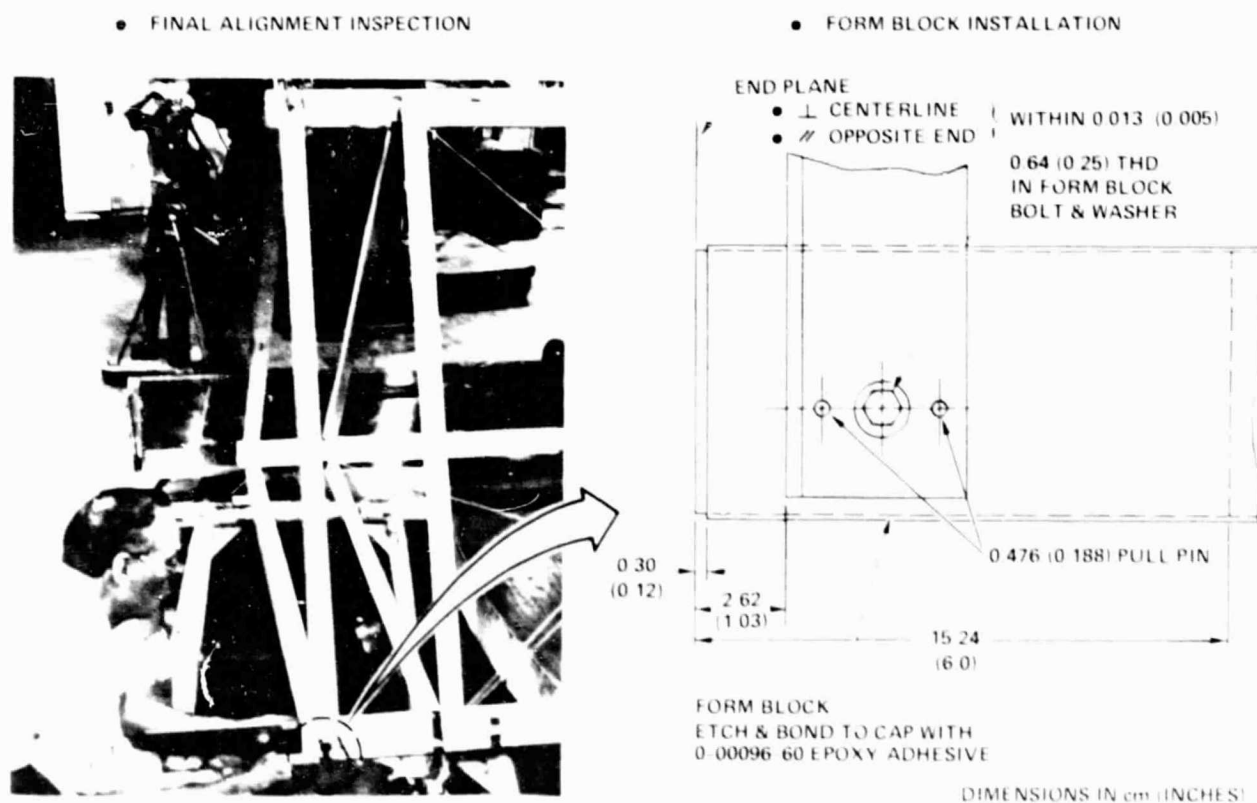


Figure 4-8. Truss load introduction fittings installation.

4.2.2 PTS INSTRUMENTATION. A total of 36 axial strain gages were installed by Convair on the PTS, as shown in Figure 4-9. All other test instrumentation was provided by JSC.

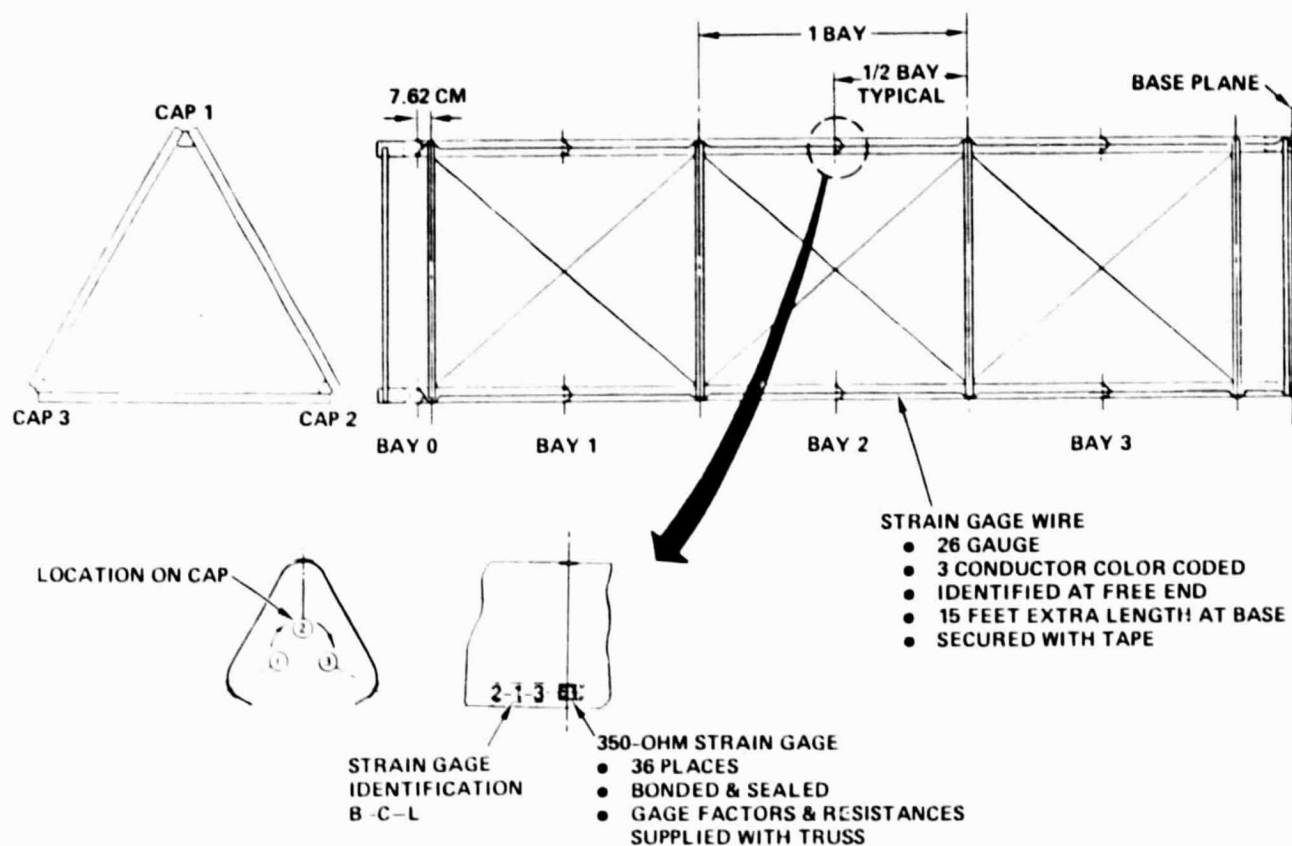


Figure 4-9. Truss strain gage installation.

The completed PTS, as shown in Figure 4-10, was skid-mounted and boxed for shipment to JSC. The PTS was shipped to JSC on 17 June 1980. Final acceptance was made at JSC on DD Form 250.

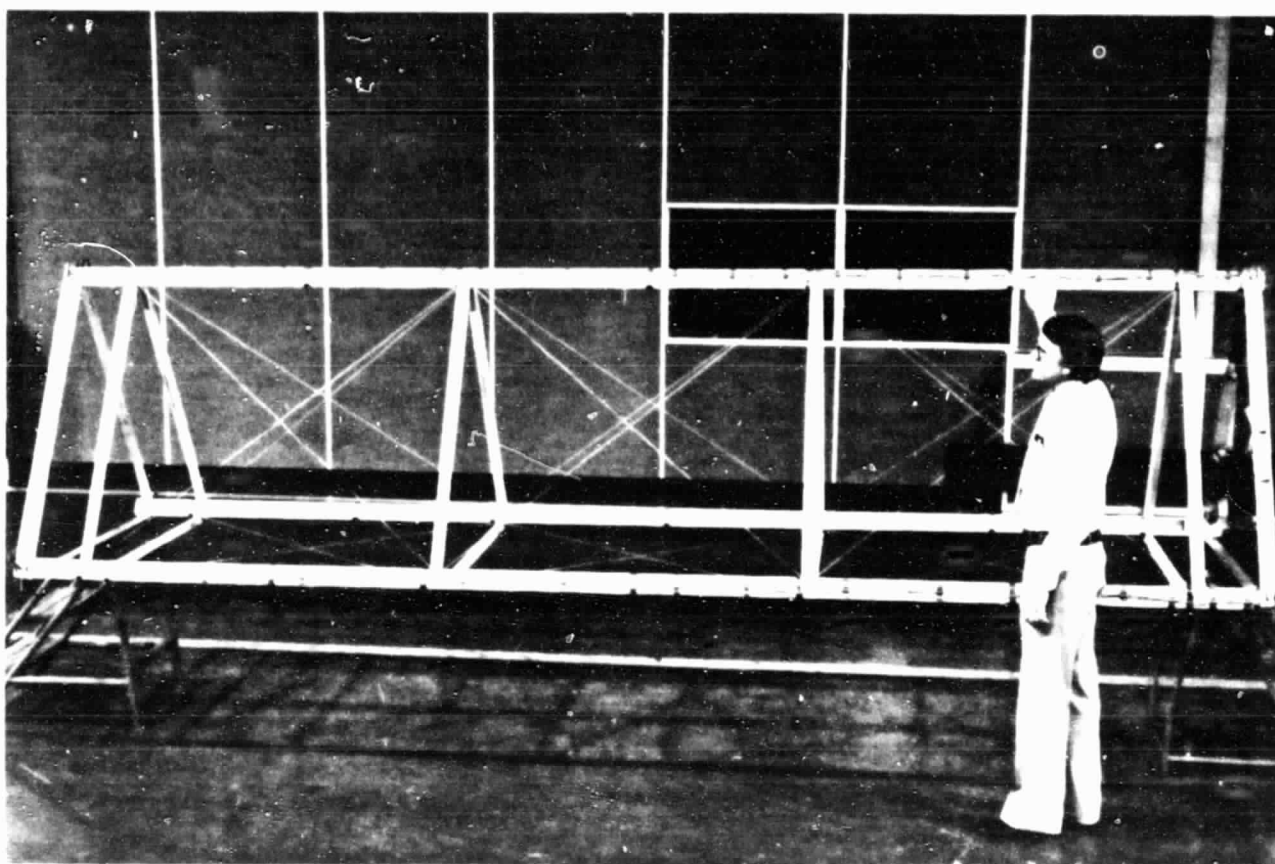


Figure 4-10. Finished prototype test truss segment.

4.3 LOCAL EFFECTS

The task flow and interrelationships for development of the local effects data is diagrammed in Figure 4-11. Local effects refers to the behavior and failure characteristics of the open section truss cap members under axial load as a column. It is known that the open section caps are subject to local buckling, column buckling, and torsional instability when subjected to column loading. To predict local effects, analysis of local stability and column stability using measured material properties was performed. The predictions were then tested by performing short column crippling tests and long column tests. A technique for measuring local cap rotation due to the effects of torsional instability was developed and tested. The results of the column tests were to be compared with the results of the PTS compression load test to determine the end constraints or end fixity of the PTS. If the end fixity of the PTS is known, the behavior of a long truss can then be predicted.

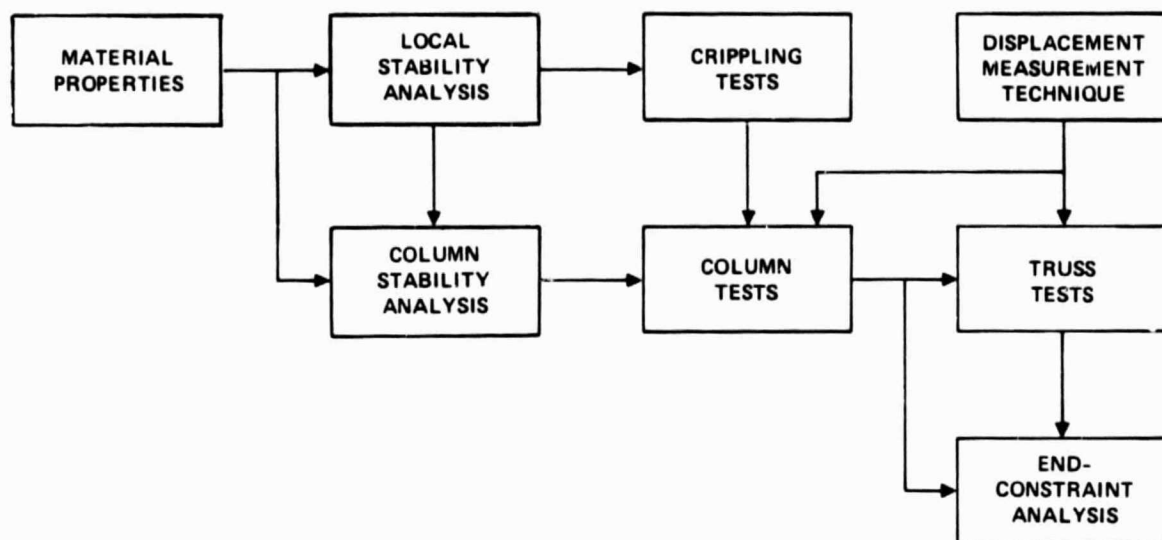


Figure 4-11. Local effects data development.

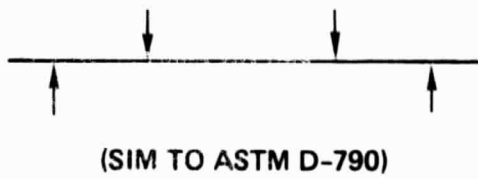
4.3.1 CAP MATERIAL PROPERTIES. The characteristics and average properties for the GR/TP composite material used for the PTS cap members are given in Sub-section 5.1.

Since elastic flexural stiffness constants cannot be derived from the basic mechanical properties data for a single-ply woven cloth material, three flexural tests were performed on coupons in the longitudinal and transverse directions. The test results were used to derive the elastic constants D_{11} , D_{22} , and D_{12} as shown in Figure 4-12 (Reference 5).

Unfortunately, the usual test methods for determining the twisting elastic constant D_{66} were not applicable to single-ply material. Accordingly, three one-edge-free buckling tests were conducted and the value of D_{66} was computed as shown in Figure 4-12.

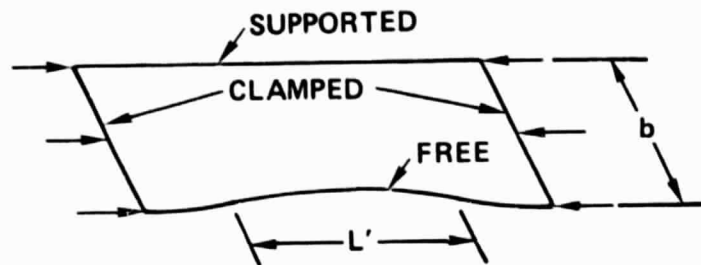
4.3.2 LOCAL STABILITY ANALYSIS AND TEST. The structural analysis of general shells STAGS computer code (Reference 2) was used for local stability analyses of the cap. Both bifurcation buckling and nonlinear collapse analyses were obtained using nominal thickness, 0.635 cm (0.025 in.), and the material properties. A diagram of the STAGS model is shown in Figure 4-13, including the half section used in analyses. STAGS is a finite difference code where rows and columns are defined as shown, respectively; also, coordinates and displacement components are indicated. There are four branches to the model and 25 rows were used with a total length (L) of 63.5 cm (25 in.). The results of both the bifurcation and nonlinear collapse analyses are

● FLEXURAL PROPERTIES
▲ FLEX SPECIMENS



$$\begin{aligned} D_{11} &= 18.5 \\ D_{22} &= 1.405 \\ D_{12} &= 0.576 \end{aligned}$$

▲ COMPRESSION SPECIMENS



$$\sigma_{cr} = \frac{\pi^2 D_{11}}{L'^2 t} + \frac{12 D_{66}}{b^2 t}$$



$$D_{66} = 0.30$$

Figure 4-12. Flexural and buckling properties tests.

STAGS MODEL

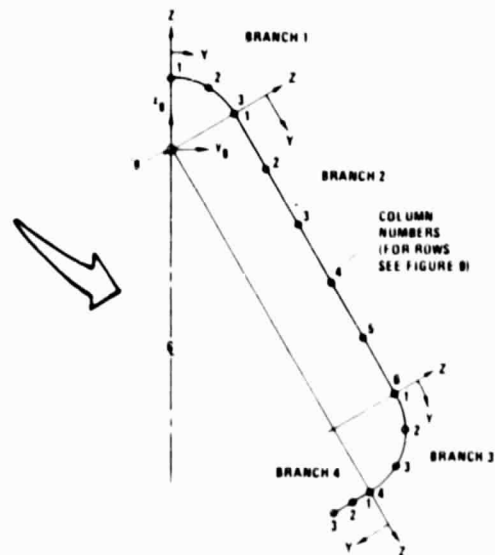
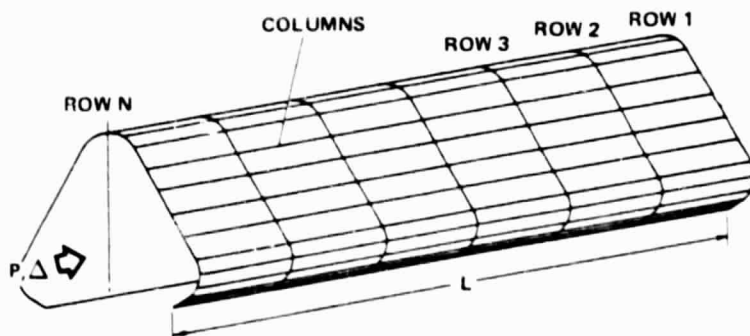


Figure 4-13. Finite-difference model for STAGS.

presented in Figure 4-14, which shows the total compression load P^c , versus the non-dimensionalized end shortening, u/L . This type of plot is an expedient means of comparing analyses with test.

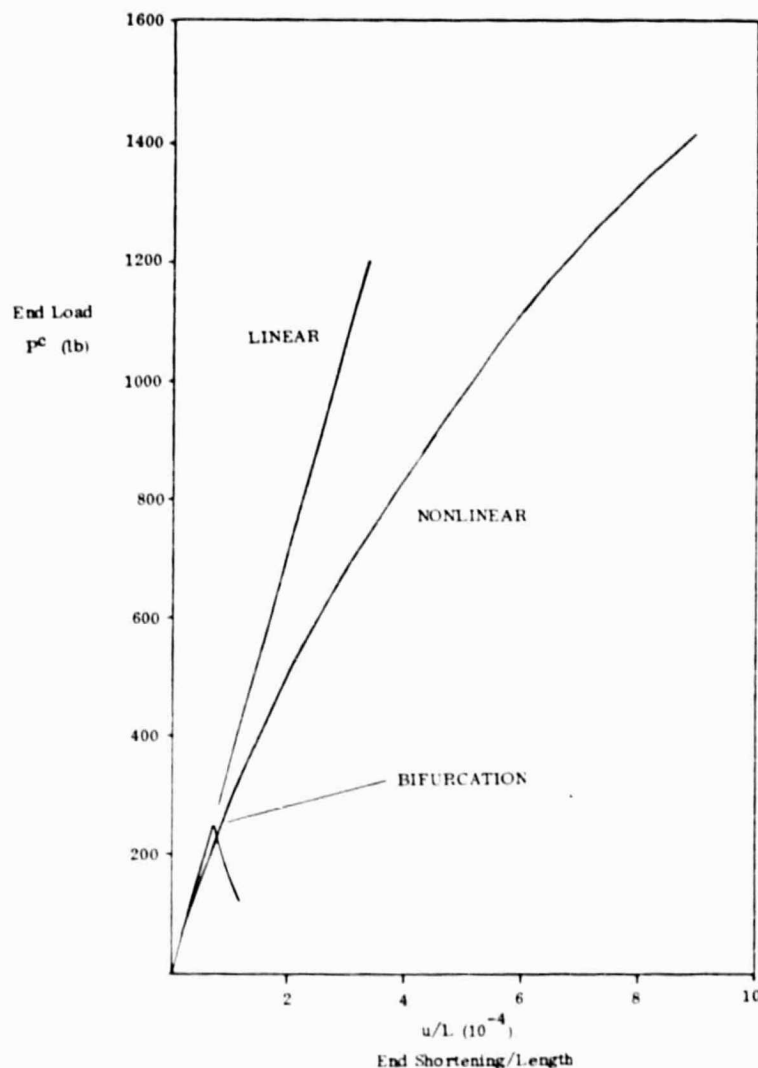


Figure 4-14. Predicted local buckling and end shortening for crippling test specimens.

4.3.3 CRIPPLING TESTS. Two crippling tests of the cap were performed which provide the local buckling strength behavior and the crippling strength. Specimens two feet in length were used for this test and the ends were carefully potted in steel blocks to obtain uniformity of the compression load.

A specimen is shown during test in Figure 4-15. Axial strain gages were installed on each of the three curved elements, but the readings were not close, probably due to irregularities in the uniformity of the material. Accordingly, the strains are not reported here.

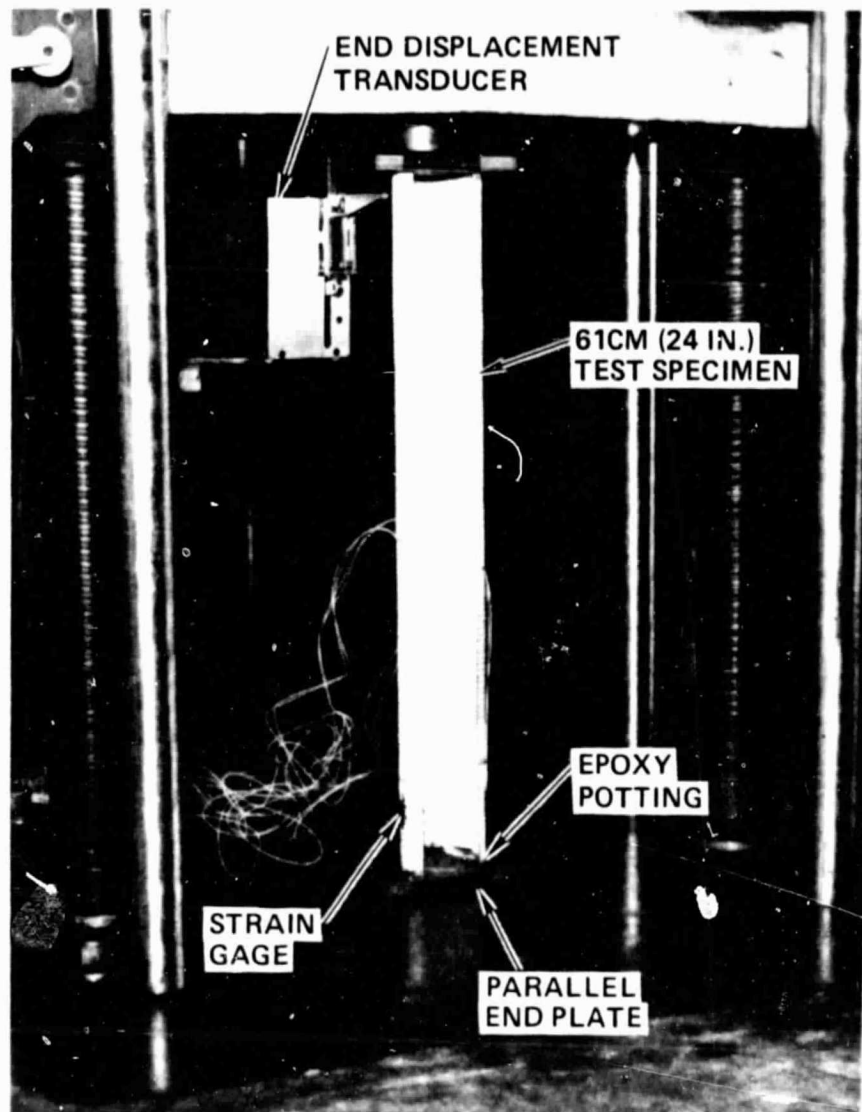
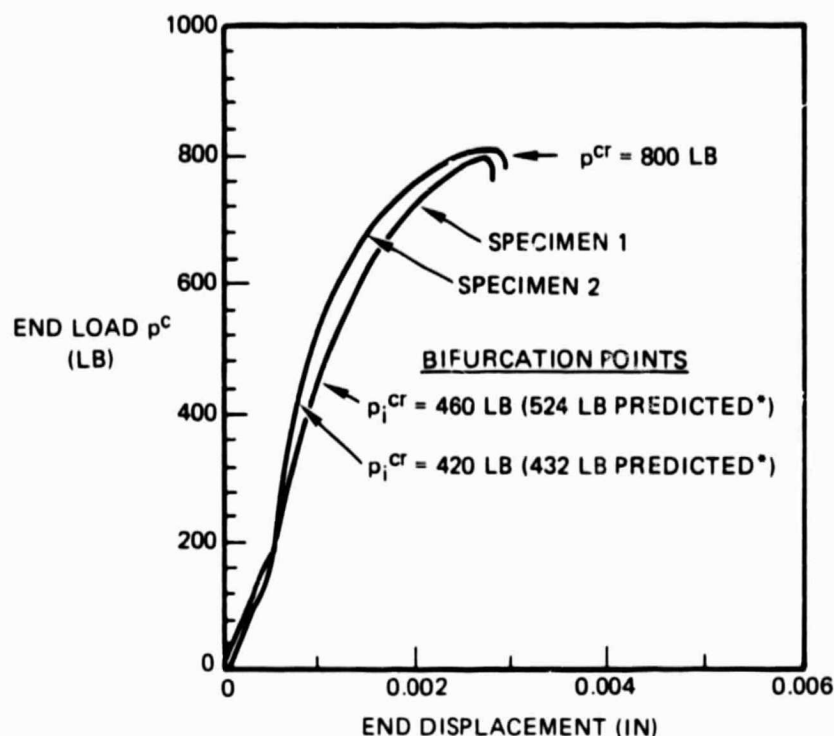


Figure 4-15. Cap column crippling test set-up.

The end-shortening plots for the two tests are presented in Figure 4-16. Both tests reached a crippling load of about 800 pounds. The bifurcation buckling loads were 420 and 460 pounds, which do not compare to the STAGS analyses shown in Figure 4-14. The reason for this is that the cap varied in thickness and ranged from 0.711 - 0.940mm (0.028 - 0.037 in.) as compared to 0.735mm (0.025 in.) used in the analysis. This thickness variation was the result of the intermittent compaction process discussed in Subsection 2.1.2.

The bifurcation buckling load is proportional to the thickness cubed. Accordingly, the calculated bifurcation buckling load may be adjusted as indicated in Figure 4-16.

Thus, the ratios of the test load to the corrected load are 0.88 for specimen 1 and 0.97 for specimen 2. These ratios do show good correlation between analyses and test, despite the fact that the specimen thickness varied along the length and there was some degree of lengthwise curvature.



p^{cr} = CRIPPLING LOAD

p_i^{cr} = INCIPIENT BUCKLING LOAD

* CORRECTED FOR THICKNESS $(p_i^{cr})_{COR} = \left(\frac{\bar{t}}{t}\right)^3 p_i^{cr}$

$t = 0.025$ ANALYSIS

$\bar{t} = 0.032$ SPECIMEN 1

$\bar{t} = 0.030$ SPECIMEN 2

Figure 4-16. Crippling test results.

4.3.3.1 Short Column Analysis. Compression buckling of the cap between lateral supports falls into the short column category, which is dependent on the crippling strength and the slenderness ratio \bar{L}/ρ where:

$$\bar{L} = L / \sqrt{C}$$

C = end-fixity coefficient at the lateral supports

ρ = minimum radius of gyration of the cross-section

The value for C is, at present, an unknown. For expediency, the nondimensional short column buckling curves presented in Figure 4-17 (Reference 6) may be used to estimate the column buckling strength. The curve for the cap would intersect the ordinate at a value of $(F^{co}/E^c) \times 10^3$.

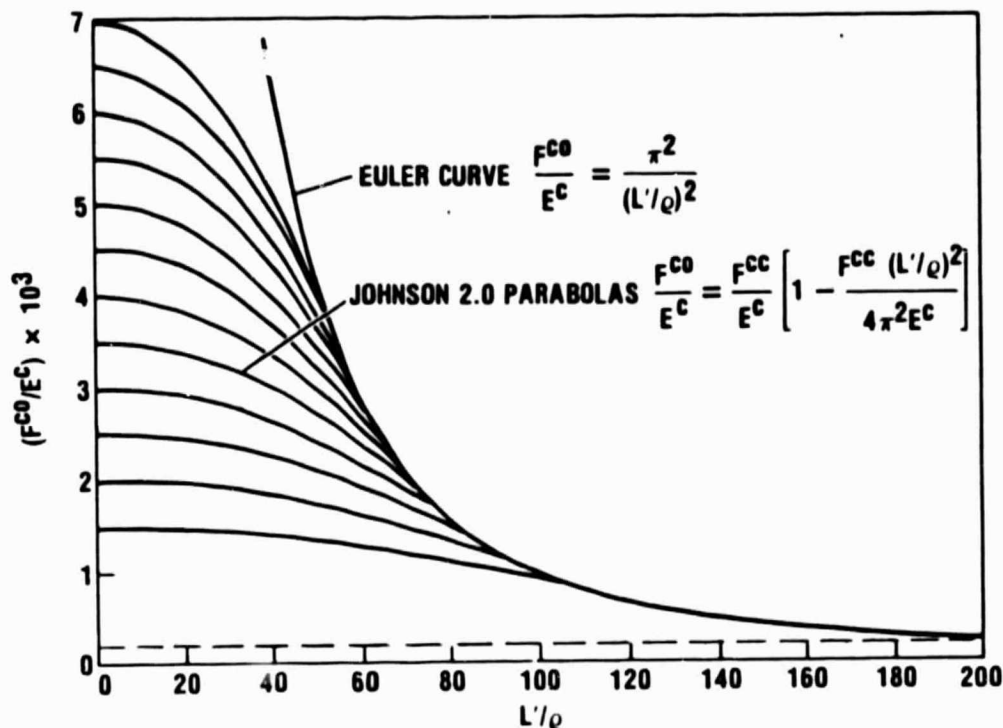


Figure 4-17. Nondimensional buckling curves.

The crippling strength is:

$$F^{cc} = P^{cr} = 800 \text{ lb}$$

The mean thickness is:

$$\approx 0.031 \text{ in.}$$

The developed length of cross section = 7.5 in.

$$F^{cc} \approx 800 / (7.5 \times 0.031) \approx 3440 \text{ psi}$$

$$E^c = 19.6 \times 10^6 \text{ psi}$$

$$(F^{co}/E) \times 10^3 = (3440 / 19.6 \times 10^6) \times 10^3 = 0.175$$

With this value of 0.175, the column curve is drawn as a dotted curve in Figure 4-17 which indicates that the short column crippling strength and the long column buckling strength are virtually the same. Consequently, the critical long column load should be about 800 pounds, were it not for the effects of torsional instability, which is discussed next.

4.3.4 TORSIONAL INSTABILITY ANALYSIS. A thin-walled open section column may exhibit torsional instability when subjected to compression loading if the free length is sufficiently large. Otherwise, the member may be subject to short or long (Euler) column buckling. In some cases, the structure may be affected by the interaction of torsional and column buckling.

For expediency in the stability analysis of the cap over one bay length, the effects of the cross members and diagonals are assumed to provide simple support at the ends and complete restraint against rotation at the ends.

The STAGS computer code with the nonlinear option was chosen for this analyses. There are two options for the STAGS finite difference model.

- a. Input user written initial imperfections that impose a maximum rotation at midspan, tapering to zero at the ends. The configuration of the imperfections is shown in Figure 4-18. Notice that these imperfections will result in torsional instability and may also impose lateral bending of the cap, which would tend to move the two free edges closer together. To accomplish the analysis of this model, local buckling of the flat sides must be precluded. This can be accomplished by arbitrarily assuming that the transverse flexural stiffness of the flat elements is large enough

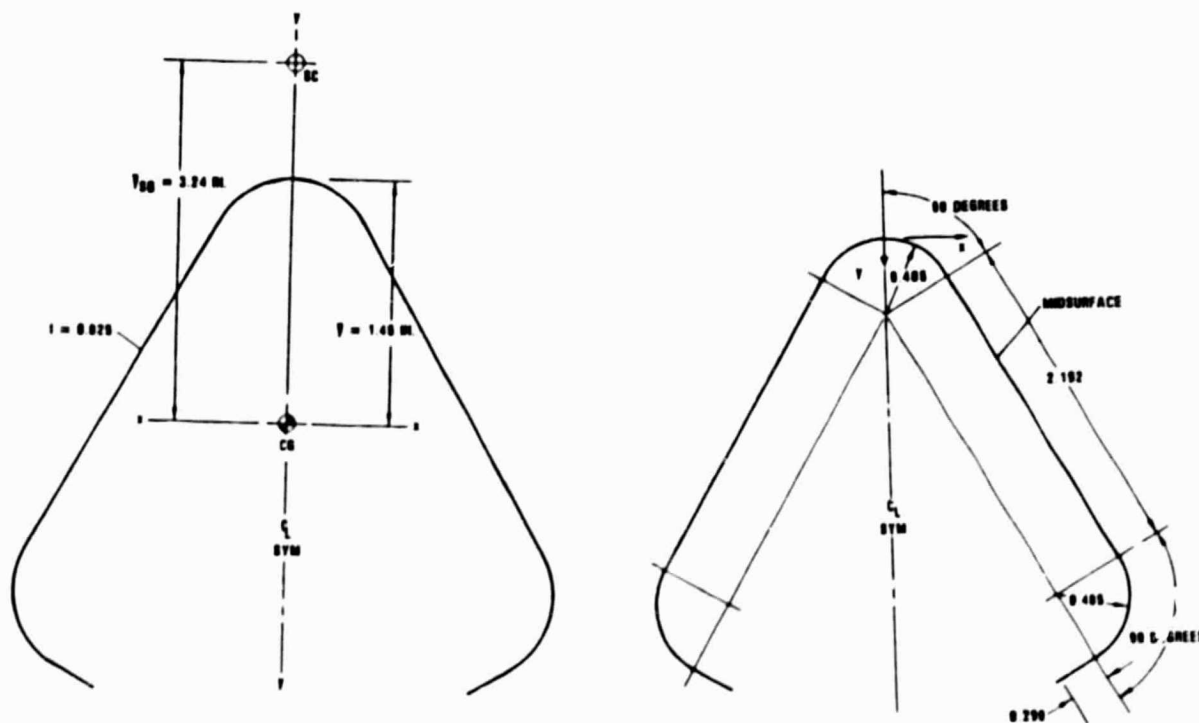


Figure 4-18. Cap cross-section

to preclude local buckling. This procedure will not affect the torsional instability analysis. In the present problem, the transverse flexural stiffness had to be eight times as large as the actual value. Accordingly, a half-model with 10 rows (See Figure 4-13) was sufficient for the analysis.

- b. Use the same model as described above, but accommodate local buckling of the flat sides instead of precluding it. This would require about 125 rows instead of 10 required in option a, so that there are a sufficient number of rows on each half-wave of the local buckling eigenvector. The local buckling model for nonlinear behavior would need an additional user-written subroutine for local imperfections to supplement the long wave imperfections discussed in option a.

Because of budget limitations and lack of prior experience similar to the analysis discussed in either option, it was decided to proceed with option a. Option b would probably require double the computer time need for option a. However, since local buckling and torsional instability were analyzed separately, interaction analysis was required, using the theory developed in Reference 3. For further analysis of the cap, certain section properties are required. For the cap shown in Figure 4-18, a user-written Hewlett-Packard program was used to obtain the following section properties:

$$\begin{aligned} A &= 0.1861 \text{ in}^2 & y &= 1.45 \text{ in} \\ I_{xx} &= 0.1583 \text{ in}^4 & I_{yy} &= 0.2215 \text{ in}^4 \end{aligned}$$

An approximate analysis for the location of the shear center was performed by use of Reference 4, and the location is as shown in Figure 4-18. The results of the STAGS analyses for nonlinear torsional instability with flexural buckling precluded is shown in Figure 4-19. Thus, the torsional collapse load is:

$$P_T^c = 900 \text{ lb}$$

and the flexural column buckling load (from Subsection 4.3.3.1) is:

$$P_T^c = 800 \text{ lb}$$

The allowable compression collapse load, accounting for interaction effects is determined as follows:

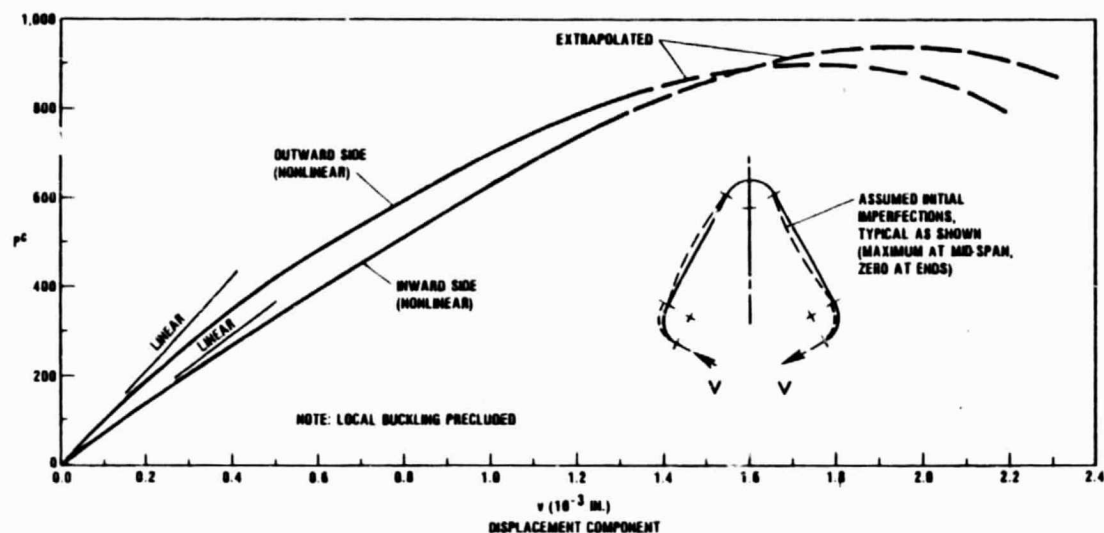


Figure 4-19. Predicted compression load versus tangential displacement of free edges due to torsional instability.

The interaction equation (Reference 3-1, Eq. 88) is in the form

$$\left(1 - \frac{P_F^c}{P_{cr}^c}\right) \left(1 - \frac{P_T^c}{P_{cr}^c}\right) = \left(\frac{\bar{Y}_{SG}}{\rho_p}\right)^2 \quad (\text{eq 4-1})$$

where

P_{cr}^c = allowable compression collapse load, and equal to the smallest root of the equation.

ρ_p = polar radius of gyration about the shear center

The value for ρ_p is computed from

$$\rho_p = \sqrt{I_{xx} + I_{yy} + A \bar{Y}_{SG}^2} / A \quad (\text{eq 4-2})$$

$$\rho_p = 3.54 \text{ in}$$

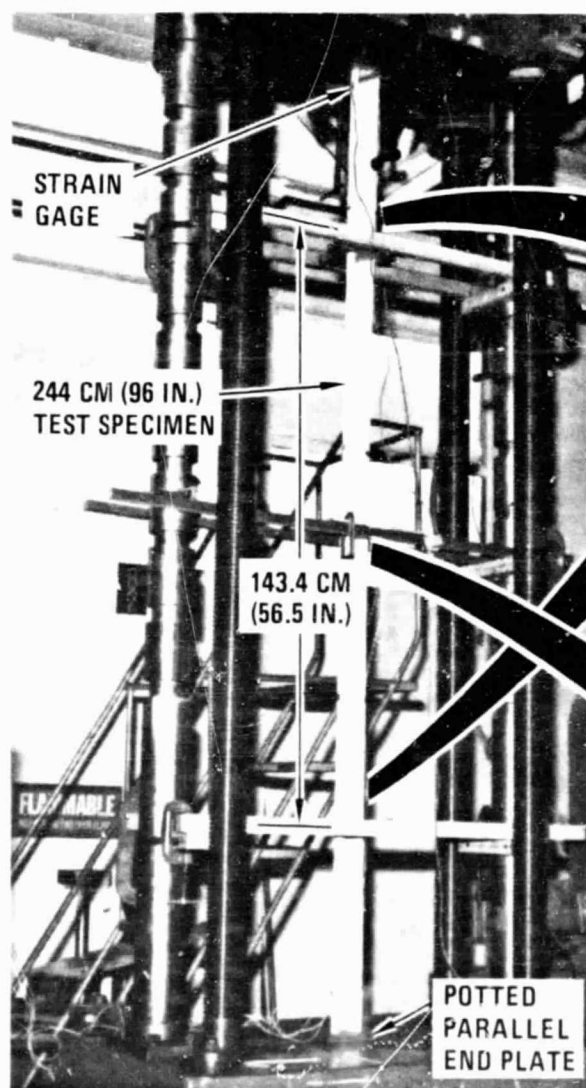
Solving equation (4-2) for the smallest root

$$P_{cr}^c = 442 \text{ lb}$$

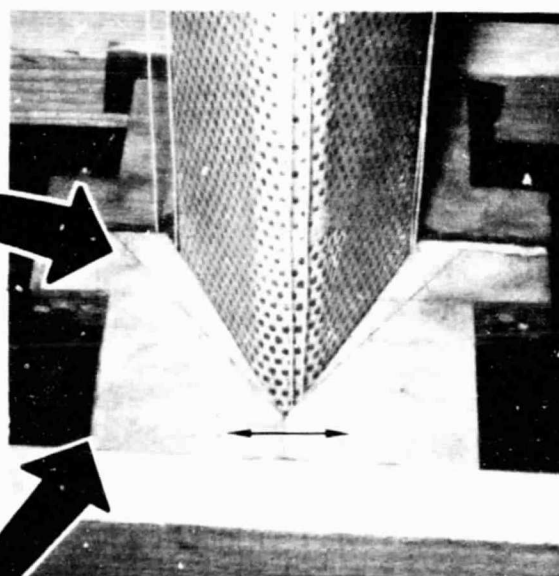
Since initial imperfections were applied in the STAGS analyses, displacements of the free edge occurred at the outset. Accordingly, the bifurcation point for torsional instability cannot be determined from Figure 4-19. Also, a STAGS bifurcation analyses was not performed because it had been found previously to be highly unconservative for some unknown reason.

4.3.5 COLUMN TESTS & DISPLACEMENT MEASUREMENT. The cap column test specimen was potted in parallel steel end plates for the purpose of testing with a uniform comparison load. It was originally planned to have a slenderness ratio ($L'/\rho = 61$) equivalent to one bay of the PTS with pinned ends. However, due to limited height of the testing machine, the specimen was reduced in length to 243.8 cm (96 in.) which resulted in a slenderness ratio of 51. Fortunately, this does not affect the column (flexural) buckling characteristic because of the insensitivity to the slenderness ratio, as indicated in Figure 4-17. The test setup for the column test is shown in Figure 4-20.

• TEST SET-UP



• FREE SLIDING FORM BLOCKS



• MID-SPAN TRAVEL BLOCK

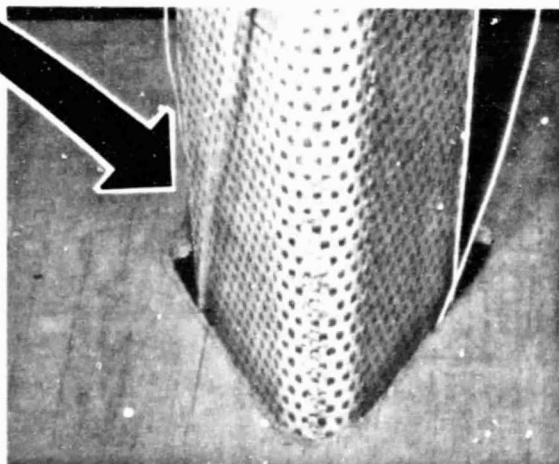


Figure 4-20. Cap column test setup.

To test for torsional instability, complete restraint to twist was provided at two locations, a distance apart equal to one bay length, 143.4 cm (56.4 in.), at the center of the specimen. These restraints were free-sliding form blocks that could be set up to allow column buckling about either principal axis. A contoured wooden stop with clearance to the outside of the cap of about 0.3 cm (0.12 in.) was provided at the center of the column for two purposes:

- a. To provide visual evidence of torsion (rotation) of the cross section.
- b. To prevent runaway torsional collapse of the specimen.

The technique used to measure cap rotation at the center is shown in Figure 4-21. A beam from a stationary 2mW laser was reflected from a small mirror bonded to the

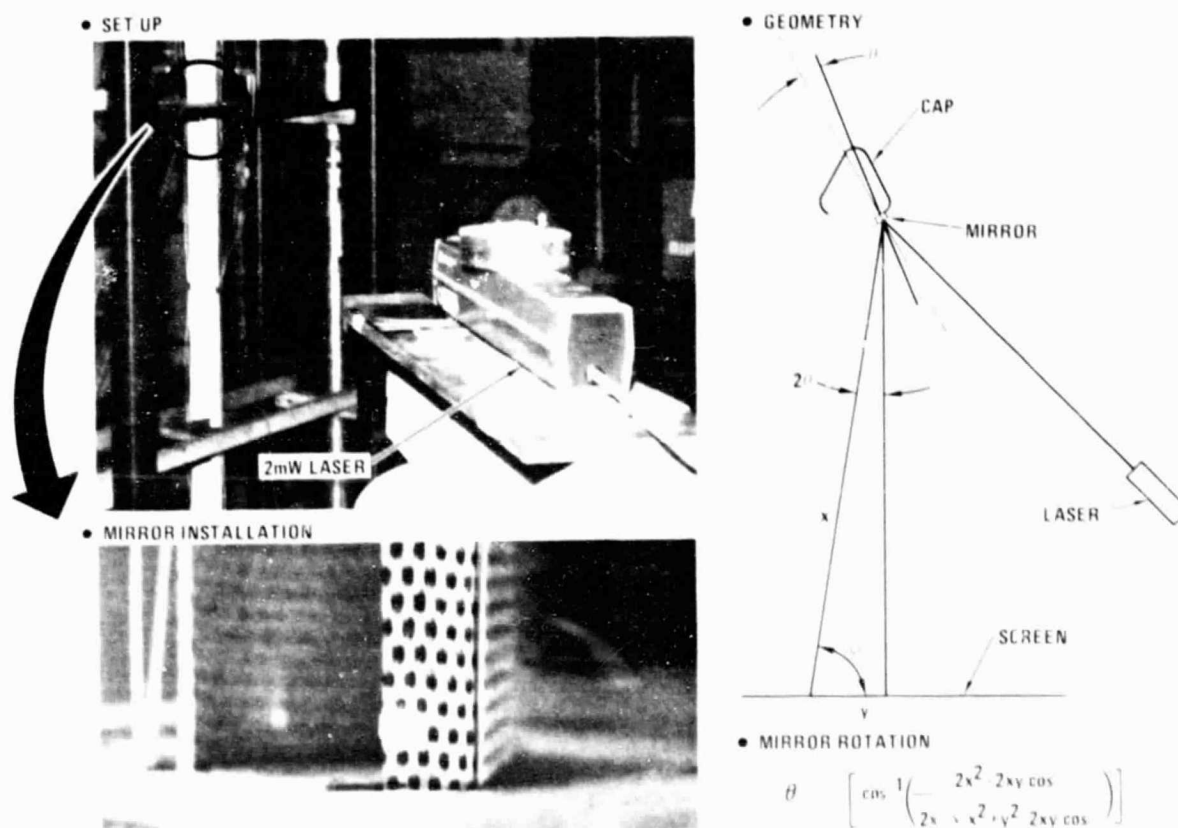


Figure 4-21. Cap rotation measurement.

top of the cap section. The reflected beam was projected onto a paper screen located 3.15 m (124 in.) from the mirror for test 1, and 4.27 m (168 in.) from the mirror for test 2. The laser was placed within 2.5m (98 in.) of the mirror. Differences in deflections of the spot on the screen were marked off as the column was loaded in 222.4N (50 lb) increments. The apparent rotation, θ , of the cap section could then be computed using the equation shown in Figure 4-21.

Other instrumentation included an end displacement transducer, a load cell to measure axial load, and three axial strain gages mounted on the outside radii of the cap near the upper end plate.

The plots of the column end displacement and apparent cap rotation versus end load for the two tests are shown in Figures 4-22 and 4-23. During test 1, it became evident that the column was experiencing combined local buckling and torsional instability, due to both upward and lateral displacement of the laser beam. The beam displacements increased with each load increment. At between 400 and 450 lb, the displacement of the beam changed abruptly and the cap contacted the center travel block. The test was terminated at this point.

Test 2 was considered to be a more critical test of actual loading conditions when installed in a truss. With the cap free to flex in the weakest direction, the interaction of column buckling and torsional instability would be the most severe. During the test it was visibly observed that the cap section at mid-span was rotating and moving laterally, and the cap edges were closing together. The cap section contacted the travel block at a load of between 375 and 400 lb. The test was terminated at this point.

Again, as with the short crippling specimen, three axial strain gages showed varied loading characteristics. This is attributable to the irregularities in the straightness and uniformity of the cap section and lateral displacement induced by column buckling.

It was not possible to show accurately what the true rotation of the cap was at mid-span. The lateral displacement had little effect on the laser beam spot displacement; however, the closing of the cap section edges could have had a significant effect on the spot displacement. It would, therefore, have been best to have placed the mirror on the apex of the cap section to preclude the effects of edge closure.

The compression collapse load is presumed to have occurred at 350 to 400 lb. Thus, there is reasonable agreement between test and theory where:

$$P_{cr}^c \text{ (experimental)} \approx 375 \text{ lb}$$

$$P_{cr}^c \text{ (theoretical)} = 442 \text{ lb}$$

The displacements of the free edges are due to the interaction of cap rotation, local distortions, and lateral bending deflections of the cap. There was insufficient nonlinear analyses performed to obtain the displacements for correlation with test.

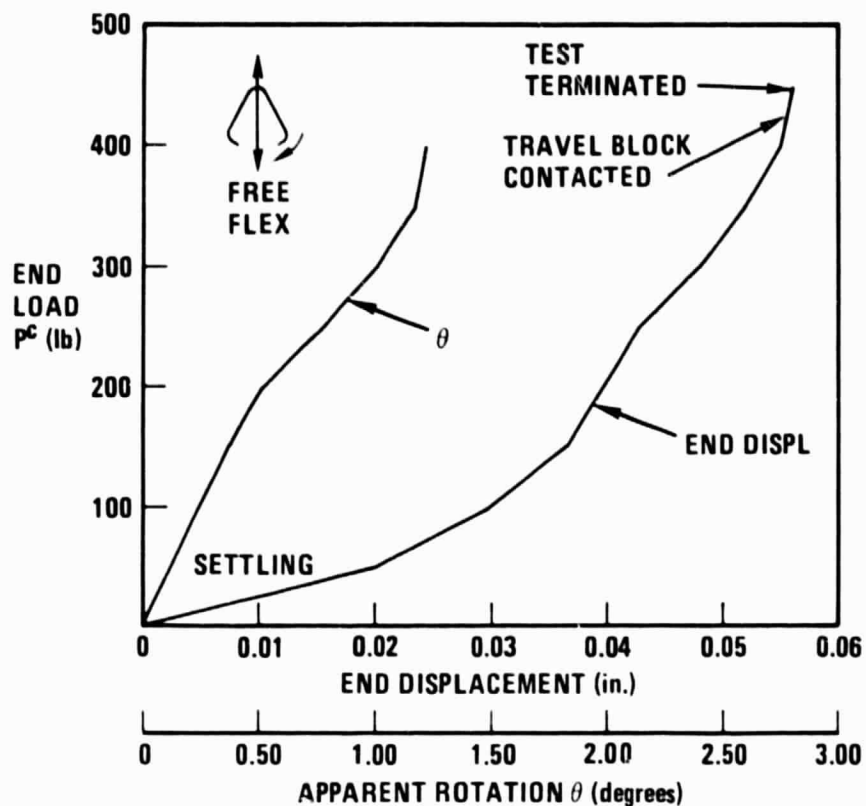


Figure 4-22. Cap column test no. 1 results.

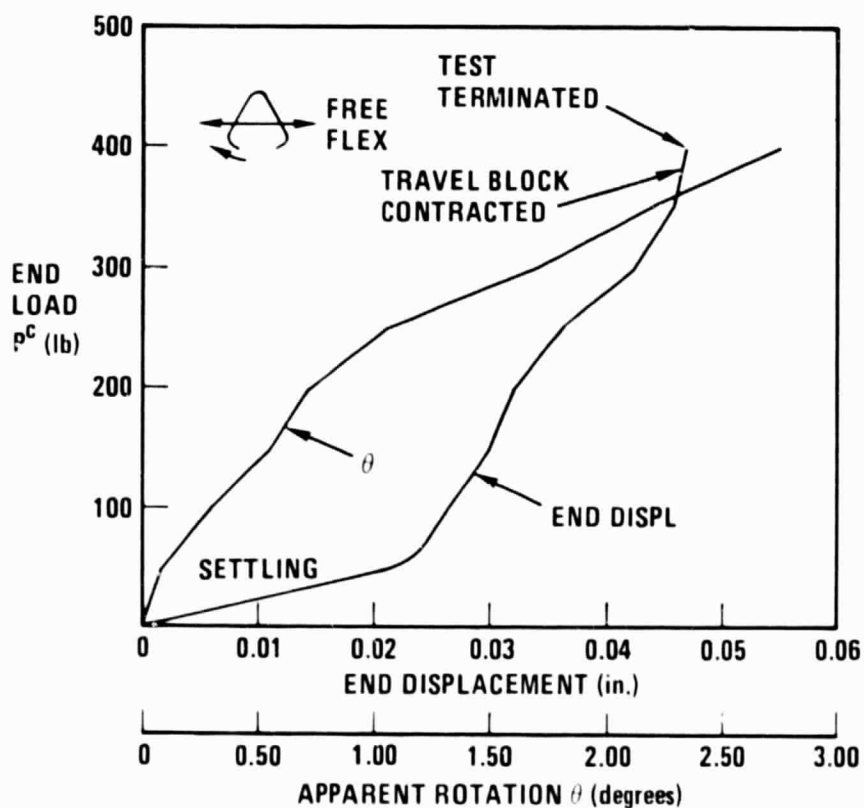


Figure 4-23. Cap column test no. 2 results.

4.4 TEST PLAN

A recommended instrumentation and test plan was prepared by Convair and submitted to NASA/JSC. This plan is included in this report as Appendix A.

4.5 PTS TEST RESULTS

The PTS was subjected to four recommended tests at JSC's Structure and Mechanics Laboratory: cap transverse stiffness, torsional stiffness, torsional damping, and axial compression. The flexural stiffness and damping tests were not performed because of scheduling conflicts with Orbiter structural tests.

The fragility of the PTS was inadvertently demonstrated during test preparations when accidental contact by personnel with the truss resulted in fracture of a crossmember, two broken cords, and elongation of one cord. Repairs were performed prior to testing to replace the three damaged cords by bonding new cords to the cap members with the proper amount of tension applied. The broken crossmember was repaired by bonding a splice section of crossmember over the damaged area. These repairs were designed to restore the PTS to a level of structural performance capability needed to complete the test sequence.

4.5.1 TEST SEQUENCE 1: CAP TRANSVERSE STIFFNESS. The cap transverse stiffness test setup is shown in Figure 4-24. A maximum load of 222.4N (50 lb) was applied in 44.5N (10 lb) increments. Deflection readings of the loaded cap were made with an LVDT located adjacent to the load application point. A dial gauge was added for runs on caps 2 and 3 to measure deflection at the crossmember station. Two load/deflection tests were performed on each cap.

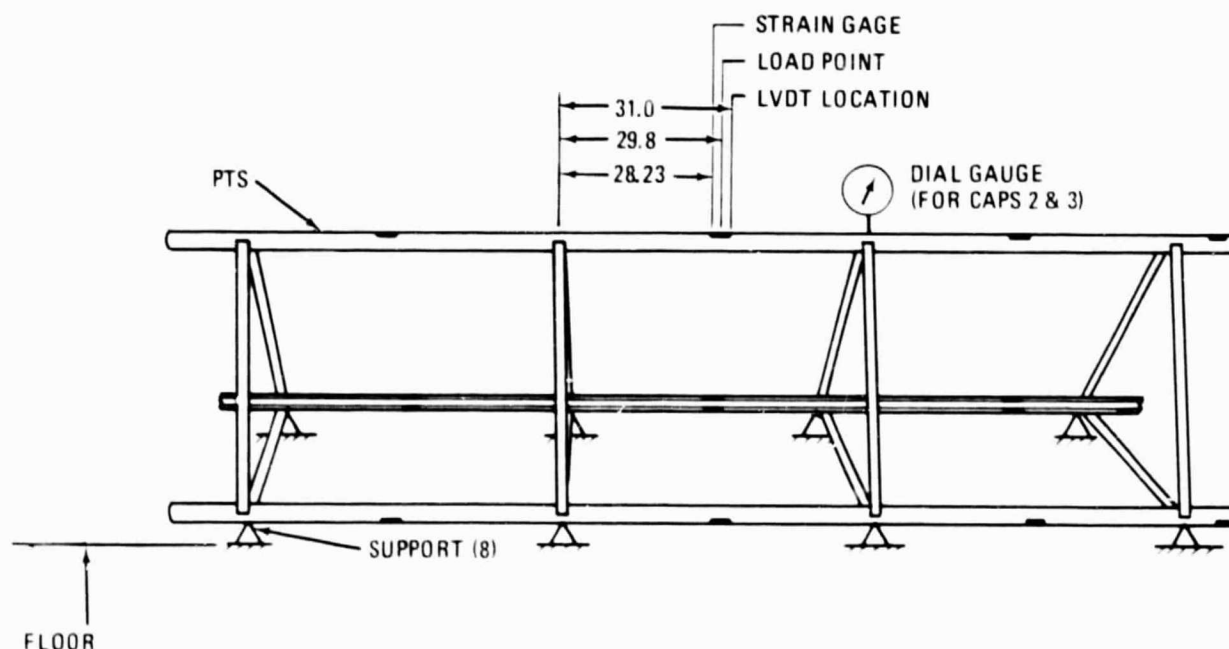


Figure 4 24. Cap transverse stiffness test setup.

The initial calculation of local cap deflection did not include the contribution of the crossmembers to the overall deflection. After performing the first cap deflection test, it was evident that the crossmember deflections were significant. A local cap deflection of nearly 6.4 mm (0.25 in.) was measured when only a 1 mm (0.04 in.) deflection had been computed. The deflection of the center of the cap member was recalculated by JSC personnel using the theorem of the cap as a continuous beam on elastically sinking supports. By measuring the deflection at a crossmember support station, the calculated mid-span deflection showed good correlation with the measured value.

Figure 4-25 shows typical results of the cap deflection tests. The average local cap transverse stiffness for the six runs was 33.5 k N/m (191.3 lb/in), with a standard deviation of ± 1.8 k N/m (± 10.3 lb/in).

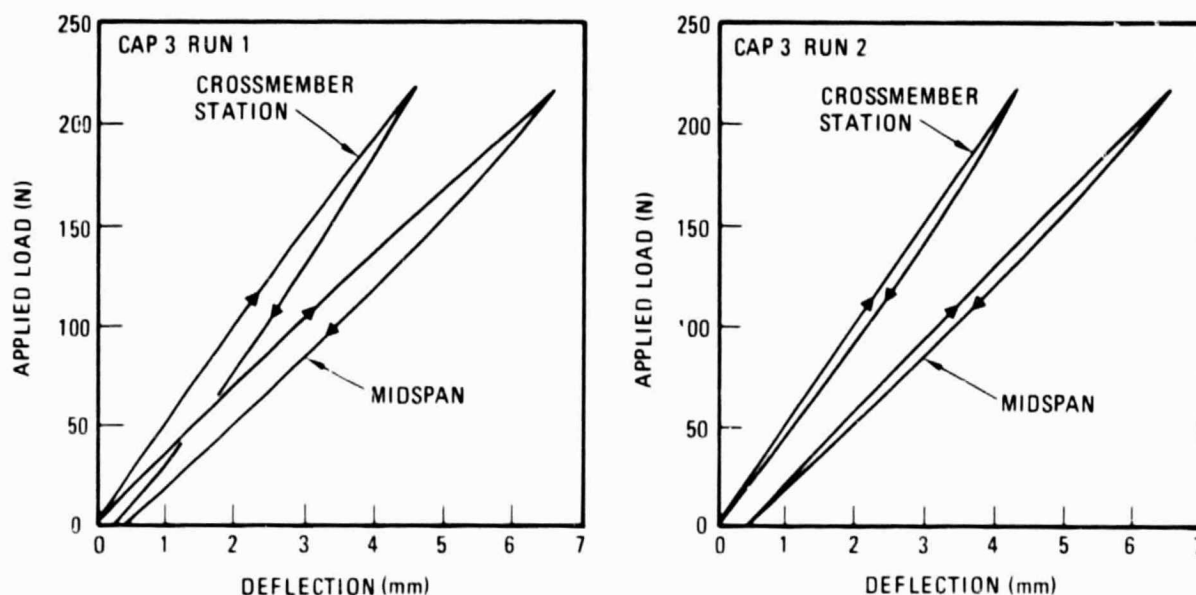


Figure 4-25. Cap transverse stiffness characteristic.

4.5.2 TEST SEQUENCE 2: TORSIONAL STIFFNESS TEST. The torsional stiffness test was performed as shown in Figure 4-26. The PTS was oriented vertically, with the base clamped to the floor of the test area. The torsion was applied manually at the top of the truss segment, with a torque-reading wrench, through the centroid of a balanced fixture. A cardboard grid marked to indicate degrees of angular rotation was installed at the top of the PTS.

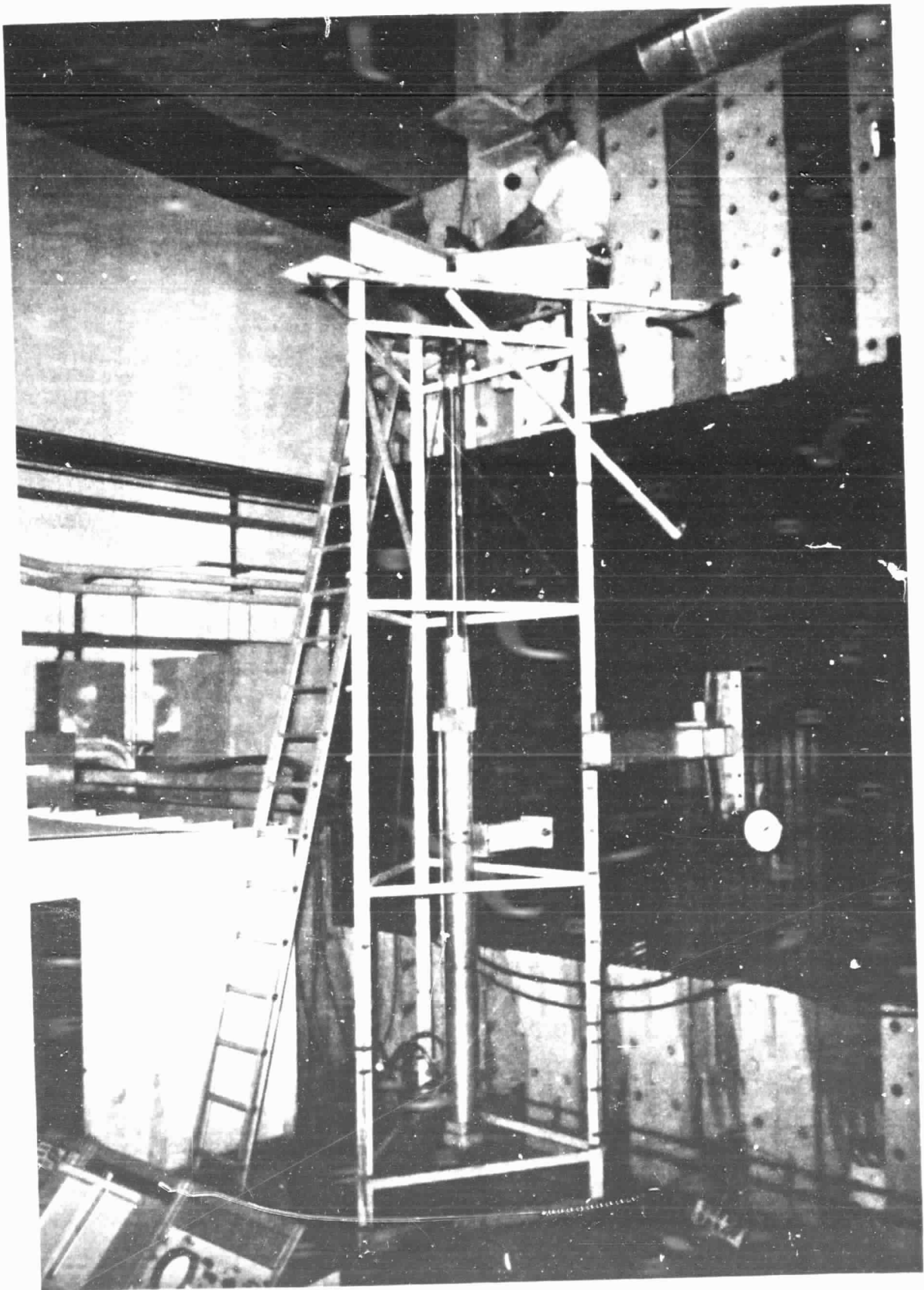


Figure 4 26. PTS torsional stiffness and damping test setup.

The truss segment was twisted in 1 degree increments up to 5 degrees, first clockwise, then counterclockwise, and the applied torque was read from the torque wrench. The torque vs. angular rotation from the clockwise and counterclockwise runs of this stiffness test are shown in Figure 4-27. From this figure, the torsional stiffness parameter, KG , may be derived from the torsional stiffness expression as follows:

$$\frac{T}{KG} = \frac{\theta}{l} \quad \text{where } \theta \text{ is rotation in radians and } l = 430.2 \text{ cm} \text{ (169.4 inches).}$$

For $\theta = 5^\circ$, $T = 135.58 \text{ N-m (100 ft-lb)}$

$$\therefore KG = \frac{(135.58)(4.302)(57.3)}{5}$$

$$KG = 6.695 \times 10^3 \text{ N-m}^2 \text{ (} 2.33 \times 10^6 \text{ lb-in}^2 \text{)}$$

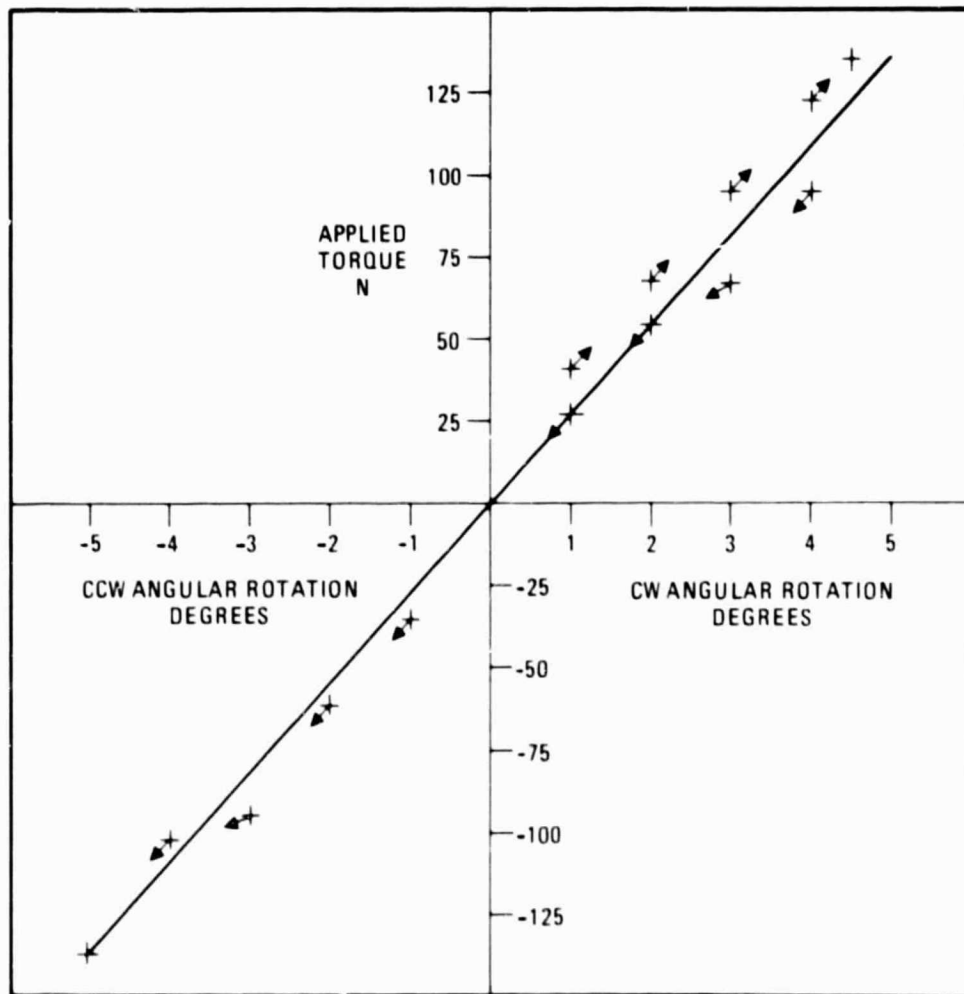


Figure 4 27. Torsional stiffness test results.

The recorded tension values for one strain gauged and load calibrated cord in Bay No. 3 for the clockwise torque application indicated a maximum increase of 60 N (13.5 lb) when the torque was increased from 0 to 135.58 N-m (100 ft-lb). This increase was about 142 N (32 lb) less than simple truss calculations would predict.

4.5.3 TEST SEQUENCE 3: TORSIONAL DAMPING TEST. The test setup for the torsional damping test was the same as that described for the torsional stiffness test. The PTS was rotated clockwise $4\frac{1}{2}^\circ$ and instantaneously released, and then 5° counterclockwise and instantaneously released. An oscillograph recording of the tangential accelerations of an accelerometer mounted at the top of cap No. 2 was made after each release of load. The natural frequency for the structure in torsion for both the clockwise and counterclockwise cases was 3.33 Hz, and the torsional damping coefficient was derived by scaling the acceleration amplitude from two successive cycles and substituting the logarithmic decrement expression:

$$C/C_{cr} = \frac{1}{2\pi} \log_n \left(\frac{X_t}{X_{t+\tau}} \right)$$

where C/C_{cr} is the ratio of the damping coefficient to the critical damping coefficient, and X is the acceleration amplitude. For the clockwise run the value of C/C_{cr} calculated is 1.2% and for the counterclockwise it is 3.2%.

The recorded acceleration amplitude for the counterclockwise test fell off abruptly after the first cycle, which indicated some high initial damping factor which cannot be explained. Since only one test run was made it is not known if this phenomenon was repeatable. There is no apparent reason why the PTS torsional damping should be dependent on the wind-up direction. The damping response of the counterclockwise test was more uniform and is considered a more valid test.

4.5.4 TEST SEQUENCES 4 & 5: FLEXURAL STIFFNESS AND DAMPING TESTS. The test sequences for the flexural stiffness and flexural damping were omitted because of a conflict with higher priority Orbiter test programs.

4.5.5 TEST SEQUENCE 6: AXIAL COMPRESSION TEST. Test Sequence No. 6 of the Structural Test Plan for the PTS was conducted in building 13 at JSC on October 27, 1980. For this test sequence, the test article was oriented vertically with the base clamped to the floor beams of the test area. The axial compression load was applied by a single hydraulic actuator via a ball and socket attachment to a loading plate on top of the test article. The loading plate distributed the single applied force equally to each of the three longitudinal cap members. A photograph of the test setup is shown in Figure 4-28.

The test plan called for three test runs: the first of which was to determine the compressive load at which local buckling of the caps occurred, the second was to evaluate post-buckling strength, and the third run was to be a loading run to failure in order to establish the ultimate compressive strength of the truss segment. The first run was successfully completed, but prior to the start of the ultimate

strength run, a compressive load of unknown magnitude was suddenly and inadvertently applied by the test operator and this load resulted in failure of the caps of the test article.



Figure 4-28. PTS axial compression test.

4.5.5.1 Instrumentation. Sixty-six channels of instrumentation consisting of 4 load cells, 7 LVDT deflections, 52 strain gauges, and 3 acoustic emission counters were electronically recorded during the test. In addition to these electronically recorded measurements, three lasers were used to measure the angular rotation of the three caps. These measurements are described as follows:

- a. Load Cells. One load cell was located between the hydraulic actuator and the loading plate to measure the total applied load to the test article, and one load cell was located between the loading plate and each of the three longitudinal caps of the PTS to measure the distribution of the applied load to each cap. The load cell at the top of Cap No. 3 can be seen in Figure 4-28.

- b. Deflection Measurements. One LVDT was located at the centroid of the loading plate and one LVDT was located at the top end of each of the three caps to measure axial deflections, and three LVDTs were mounted in Bay 2 to measure the lateral deflection of each cap.
- c. Strain Gauges. Fifty-one strain gauges were installed on the PTS cap members and one strain gauge was glued to one of the diagonal cords in Bay 3.
- d. Acoustic Emission. Microphone transducers were mounted on each of the three beam caps in Bay 3 in order to monitor the acoustic emissions during loading of the PTS.
- e. Laser Beam Measurements. The angular rotation of the PTS cap members was obtained using three C.W. Radiation, $\frac{1}{2}$ milliwatt helium-neon lasers. The laser beams were reflected by 1/8-inch diameter front silvered mirrors attached to the apexes of the PTS cap members at all mid-bay points onto flat target surfaces located 5.36 m and 6.02 m away. Each laser was installed in-plane with three mid-bay mirrors to allow the beam to be directed to each mirror by rotating the laser.

Cardboard was attached to the flat target surfaces with graph paper taped to the cardboard. A permanent record of reflected laser beam positions could thus be obtained by placing a pencil mark where the beam struck the paper.

A reference mirror was attached to a dial indicator magnetic stand and supported from the backstop for each laser. This allowed any change in the position of a laser to be detected.

4.5.5.2 Compression Test Results. The maximum applied compressive load for the bifurcation test run was 3.43 kN (772 lb). The load cells at the top of each cap indicated that this applied load was distributed equally within about 1.5% to the three longitudinal caps. The axial deflection measurements of the caps were used during this test run to indicate the onset of initial local buckling of the caps. The axial and angular deflection versus axial load in cap No. 1 and cap No. 3 is shown in Figure 4-29. The LVDT at the top of cap No. 2 gave very erratic readings and was disconnected. From these deflection plots, it appears that the cap load at which local buckling first appears is between 756N and 800N (170-180 lb). The magnitude of the cap strains at the maximum applied load were all relatively small (less than 500 $\mu\text{m}/\text{m}$). The magnitude of the maximum cap load applied was not sufficient to produce meaningful strain gauge data.

The acoustic emissions which were monitored during the first test run showed the number of recorded emissions increased with increasing load in an orderly fashion and there was no asymptotic increase in the acoustic emission counts which is the signal for impending failure.

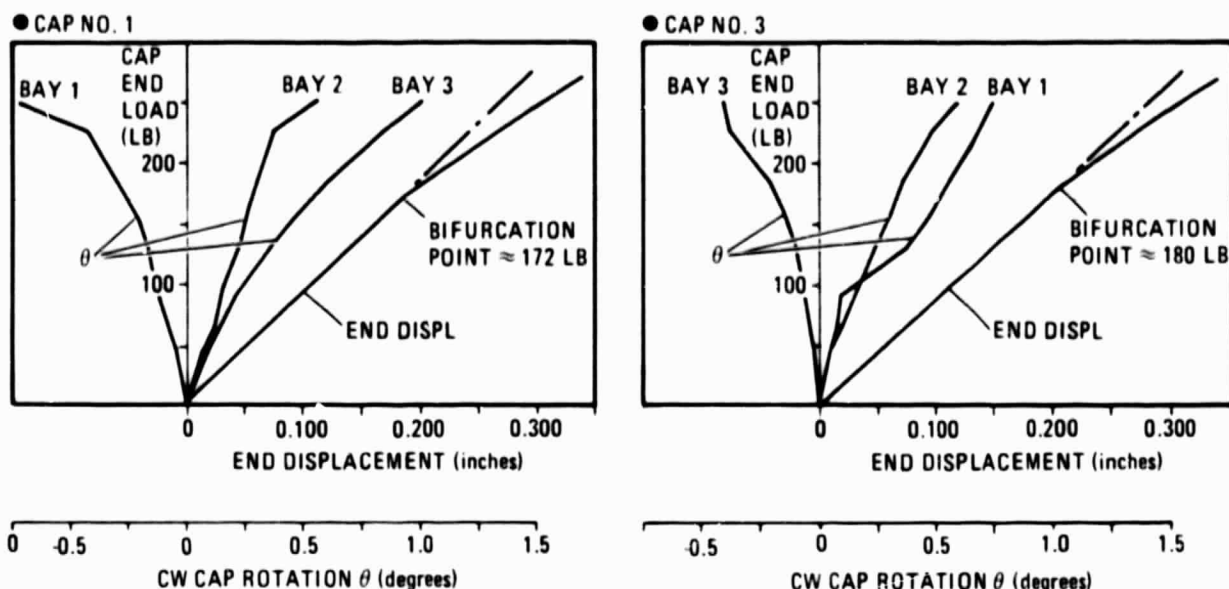


Figure 4-29. Cap displacement and rotation versus end load.

The bifurcation test for onset of initial buckling and/or torsional instability was not repeated because the test article was accidentally destroyed while setting up for the next run. The cap rotation measurements from the test that was performed indicated that the caps do rotate very gradually as load is applied and the rate of rotation shows a tendency to increase after the bifurcation point is reached. The strain gauge data suggested that local buckling is also developing as load is applied; however, the data were inconclusive as to buckling behavior after the bifurcation point is reached.

4.5.6 DISCUSSION OF PTS TEST RESULTS. Although the PTS test program was only partially completed, it did yield a number of important findings about its design and characteristics. These include the following:

- a. The diagonal cord members are not easily seen when working in proximity to the truss. This makes them vulnerable to breakage. It was also found that the cords are easily broken because the cord capture weld may cause a localized weak spot right at the edge of the weld. These findings indicate the need for further improvements in the cord and weld joint design.
- b. The cap transverse stiffness test indicated the need to provide more stiffness at the crossmember stations to minimize the deflections of the caps at mid-bay when subjected to a local transverse load. These are the loads that would be imposed by the devices which would handle the truss beams on an assembly jig during in-space assembly of large platforms.
- c. The axial load test shows the truss to be structurally adequate for a SCAFE application where maximum predicted loads on the cap members are less than 445 N (100 lb). Further testing would reveal to what extent the truss could operate in the post-buckling load range without damage or deterioration. Also, more testing and analysis of material characteristics and open section cap members would lead to much more precise methods of predicting the structural performance of the truss.

5

GRAPHITE COMPOSITE MATERIAL

In addition to the forming, welding, truss manufacture and local effects tasks, Convair provided samples of graphite/thermoplastic (GR/TP) consolidated strip material for testing in a NASA/LaRC material space environmental test program. This section describes the material used in this program, the material provided to LaRC, and the nature of the environmental tests which were performed by LaRC.

5.1 FORMING, WELDING & TRUSS MATERIAL

The GR/TP composite material used in each of the program tasks reported in the preceding sections is a hybrid single-ply woven graphite and glass cloth impregnated with Union Carbide's P-1700 polysulfone resin and coated with TiO₂ pigmented P-1700 resin. The material characteristics are as shown in Figure 5-1. The extensional properties were measured at room temperature after consolidation.

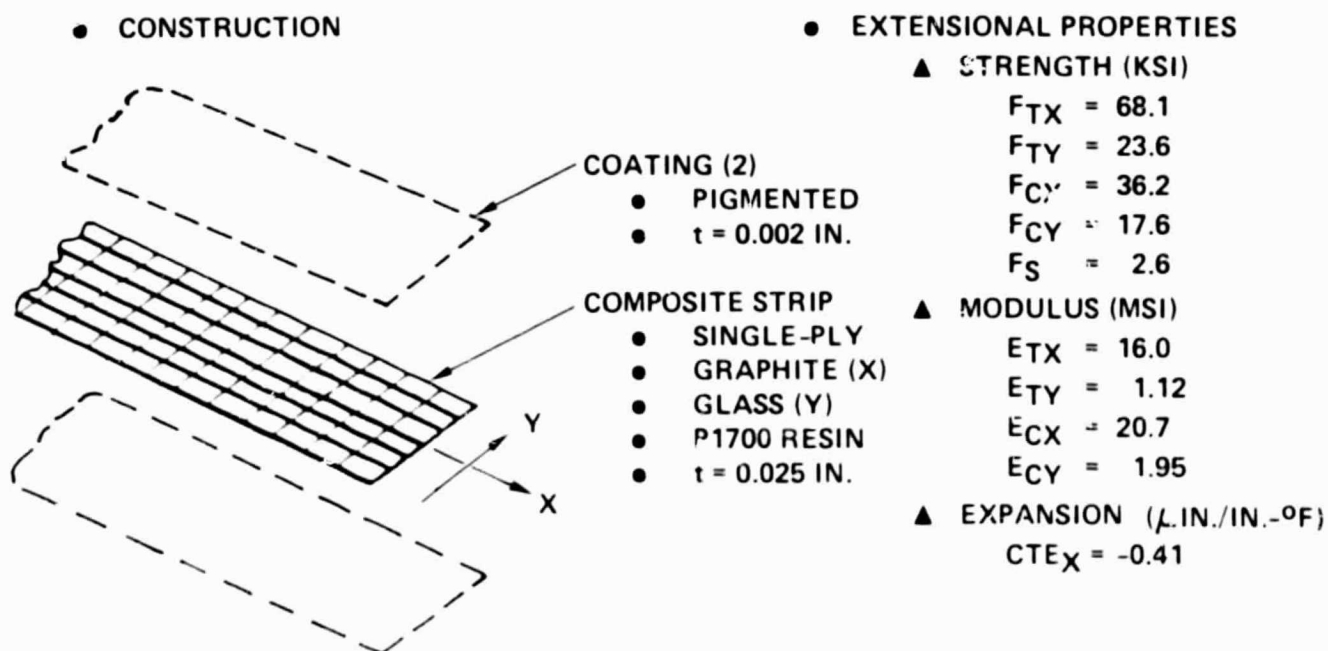


Figure 5-1. Material characteristics.

All forming, welding, and truss fabrication was performed with strip material from the same batch. This material was procured from Fiberite, Corp., and delivered to Convair in March 1979. It was the fourth in a series of material designs developed and tested by Convair in conjunction with automated in-space fabrication technology IRAD.

5.2 SPACE ENVIRONMENTAL TEST MATERIAL

The GR/TP composite material supplied to NASA/LaRC for their space environmental test program was similar to the material used in the forming, welding, and truss fabrication tasks. The 968 cm² (150 in.²) of consolidated strip material delivered to NASA/LaRC on 7 November 1979 was taken from the previous batch of hybrid graphite/glass polysulfone composite material tested by Convair. A detailed description of this composite strip material is as follows:

- a. Fiber (56% by volume):
 - (1) Warp: PAN 50 Graphite; 6K tows; 44 per inch
S-Glass; 12 end roving; 11 per inch
 - (2) Fill: S-Glass; 12 end roving; 12 per inch
 - (3) Construction: Single-ply; 5-harness satin skip-draw
- b. Resin (44% by volume): P-1700 Polysulfone
- c. Processing:
 - (1) Weaving and prepregging by vendor (Fiberite)
 - (2) Delivered to GDC in March 1978
 - (3) Consolidation by heated press at GDC; final thickness $\approx .032$
 - (4) Stored in materials lab ambient environment
- d. Properties (Room temperature test values):
 - (1) Strength (KSI):

$$F_{TX} = 82.3; F_{CX} = 43.1 \quad F_S = 3.6$$

$$F_{TY} = 19.2; F_{CY} = 10.8$$
 - (2) Modulus (MSI):

$$E_{TX} = 17.1; E_{TY} = 1.0$$

NASA/LaRC planned to perform flexure tests on miniature material coupons to determine mechanical properties before and after exposure to the following radiation levels:

- a. 1 MeV electrons
- b. 1×10^{10} rads (\approx 30 years at GEO)
- c. 20°C and 120°C each exposure

The results of this testing are to be published by LaRC.

6

CONCLUSIONS AND RECOMMENDATIONS

This section summarizes the conclusions drawn from the Graphite Composite Truss Welding and Cap Section Forming Subsystems program and provides recommendations for subsequent technology development efforts associated with these key beam-builder elements.

6.1 CONCLUSIONS

Conclusions are presented in the subject sequence of the preceding text.

6.1.1 CAP FORMING TECHNOLOGY

- a. The Convair-developed roll forming process represents a viable and efficient solution to the problem of roll forming graphite composite material beam cap members in an automated beam builder system for in-space fabrication of large space structures.
- b. Minor irregularities observed in cap sections due to unresolved heating effects can be corrected by simple changes to the heater reflectors.
- c. Curvature of cap members can be resolved by using strip material of uniform thickness.
- d. The lack of capability to produce continuous strips of high quality preprocessed graphite/thermoplastic (GR/TP) material will impede progress in beam builder and large space structures technology as follows:
 - (1) Small batch production and processing will become prohibitively expensive as greater experimental quantities are required to support beam builder development.
 - (2) The effects of improper preprocessing techniques on material structural and long-term operating behavior.
- e. The baseline SCAFEDS beam builder drive speed produced no speed-related defects in roll formed caps.
- f. The Rolltrusion roll forming process can be adapted to drive speeds between 10.1 cm/sec (4.0 in./sec) and 30.5 cm/sec (12.0 in./sec) through further development.

6.1.2 ULTRASONIC WELDING TECHNOLOGY

- a. Ultrasonic welding in vacuum produced no identifiable effect on weld strength or resin flow characteristics.
- b. Welding GR/TP material which has been properly conditioned to remove moisture and volatiles produces no outgassing in vacuum.
- c. Ultrasonic welder electronic amplifiers and controllers that are vacuum-compatible will have to be specially designed and developed for the beam builder.
- d. The piezoelectric ultrasonic transducer will operate in vacuum when properly evacuated.
- e. Ultrasonic welding in vacuum produced no change in the efficiency of the welder and no significant heating effects on the weld horn or transducer.
- f. Weld heat is conducted away from the weld primarily in the direction of the graphite fibers, and the rate of cooling is not significantly different between welds produced in air and in vacuum.
- g. Welder performance is affected by gravity but would not be affected by zero-gravity.
- h. Gravity effects on the welder performance can be compensated for by adjusting weld pressure and weld time. Also, the stiffness of the weld horn can be changed to preclude gravity effects.
- i. The weld power characteristic during welding is sensitive to material thickness and surface conditions, and the amount of weld energy applied correlates well with weld strength. Weld energy and weld power profile monitoring should be considered as in-process quality control parameters for the beam builder system.
- j. A beam builder ultrasonic welder will require automatic frequency compensation for weld horn temperature changes.

6.1.3 PROTOTYPE TEST TRUSS

- a. Minor modification of the truss welding horn is required to allow the cord to be maintained in full tension without breaking during welding.
- b. Fabrication and assembly of the PTS proved that the SCAFEDS beam builder concept is sound and no major technical problems exist that preclude its development.

- c. The incipient buckling loads measured for the crippling test specimens showed good correlation with the predicted load when corrected for thickness.
- d. The critical column buckling load for cap members would be nearly the same as the short column crippling strength in the absence of torsional instability.
- e. Interaction analysis of the combined effects of column buckling and torsional instability for the open section cap member when compared with the column test results, showed only fair correlation. A better test specimen and a STAGS analysis which accommodates both torsional instability and local buckling is required to demonstrate that the load effects analysis is producing reasonable results.

6.2 RECOMMENDATIONS

The work completed on the Graphite Composite Truss Welding and Cap Section Forming Subsystems program indicates the need for continued technology and hardware development if a truly useable beam builder and large space structures construction system are to become a reality.

6.2.1 BEAM BUILDER TECHNOLOGY

- a. Design, develop, manufacture, and test a flight qualifiable cap forming module as defined in JSC specifications BB-SS-100 and BB-CFS-101, to accomplish the following:
 - (1) Conduct ground test and evaluation of vacuum and gravity effects.
 - (2) Develop a precision cap drive and control technique.
 - (3) Optimize heaters, temperature sensor, and temperature controls for an operational space system.
 - (4) Conduct in-space cap forming experiments to ensure flight and in-space operational compatibility.
- b. Design, develop, manufacture, and test a flight qualifiable ultrasonic welder for the beam builder per the requirements of JSC specification BB-BJS-101, to accomplish the following:
 - (1) Optimize weld head size, weight, and efficiency.
 - (2) Provide a space compatible weld power and control module.
 - (3) Incorporate automatic in-process quality assurance functions and assess reliability of welds.

- (4) Conduct ground test and evaluation of the effects of long term operation of the welder in vacuum.
- (5) Conduct in-space ultrasonic welding experiments to ensure flight and in-space operational compatibility.

6.2.2 GRAPHITE THERMOPLASTIC MATERIALS TECHNOLOGY

- a. Continue the analysis and test of single-ply woven fabric material as follows:
 - (1) Determine the effects of manufacturing techniques on material properties.
 - (2) Conduct experiments to assess how closely the coefficient of thermal expansion of the material can be controlled and how stable it remains with time, temperature, and load.
 - (3) Determine the fatigue of repeated loading and thermal cycling.
 - (4) Establish the behavioral characteristics of single-ply versus laminated GR/TP materials.
- b. Establish manufacturing requirements for GR/TP strip material which will define the techniques required for continuous compaction, coating, conditioning and quality assurance.

6.2.3 LARGE SPACE STRUCTURES TECHNOLOGY

- a. Continue to analyze, fabricate, and test prototype structure and structural elements.
 - (1) Test cap members for post buckling fatigue life.
 - (2) Perform a STAGS analysis of the combined effects of local buckling, column buckling, and torsional instability on cap load carrying capability.
- b. Conduct tests to determine the endurance of truss weld joints under cyclic loading and long term static loading.



REFERENCES

1. Browning, D. L., Space Construction Automated Fabrication Experiment Definition Study (SCAFEDS) Part III, Final Report, CASD-ASP78-016
29 June 1979.
2. Almroth, B. O., et al, "Structural Analysis of General Shells, User Instruction for STAGSC," Volume III, Report No. LMSC D50277, Lockheed, Structural Mechanics Laboratory, Lockheed Palo Alto.
3. Structural Principles and Data, Handbook of Aeronautics, No. 1, Sir Isaac Pitman & Sons, Ltd., London, 1952, Section 12.5.4.
4. Bleich, Friedrich, Buckling Strength of Metal Structures, McGraw-Hill 1952, Pg 121.
5. Advanced Composites Design Guide, Volume II - Analysis, Air Force Materials Laboratory, Advanced Development Division, Dayton, Ohio, January 1973.
6. Structures Manual, NASA Marshall Space Flight Center, Huntsville, Alabama, Section C1, Pg 20.

APPENDIX A

INSTRUMENTATION AND TEST
REQUIREMENTS FOR
PROTOTYPE TRUSS SEGMENT (PTS)

APPENDIX A

TABLE OF CONTENTS

<u>Section</u>	<u>Page</u>
1.0 SCOPE	A-3
2.0 OBJECTIVE	A-3
3.0 APPROACH	A-3
4.0 REQUIREMENTS	A-3
4.1 GDC Responsibilities	A-3
4.1.1 PTS Configuration and Manufacture	A-3
4.1.2 Strain Gages	A-3
4.1.3 End Fittings	A-4
4.2 NASA/JSC Responsibilities	A-4
4.2.1 General	A-4
4.2.2 Test Preparation	A-6
4.2.2.1 Setup	A-6
4.2.2.2 Instrumentation	A-7
4.2.3 Testing	A-10
4.2.3.1 Cap Transverse Stiffness	A-10
4.2.3.2 Torsional Tests	A-12
4.2.3.3 Flexural Tests	A-12
4.2.3.4 Compression Tests	A-12
5.0 TEST DATA ANALYSIS	A-13
5.1 Analysis of PTS End Constraint Effects	A-13

1.0 SCOPE

This document establishes the requirements for instrumentation, test preparation, test and evaluation of the Prototype Truss Segment (PTS) to be manufactured by General Dynamics Convair (GDC) and tested by the National Aeronautics and Space Administration, Johnson Space Center (NASA/JSC), in accordance with Contract NAS9-15973.

2.0 OBJECTIVE

The objectives of this program are to measure the principal structural characteristics of the 3-bay PTS, and to establish corresponding characteristics for beams of identical construction and arbitrary length, free of test length and fixity constraints. Characteristics of interest are: truss critical axial compression load; truss axial compressive, torsional and flexural stiffnesses; truss dampint in torsion and flexure; and individual cap transverse stiffness. The resulting values will replace those currently given in the Beam Builder System Specification, BB-SS-100.

3.0 APPROACH

A 3-bay truss segment, which conforms to the SCAFEDS Part III baseline beam configuration, will be manufactured by GDC and test by NASA/JSC. Analyses will then be performed to: (1) determine the effects of PTS length and end constraint on the measured structural characteristics; and (2) establish corresponding characteristics for long, unconstrained beams. The analytical approach employs data from both the PTS tests and GDC single-cap tests, and is also presented in this document. The specific requirements contained in this document for instrumentation, setup, and test of the PTS, are recommended by GDC to provide sufficient data to properly perform the concluding analyses.

4.0 REQUIREMENTS

To accomplish the objectives of the test program, the PTS shall be prepared for test and tested in accordance with the requirements of this section.

4.1 GDC RESPONSIBILITIES

4.1.1 PTS CONFIGURATION AND MANUFACTURE. The PTS shall conform to the requirements and dimensions of drawing LSST-001.

4.1.2 STRAIN GAGES. Strain gages shall be installed per Figure A-1 to: (1) verify proper shimming during setup to assure equal axial load application to the three individual PTS cpps; and (2), characterize cap behavior during the various test phases.

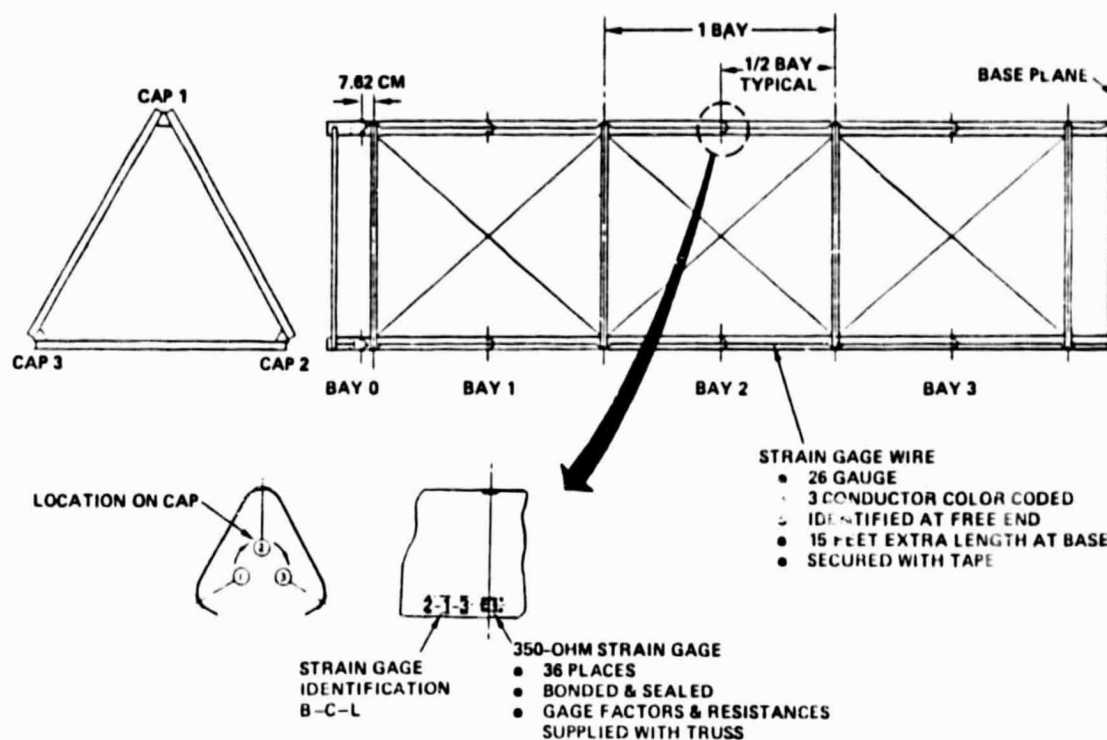


Figure A-1. Strain gage installation.

Gage type and quantity shall be per Table A-1. All gages shall be installed and wired per drawing SKDV 800418 (TBS-GDC) with an additional 15 ft. of wire length provided at the base end of the truss.

4.1.3 END FITTINGS. Metallic fittings shall be fabricated and bonded into the cap ends per drawing SKDV 800418 (TBS-GDC) and braced with aluminum angle to facilitate truss vertical support and test load introduction. The mass properties of these items shall be determined and recorded.

4.2 NASA/JSC RESPONSIBILITIES

4.2.1 GENERAL

- a. The following tests shall be conducted:
 - (1) Cap Transverse Stiffness
 - (2) PTS Torsional Stiffness
 - (3) PTS Torsional Damping
 - (4) PTS Flexural Stiffness (optional)

Table A-i. Instrumentation requirements.

Code	Type Function	Characteristics (Type/Sensitivity/Range)	Quantity			Installation		Test Applicability					
			LOCS	PTS LOC	Σ	By	Per	1	2	3	4	5	6
A	Acceleration	TBD	3	1	3	NASA	Fig 5			X		X	
D	Displacement - Lateral - Axial	0-1.0 In. Range	9	3	27	NASA	Fig 4	*	X	†	X	†	X
		0-0.25 In. Range	4	1	4	NASA	Fig 4				X		X
L	Load - Axial - Lateral	0-2400 lb. Range	3	1	4	NASA	Fig 3,4				X		X
		0-50 lb. Range	1	1	1	NASA	‡	X			X		
M	Motion Pictures	Speed TBD	2	1	2	NASA	Fig 5			X		X	
P	Still Photo	Conventional Equip	TBD	TBD		NASA	—	X	X	X	X	X	X
R	Rotation	Protractor/TBD	1	1	1	NASA	Fig 5		X	X			
S	Strain	350 Ohm	12	3	36	GDC	Fig 1	*	X	X	X	X	X
T	Torque	Com'l Torque Wrench	1	1	1	NASA	—		X	X			

* Measurements required on loaded cap only. Ref. Figure 2.

† Measurements optional, in upper bay, if response sufficient to follow cap motion.

‡ Relocate load cell to suit test requirements.

- (5) PTS Flexural Damping
- (6) PTS Axial Compression
 - (a) Case 1: Axial Stiffness
 - (b) Case 2: Cap Buckling
 - (c) Case 3: Ultimate Strength (optional)

- b. All tests shall be conducted in the JSC structural test facility (Bldg.13), in the ambient environment.
- c. Handling of the PTS by personnel not directly involved in necessary test setup and operations shall be prohibited.

Test details will be discussed in Subsection 4.2.3.

To minimize truss handling and setup time, tests should be conducted in the above sequence. (If optional test 6-3 is omitted, test 1 can be performed after test 6-2.)

4.2.2 TEST PREPARATION

4.2.2.1 Setup. Test 1 (Cap Transverse Stiffness) shall be performed with the PTS in a horizontal position as shown in Figure A-2. To facilitate PTS rotation (to lead each

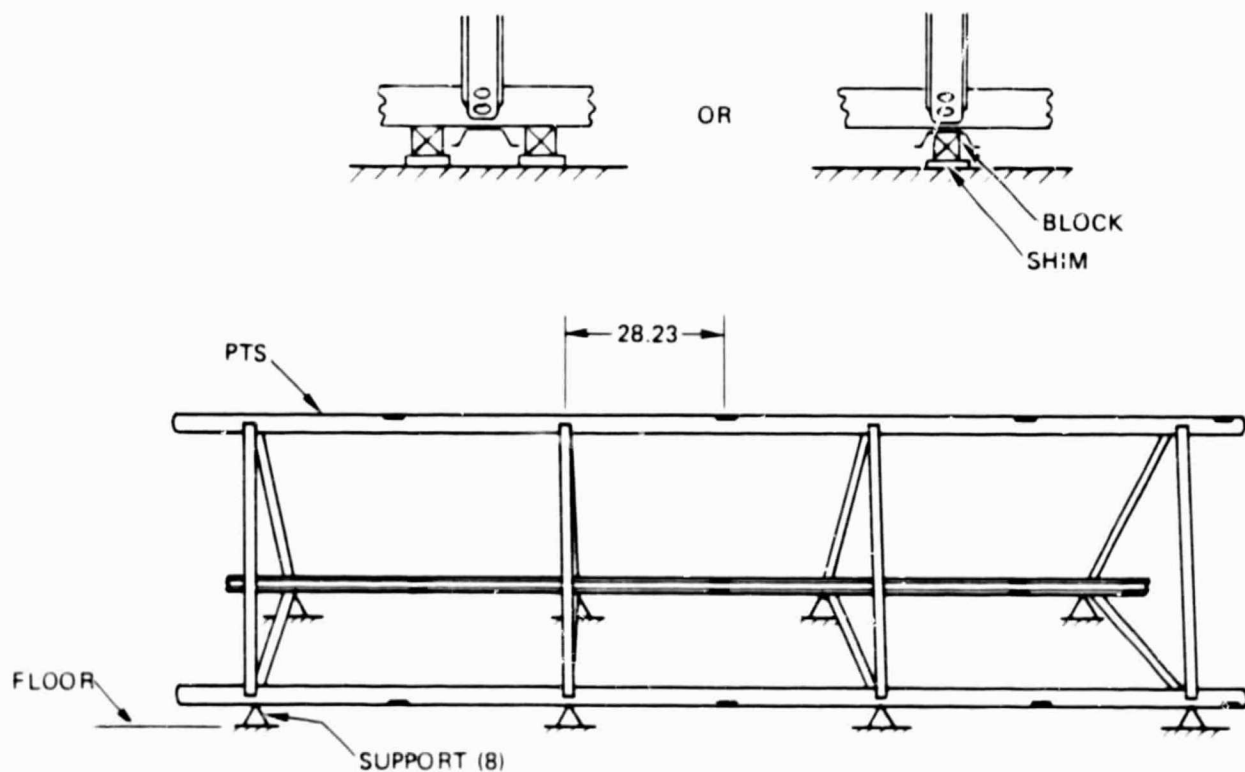


Figure A-2. Setup for test 1. (cap transverse stiffness)

cap successively) the eight supports should consist of simple bearing blocks, either nesting in or straddling each crossmember. In each setup position, gaps at the support points should be eliminated by appropriate shimming, and two load cycles (to 20% of the maximum test value) should be applied to "set" the PTS and the instrumentation. If the caps distort due to end fitting weight with the PTS horizontal, provisions shall also be made to interconnect and support each set of fittings.

All other tests shall be performed with the PTS in a vertical position. Setup and load fixture provisions for vertical testing shall be similar to those employed for previous testing of the SCAFEDS prototype truss. (Ref. Figure A-3 and NASA/JSC drawing ES6-STA6-17.) The design of the PTS cap/loading plate interface shall consider the possibility of different cap end fixity requirements among the various tests.

Mass properties of all setup/fixturing elements which apply inertia load to the PTS in any test shall be determined and recorded.

4.2.2.2 Instrumentation. Table A-1 summarized the minimum instrumentation required to characterize and fully document PTS test behavior and to satisfactorily complete the subsequent analyses. Strain gage locations were shown in Figure A-1.

Displacement and load measurement locations and component axes, shall be per Figure A-4. Separation shall be maintained between strain gages and the contact/attach points of cap lateral displacement measurement devices, as noted. Load cells on each cap shall supplement the actuator load cell (Figure A-3) to equalize axial load distribution among the three PTS caps during setup and to monitor load distribution during compression tests (for bifurcation onset and post-buckling behavior). Axial displacement shall also be measured at all load cell locations.

Accelerometer locations and axes, for determining PTS vibration decay (Tests 3 and 5) shall be per Figure A-5. A visual record of the vibration decay characteristics shall also be made, using a minimum of two motion picture cameras: one looking horizontally at the full length PTS, the other looking down the PTS axis from above. The use of a "t = 0" flash and the illustrated fixed reference grids would also aid post-test data evaluation and correlation.

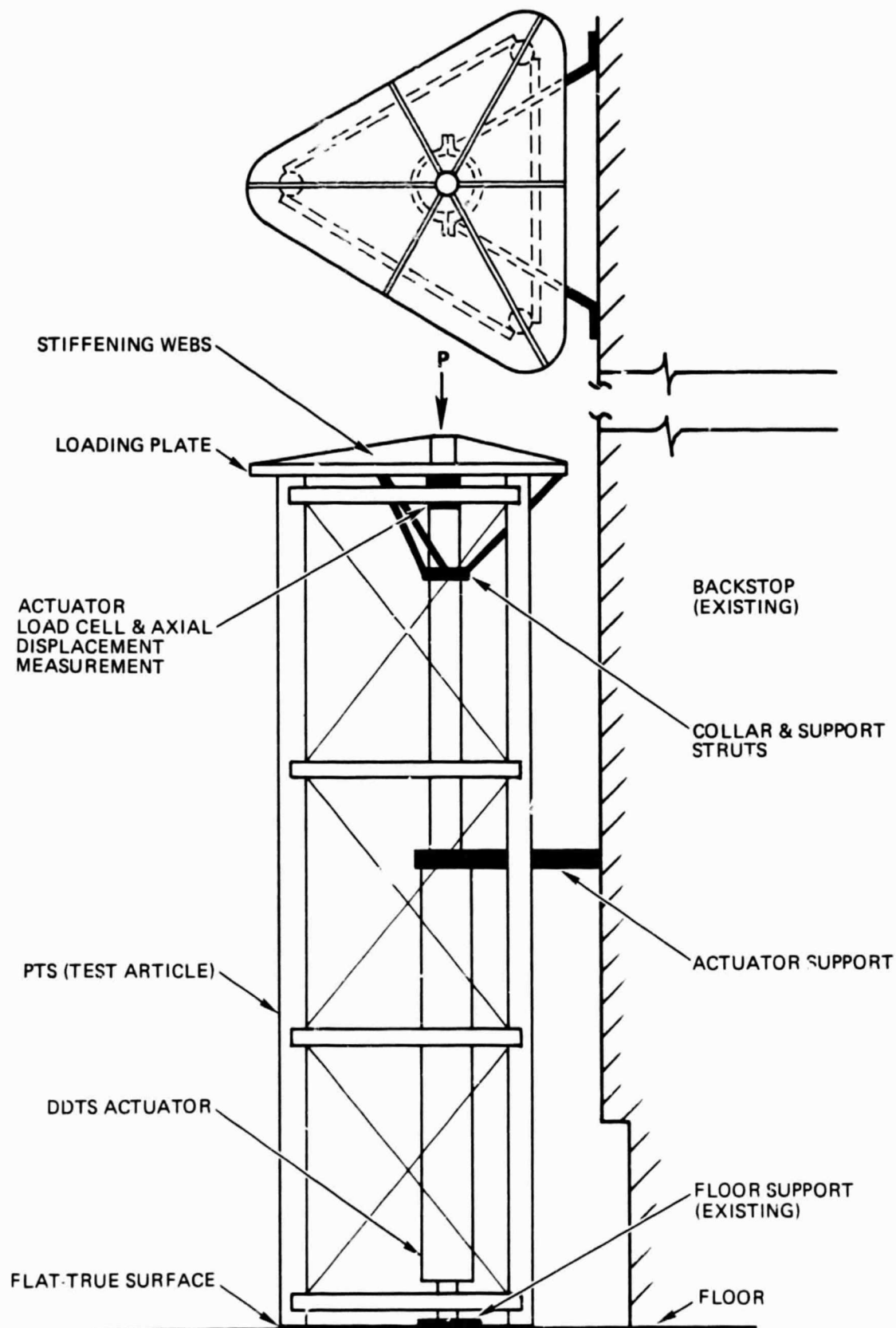


Figure A-3. Setup and fixture provisions for vertical tests.

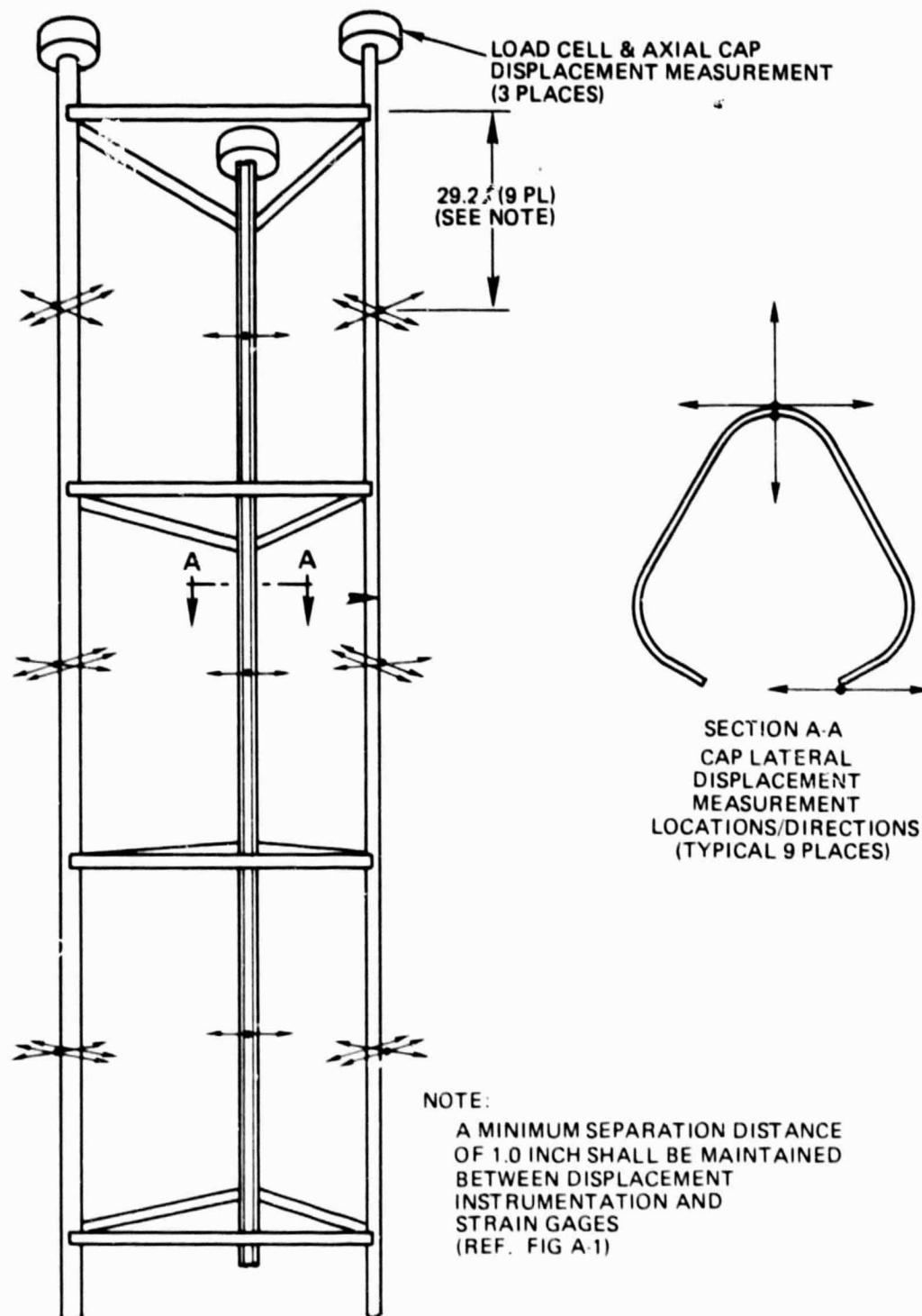


Figure A-4. Displacement and load instrumentation.

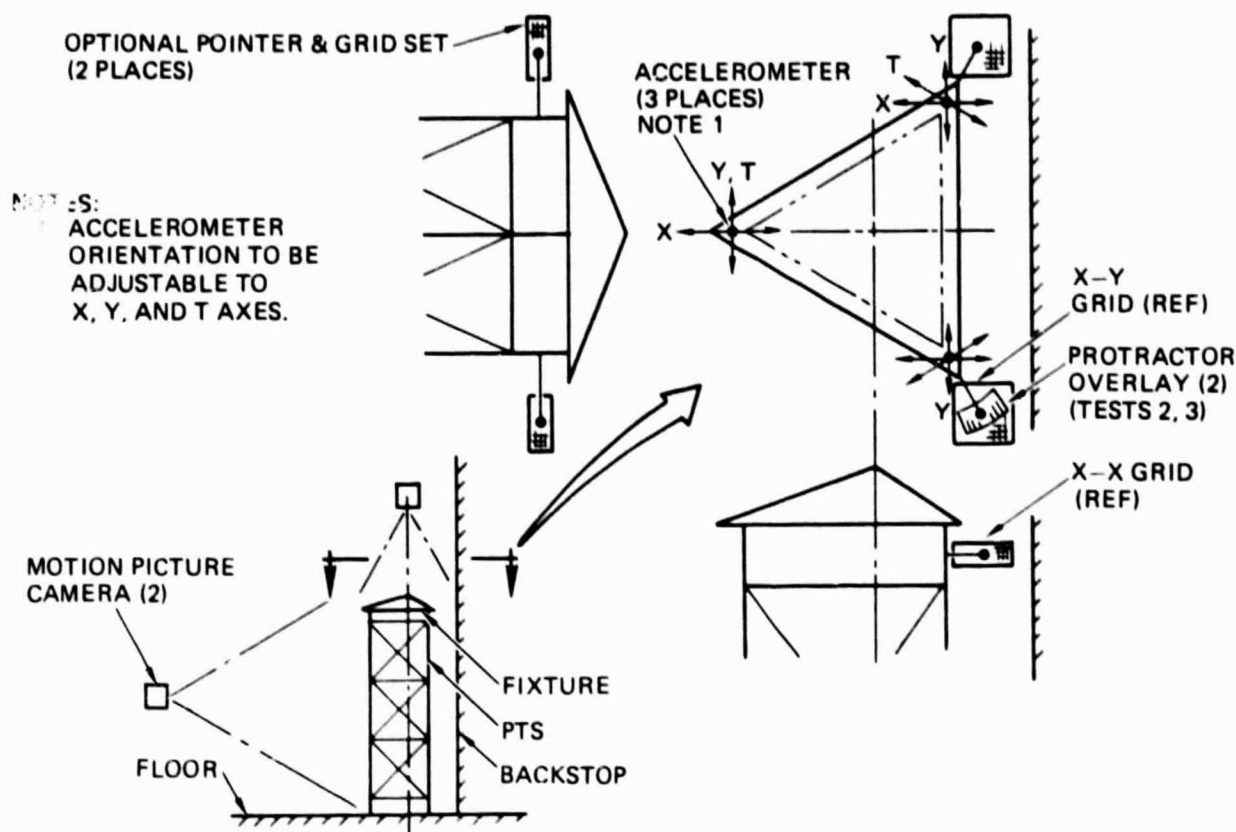


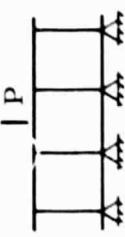
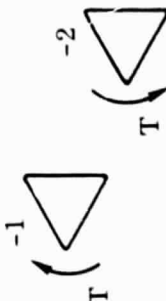
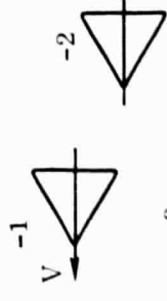
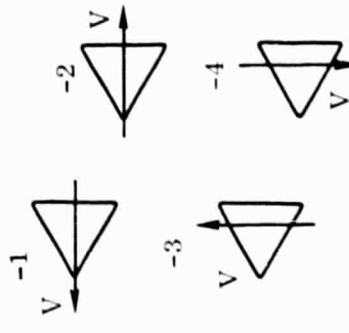
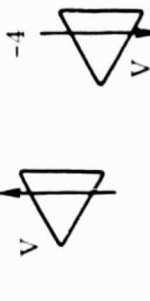
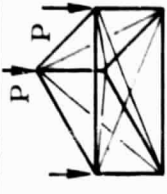
Figure A-5. Vibration decay instrumentation.

4.2.3 TESTING. The PTS test program shall consist of the tests summarized in Table A-2. Tests 1 and 4 are optional, but strongly recommended. Test 6-3 is also optional, depending on JSC plans for future use of the PTS for display or additional testing.

With the exception of Test 6-3 (Ultimate Compression), all tests shall be nondestructive. Maximum test loads and deflections shall be determined accordingly from the applicable analytical and component test data. Inertia effect of test setup/fixtures elements shall be considered in establishing maximum loads for all tests. If at any time, during any test, unexpected indications of potential or impending damage occur (e.g., audible cracking, significant deflection, increased deflection rate, etc.) the test shall be terminated immediately, followed by data review and detailed PTS examination prior to test resumption.

4.2.3.1 Cap Transverse Stiffness. The purpose of this test is to establish the spring rate under a cap midspan load. This condition occurs during beam longitudinal translation on an assembly fixture and represents the "softest" case for dynamic response analysis. To obtain a representative average value, as well as to assess cap-to-cap differences, this test should be performed successively on each of the three PTS caps.

Table A-2. PTS test matrix.

Test		Setup		Load Conditions					Instrumentation									
Seq	Type	H	V	Case	Orientation	Reps	Max Value	Increment		A	D	L	M	P	R	S	T	
1	Cap Transverse Stiffness	✓		-1 -2 -3		2 2 2	50 lb 50 lb 50 lb	20% 20% 20%	20% 20% 20%	X X X	X X X			X X X		X X X		
2	Torsional Stiffness		✓	-1 -2		2 2	100 ft-lb* 100 ft-lb*	20% 20%	20% 20%	X X				X X	X X	X X	X X	
3	Torsional Damping		✓	-1 -2		2 2	100 ft-lb* 100 ft-lb*	20% 20%	Abrupt Abrupt	X X	X X			X X	X X	X X	X X	
4	Flexural Stiffness		✓	-1 -2 -3 -4		2 2 2 2	100 lb 100 lb 100 lb 100 lb	20% 20% 20% 20%	20% 20% 20% 20%	X X X X	X X X X			X X X X		X X X X		
5	Flexural Damping		✓	-1 -2 -3 -4		2 2 2 2	TBD TBD TBD TBD	20% 20% 20% 20%	Abrupt Abrupt	X X X X	X X X X			X X X X		X X X X		
6	Axial Compression		✓	-1 -2 -3		3 3 1	450-900 lb 1200-2400 lb 1200-2400 lb	10% 5% 5%	20% 20% —	X X X	X X X			X X X	X X X	X X X		

*or 5° rotation, whichever occurs first.

For each load case, only the instrumentation on the loaded cap need be measured. Care should be taken to avoid load application directly on the cap apex strain gages (or wiring) at the load point.

4.2.3.2 Torsional Tests. To obtain representative average values, as well as to assess the effects of alternating cord crossover along each of the three PTS sides, these tests should be performed with both CW and CCW torques about the PTS axis.

The maximum load value (and twist angle) shall be the same for Tests 2 and 3.

4.2.3.3 Flexural Tests. Each flexural test case involves PTS lateral displacement, without twist, under a transverse shear load. Normally in such an equilateral/equal-cap-area structure, the proper line of action for this load would be through longitudinal (centroidal) axis. However, coupon tests of the cap material indicate different moduli of elasticity in longitudinal tension and compression. Consequently the flexural axis for the four symmetrical load cases (4-1, 4-2, 5-1, and 5-2) is expected to shift off the PTS axis, but a symmetric line of action should still result in twist-free deflection for these cases.

For the remaining four cases (4-3, 4-4, 5-3, and 5-4) the shear load does not lie in a plane of symmetry, and its "zero-twist" line of action should be found by trial and error during setup.

The maximum load value (and deflection) shall be the same for Tests 4 and 5.

4.2.3.4 Compression Tests. Prior to the first test in this sequence, the equality of load introduction to the three PTS caps should be reverified, and the setup adjusted as necessary to achieve this condition. If setup changes are required, the adjusted structure should be cycled at least two times to 20% of the case 6-1 maximum load, to "set" the PTS and its instrumentation.

Case 6-1 should be run to the predicted bifurcation load per Table A-2. If bifurcation is observed at a load less than the predicted value, the observed load should be adopted as the target value for the next two repetitions. If bifurcation has not yet occurred at the predicted value, the load should be increased in similar increments until bifurcation is observed, and this load value adopted as the target for the next two repetitions.

Case 6-2 should non-destructively investigate the post-bifurcation behavior of the PTS. Loading to the bifurcation point should duplicate case 6-1, and further loading into the post-buckling region should be applied in 5% increments. Specific load/displacement targets, based on GDC long column tests and analysis, should be used to govern the extent of safe progress into the post-buckling region.

5.0 TEST DATA ANALYSIS

5.1 ANALYSIS OF PTS END CONSTRAINT EFFECTS

The end fixity coefficient of the cap beam structure between lateral supports may be determined by the expression

$$C = P_{pts}^{cap} / P_{gdc}^{cap}$$

where P_{gdc}^{cap} = column or torsional instability load from single cap test at GDC

P_{pts}^{cap} = column or torsional instability load for one cap in the prototype truss structure.

If the failure mode is found to be similar for both tests, the value for C becomes: for torsional instability, $C = 1.0$ implies complete restraint to twist at the ends. Thus, the value for C should be equal to or less than 1.0, and the value represents the percent resistance to twist.

For column buckling, $C = 1.0$ implies simple-support at the ends. Here, the value for C will be qualitative, not quantitative; i.e., equal to simple-support ($= 1.0$), better than simple-support (> 1.0), or not as good as simple-support (< 1.0).